Title

Identifying a non-dopaminergic system as a target for treating Parkinson's Disease

Permalink

https://escholarship.org/uc/item/16w2n90d

Author

Alhassen, Sammy T.

Publication Date

2023

UNIVERSITY OF CALIFORNIA,
IRVINE

Identifying a non-dopaminergic system as a target for treating Parkinson's Disease

DISSERTATION

submitted in partial satisfaction of the requirements

for the degree of

DOCTOR OF PHILOSOPHY

in Pharmacological Sciences

by

Sammy T. Alhassen

Dissertation Committee:
Professor Amal Alachkar, Chair
Professor Olivier Civelli
Professor Geoffrey Abbott

2023

DEDICATION

This thesis is dedicated to my father, Lamees, Wedad, Kareem, and Mansoor for all of the encouragement you've given me and sacrifices that you all have made for this achievement to be possible.

TABLE OF CONTENTS

TABLE OF CONTENTS

LIST OF FIGURES AND TABLES

LIST OF FIGURES AND TABLES

LIST OF FIGURES AND TABLES

ACKNOWLEDGEMENTS

I would like to express my deepest appreciation to Dr. Amal Alachkar above all. I am grateful for the opportunity you have given me and for the guidance and encouragement that you have provided throughout my journey. Your patience, understanding, and words of wisdom have been invaluable to me. Your passion and dedication to the pursuit of knowledge in the field of science are truly remarkable and have been a constant source of inspiration to me. I feel incredibly fortunate to have had you as my PhD advisor and I could not have asked for anyone better.

I would like to express my gratitude to Dr. Olivier Civelli for his exceptional mentorship and for sharing his vast knowledge in the field. It has been a great privilege to have the opportunity to discuss my research with you and to benefit from your insightful feedback.

I would also like to thank the final member of my committee, Dr. Geoffrey Abbott. I truly appreciate you taking the time to meet with me and the rest of the committee and the feedback that you provided.

Thank you to the Alachkar and Civelli lab - your support and help throughout these years have been invaluable and I am forever appreciative of what you all have done for me. I would like to extend a special thanks to Dr. Ryan Yoshimura, whose vast knowledge and patience were instrumental in guiding me during my early days; Dr. Derk Hogenkamp, who has been incredibly helpful and a joy to work with; and Dr. Mehmet Senel, whose unique perspective and creativity were truly inspiring. I would also like to thank all of our collaborators who have contributed in numerous ways to our work.

Finally, I would like to express my gratitude to all my friends and family, some of whom were instrumental in helping me reach this achievement, and I am fully aware that without your support, this accomplishment would not have been possible.

Chapter 2 of this dissertation is a reprint of the material as it appears in Surface Plasmon Resonance Identifies High-Affinity Binding of l-DOPA to Siderocalin/Lipocalin-2 through Iron-Siderophore Action: Implications for Parkinson's Disease Treatment. ACS Chem Neurosci. 2022 Jan 5;13(1):158-165. Used with permission from the American Chemical Society. The co-authors listed in this publication are Mehmet Senel and Amal Alachkar. Amal Alachkar directed and supervised research which forms the basis for the thesis/dissertation.

Chapter 6 of this dissertation is a reprint of the material as it appears in Intergenerational trauma transmission is associated with brain metabotranscriptome remodeling and mitochondrial dysfunction. Commun Biol. 2021 Jun 24;4(1):783. Used with permission from Communications Biology. The co-authors listed in this publication are Siwei Chen, Lamees Alhassen, Alvin Phan, Mohammad Khoudari, Angele De Silva, Huda Barhoosh, Zitong Wang, Chelsea Parrocha, Emily Shapiro, Charity Henrich, Zicheng Wang, Leon Mutesa, Pierre Baldi, Geoffrey W Abbott, Amal Alachkar. Amal Alachkar directed and supervised research which forms the basis for the thesis/dissertation.

VITA

Sammy T. Alhassen

EDUCATION

University of California, Irvine 2018-2023
Doctor of Philosophy in Pharmacological Sciences

University of California, Berkeley 2016-2017
Masters of Science in Bioengineering

University of California, Riverside 2015-2016
Bachelor of Science in Bioengineering

PUBLICATIONS

1. Alhassen W, **Alhassen S**, Chen J, Monfared RV, Alachkar A. Cilia in the Striatum Mediate Timing-Dependent Functions. Mol Neurobiol. 2023 Feb;60(2):545-565.
2. Alachkar A, Lee J, Asthana K, Vakil Monfared R, Chen J, **Alhassen S**, Samad M, Wood M, Mayer EA, Baldi P. The hidden link between circadian entropy and mental health disorders. Transl Psychiatry. 2022 Jul 14;12(1):281.
3. **Alhassen S**, Senel M, Alachkar A. Surface Plasmon Resonance Identifies High-Affinity Binding of l-DOPA to Siderocalin/Lipocalin-2 through Iron-Siderophore Action: Implications for Parkinson's Disease Treatment. ACS Chem Neurosci. 2022 Jan 5;13(1):158-165.
4. Chen S, Lee J, Truong TM, **Alhassen S**, Baldi P, Alachkar A. Age-Related Neurometabolomic Signature of Mouse Brain. ACS Chem Neurosci. 2021 Aug 4;12(15):2887-2902.
5. **Alhassen S**, Chen S, Alhassen L, Phan A, Khoudari M, De Silva A, Barhoosh H, Wang Z, Parrocha C, Shapiro E, Henrich C, Wang Z, Mutesa L, Baldi P, Abbott GW, Alachkar A. Intergenerational trauma transmission is associated with brain metabotranscriptome remodeling and mitochondrial dysfunction. Commun Biol. 2021 Jun 24;4(1):783.
6. Senel M, Dervisevic E, **Alhassen S**, Dervisevic M, Alachkar A, Cadarso VJ, Voelcker NH. Microfluidic Electrochemical Sensor for Cerebrospinal Fluid and Blood Dopamine Detection in a Mouse Model of Parkinson's Disease. Anal Chem. 2020 Sep 15;92(18):12347-12355.
7. Senel M, Dervisevic M, **Alhassen S**, Alachkar A, Voelcker NH. Electrochemical Micropyramid Array-Based Sensor for In Situ Monitoring of Dopamine Released from Neuroblastoma Cells. Anal Chem. 2020 Jun 2;92(11):7746-7753.

AWARDS

Henry Wood Elliott Graduate Student Award 2022

ABSTRACT OF THE DISSERTATION

Identifying a non-dopaminergic system as a target for treating Parkinson’s Disease

By

Sammy T. Alhassen

Doctor of Philosophy in Pharmacological Sciences

University of California, Irvine

Professor Amal Alachkar, Chair

In this thesis I will discuss my work on two distinct projects, one of which is the main focus of my work and this thesis, and, as reflected in the title, aims to find non-dopaminergic systems that can act as targets for treating PD. The other project investigates the impact of intergenerational trauma, specifically, how prenatal stress exposure affects the offspring in mice.

Parkinson’s disease is a neurodegenerative disease that is characterized by the degeneration of dopaminergic neurons. After sufficient degeneration has occurred, many motor and non-motor symptoms begin to appear. This study focuses on treating the motor symptoms, which include tremors, bradykinesia, rigidity and postural instability. In mice, this manifests itself as a decrease in overall locomotor activity. Currently, we cannot stop the degeneration that occurs, so the motor symptoms are usually what is treated in an attempt to improve the quality of life for the patient. Typically, Parkinson’s disease is treated with various forms of dopamine replacement therapy, most commonly through the use of levodopa (L-DOPA), which gets converted to dopamine via the enzyme dopa decarboxylase. Despite its ability to improve motor

function, after continual use, its effectiveness begins to decline and it has the very high potential of causing other motor complications such as dyskinesias. Because of this, there is a considerable need to find alternative treatments that are able to treat the motor symptoms, while not losing effectiveness or causing other complications.

We were able to characterize a bit of the promiscuity of L-DOPA as many other studies have observed a similar characteristic of L-DOPA binding to many different things in the brain. L-DOPA frequently binds to iron in the brain, but what happens to this complex is fairly unknown. We found that L-DOPA was able to form a stable complex with iron and siderocalin and in doing so, we speculate that this may be one of the reasons why L-DOPA efficacy is reduced as the amount of free L-DOPA available decreases due to forming these complexes.

In this study, we were able to induce locomotor activity in our Parkinson's disease modeled mice to much greater effect than what is currently used. After inducing the Parkinson's disease model in the mice, we treated the mice with L-DOPA and NSD1015, a central acting dopa decarboxylase inhibitor. In doing so, we are preventing the conversion of L-DOPA to dopamine. After a brief delay, we see that the animals display locomotor activity at a level significantly higher than that of animals treated with just L-DOPA which gets converted to dopamine. Not only this, but we were also able to confirm that our treatment does not involve the dopamine system as there is no dopamine at all in the animals when the locomotor activity is induced. Because of this, we are able to design a treatment around this new system and won't see the same complications that other dopamine-related treatments may have.

After performing a metabolomic study, we were able to identify different metabolites and observed how they changed after our new treatment. In doing so, we observed one metabolite experience a significant fold change vastly greater than the rest. This metabolite was ophthalmic acid and had experienced an approximated 20-fold increase in the animals treated with L-DOPA and NSD1015 compared to those just treated with L-DOPA. Very little research has been done on this tripeptide analog of glutathione and what little has been done has no links to motor function. What we found was that ophthalmic acid when administered via intraperitoneal injection showed no improvements in the animals locomotor activity, but that was because we later found that it does not cross the blood-brain barrier. After that discovery, we administered ophthalmic acid via intracerebroventricular injection and were able to induce locomotor activity in the disease modeled animals.

Although we found the non-dopaminergic compound responsible for inducing locomotor activity, we wanted to understand the mechanism of action for this compound. In this study, we identified that the target for ophthalmic acid is the calcium sensing receptor. Interestingly, many studies have shown the calcium sensing receptor to be expressed in many regions of the brain that are involved in the regulation of movement, such as the basal ganglia. Here we show that ophthalmic acid is able to bind and activate the calcium sensing receptor and is able to do so with a respectable affinity. Lastly, we were able to show that the hyperactivity induced via ophthalmic acid injection was able to be blocked using a calcium sensing receptor antagonist. That, alongside the rest of the evidence presented in this paper, prove that ophthalmic acid is able to induce locomotor activity in Parkinson's disease modeled mice through its interactions with the calcium sensing receptor. This study not only identifies some of the potential problems with L-DOPA being used as a treatment for Parkinson's disease, but also suggests the calcium sensing receptor as a potential therapeutic target as an alternative to the very problematic system that is the dopamine system.

As part of a separate study, we investigated the effects of intergenerational trauma on offspring. Stress during pregnancy has been shown many times to have negative effects on the child, such as increased lifetime susceptibility to depression and other psychiatric disorders. Despite that, whether the trauma that is passed down is a consequence of in-utero development or early mother-infant interactions isn’t well known. In our study, we are able to demonstrate that the trauma exposure during pregnancy induces social deficits and depressive-like behavior. We also show that good caregiving by normal mothers via cross-fostering was unable to reverse prenatal trauma-induced deficits. This suggests that there is a two-hit mechanism, with both in-utero abnormalities and poor parenting both playing a role in the developmental deficits. We noticed significant increases in mitochondria hypoxia marker and epigenetic modifier 2-hydroxyglutaric acid in the brains of neonates and adults exposed to prenatal stress. Bioinformatics analyses revealed long-lasting alterations in mitochondrial energy metabolism and epigenetic processes. Lastly, we were able to show that early intervention with acetyl-L-carnitine supplements produced long-lasting protection against the intergenerational trauma-induced depression.

Chapter 1:

INTRODUCTION

The main aim of this project is to search for alternative, non-dopaminergic targets for treating Parkinson’s disease. To understand why there is a need for these other possible targets, it is necessary to understand what the disease is and what areas of the brain it impacts, the pathology and etiology of the disease, and the current treatments of the disease.

Separately, I will also be discussing my study on the impact of transgenerational stress. To better understand that work, I will introduce what foundational knowledge is currently established in the field.

1.1 Parkinson’s Disease

1.1.1 Pathology

PD is a neurodegenerative disorder characterized by the progressive loss of dopaminergic neurons in the substantia nigra pars compacta and the subsequent depletion of dopamine in the striatum. Lewy bodies, intracellular inclusions composed of aggregated α-synuclein protein, are another hallmark of PD pathology. Lewy bodies are found not only in the substantia nigra, but also in other regions of the brain, including the cortex, thalamus, and brainstem. The accumulation of Lewy bodies and α-synuclein aggregates has been shown to contribute to neuronal dysfunction and death in PD [1].

In addition to Lewy bodies, other pathological changes have been observed in the brains of individuals with PD. These include mitochondrial dysfunction, oxidative stress, inflammation, and impaired protein degradation [2]. Mitochondrial dysfunction is particularly relevant to PD because dopaminergic neurons in the substantia nigra have high energy demands and are therefore vulnerable to oxidative stress caused by mitochondrial dysfunction. Oxidative stress, in turn, leads to the accumulation of reactive oxygen species and damage to cellular components such as DNA, lipids, and proteins. Chronic inflammation has also been implicated in PD pathology, as it can contribute to neurodegeneration through the release of pro-inflammatory cytokines and activation of microglia [3].

The role of protein degradation pathways in PD pathology has also been observed. The ubiquitin-proteasome system and the autophagy-lysosomal pathway are responsible for degrading misfolded or aggregated proteins in the cell. Dysfunction in either of these pathways can lead to the accumulation of toxic protein aggregates, such as α-synuclein, and contribute to neurodegeneration in PD [4].

1.1.2 Basal Ganglia

The basal ganglia consist of a collection of nuclei, including the striatum, globus pallidus, substantia nigra, and subthalamic nucleus, which are interconnected and work together to regulate motor and cognitive functions [5]. The striatum, which is the largest nucleus in the basal ganglia, is divided into two main subregions: the caudate nucleus and the putamen [6]. These two subregions receive input from different cortical areas and send output to different targets within the basal ganglia circuitry [7]

The function of the basal ganglia is complex and multifaceted, but a large body of research has implicated these structures in the regulation of movement and motor learning. The basal ganglia are thought to play a key role in the selection and initiation of voluntary movements, as well as the suppression of unwanted or inappropriate movements [8,9]. Additionally, the basal ganglia have been shown to be involved in the acquisition and consolidation of motor skills, particularly those that involve implicit or procedural learning

[10,11]. In addition to their role in motor function, the basal ganglia are also involved in a variety of cognitive processes, including reward-based learning and decision-making [12].

Any dysfunction of the basal ganglia may lead to a variety of movement disorders, such as Parkinson's disease, Huntington's disease, and dystonia. These disorders are characterized by abnormal movements, including tremors, rigidity, bradykinesia (slowness of movement), and dyskinesias (involuntary movements) [13-15].

1.1.3 Striatum

The striatum is a subcortical structure in the basal ganglia that plays a key role in motor control, reward processing, and learning. It is composed of two main regions, the dorsal striatum (caudate nucleus and putamen) and the ventral striatum (nucleus accumbens). The striatum receives inputs from cortical and thalamic regions, which are then integrated and processed by distinct populations of GABAergic projection neurons (GPNs) that give rise to the direct and indirect pathways [16].

Studies have shown that the striatum is involved in a range of behaviors, including action selection, habit formation, and reward processing. In particular, the direct pathway is thought to promote movement initiation and facilitate the selection of appropriate actions, while the indirect pathway is thought to suppress unwanted actions and promote behavioral flexibility [8].

Dopamine is a key modulator of striatal function and is essential for the proper functioning of the direct and indirect pathways. Dopamine acts on two main classes of receptors, D1 and D2, which are expressed on distinct populations of GPNs. Activation of D1 receptors promotes the activity of the direct pathway, while activation of D2 receptors promotes the activity of the indirect pathway [17-18].

1.1.4 Substantia Nigra Pars Compacta

The substantia nigra pars compacta (SNc) is a midbrain region that plays a key role in the control of voluntary movement. It is primarily composed of dopaminergic neurons, which project to the striatum and other basal ganglia nuclei. Loss of dopaminergic neurons in the SNc is a hallmark feature of PD and is associated with the motor symptoms of the disease [19].

Research has shown that the activity of dopaminergic neurons in the SNc is regulated by a complex interplay of inputs from other brain regions, including the subthalamic nucleus, globus pallidus, and striatum [20]. Additionally, the activity of SNc neurons is modulated by a range of neurotransmitters and neuromodulators, including glutamate, GABA, acetylcholine, and serotonin [21].

One key feature of SNc dopaminergic neurons is their ability to fire in a phasic, or burst-like, pattern. This pattern of firing is thought to be critical for the transmission of information to the striatum and is disrupted in PD [22]. Research has also shown that the phasic firing of SNc dopaminergic neurons is modulated by feedback from the striatum and other basal ganglia nuclei [23].

1.1.5 Substantia Nigra Pars Reticulata

The substantia nigra pars reticulata (SNr) is a major output nucleus of the basal ganglia and is involved in the regulation of movement and cognitive function. The SNr receives inputs from the striatum and globus pallidus, and it projects to several targets including the thalamus and brainstem. In addition to its role in motor control, the SNr has been implicated in the regulation of affective behavior and the modulation of pain perception [24].

The SNr has also been implicated in several neurological and psychiatric disorders. In Parkinson's disease, degeneration of dopaminergic neurons in the substantia nigra leads to a decrease in dopamine signaling in the striatum, which can lead to motor symptoms. In dystonia, a disorder characterized by involuntary muscle contractions, abnormal activity in the SNr has been observed [25]. The SNr has also been implicated in the pathophysiology of Tourette syndrome, a disorder characterized by tics and other motor and vocalizations [26].

1.1.6 Etiology

The cause of PD is fairly unknown, but appears to be multifactorial with genetic and environmental factors appearing to play key roles in its development. There is evidence that also suggests that oxidative stress and inflammation play a role in the pathogenesis of PD as well [27,28].

Mutations in several genes have been linked to familial forms of PD, including alpha-synuclein, parkin, PINK1, DJ-1, and LRRK2 [29]. These genes are involved in various cellular processes such as protein degradation, mitochondrial function, and oxidative stress response. Additionally, genome-wide association studies have identified several risk loci for sporadic PD, including SNCA, LRRK2, and GBA [30]. However, the precise mechanisms by which these genetic factors contribute to PD pathology are still not fully understood.

Environmental factors such as exposure to pesticides and heavy metals have also been implicated in the development of PD [31,32]. These toxins can induce oxidative stress and inflammation, leading to neuronal damage and degeneration. Additionally, there is growing evidence to suggest that the gut microbiome may play a role in PD, as alterations in gut microbial composition have been observed in PD patients [33].

1.1.7 Symptoms of Parkinson's Disease

PD is characterized by a range of motor and non-motor symptoms. Motor symptoms include tremors, bradykinesia or slowness of movement, rigidity, and postural instability, while non-motor symptoms include depression, anxiety, sleep disturbances, and cognitive impairment [34]. Tremors are often the first symptom and typically occur at rest, affecting the hands, arms, legs, or jaw [35]. Bradykinesia refers to a slowness of movement, which can affect simple activities such as walking, writing, and getting dressed. Rigidity, or stiffness in the limbs or trunk, can result in muscle pain or discomfort, and postural instability can lead to balance problems and falls [36].

Non-motor symptoms can occur before the onset of motor symptoms and can be more disabling than the motor symptoms themselves [37]. Depression is a common non-motor symptom of Parkinson's disease, affecting up to 50% of patients [50]. Anxiety and panic attacks can also occur, as well as sleep disturbances, including insomnia and excessive daytime sleepiness [38]. Cognitive impairment, including memory loss and difficulties with executive function, can occur in up to 50% of patients with Parkinson's disease [39]. Other non-motor symptoms include loss of sense of smell, constipation, and urinary problems [40].

1.1.8 Treatments for Parkinson's Disease

Treatment for PD includes both pharmacological and non-pharmacological interventions. Dopamine replacement therapy is the cornerstone of PD treatment, with levodopa being the most effective drug [41]. However, the long-term use of levodopa (L-DOPA) can lead to motor complications such as dyskinesias and motor fluctuations [42]

Other drugs used in the treatment of PD include dopamine agonists, such as pramipexole and ropinirole, and monoamine oxidase type B (MAO-B) inhibitors, such as selegiline and rasagiline [43]. These drugs can be used as monotherapy or in combination with levodopa to enhance its efficacy and reduce the risk of motor complications [44].

Deep brain stimulation (DBS) is a surgical treatment option for PD that involves implanting electrodes in the brain, typically in the subthalamic nucleus or globus pallidus internus. DBS has been shown to improve motor symptoms, reduce medication requirements, and improve quality of life in patients with PD [45].

Non-pharmacological interventions for PD include physical therapy, occupational therapy, and speech therapy. Exercise has been shown to improve motor symptoms and quality of life in patients with PD [46]. More recent advances in PD research have led to the development of new treatments, including gene therapy and immunotherapy. Gene therapy involves using viral vectors to deliver genes that produce dopamine to the brain. Immunotherapy aims to target the misfolded protein alpha-synuclein, which is thought to play a role in the pathogenesis of PD. In addition, there has also been interest in the potential neuroprotective effects of certain medications, such as rasagiline and safinamide, which may slow the progression of PD [47,48] Although current treatments, such as dopaminergic medications and deep brain stimulation, can improve symptoms in many patients, they do not cure the disease or slow its progression. Additionally, these treatments can have significant side effects, and some patients may not respond well to them. Therefore, there is a need for ongoing research to develop new therapies for PD, including gene therapy, stem cell therapy, and novel pharmacological approaches.

1.1.9 Siderocalin in Parkinson's Disease

Siderocalin (Scn) is a member of the lipocalin family of heterogeneous secretory proteins. It is known for its ability to bind to both bacterial and mammalian catechol siderophores. Scn has several alternative names such as lipocalin-2 (LCN2), neutrophil gelatinase-associated lipocalin, and 24p3 [49]. When Scn binds to bacterial siderophores, it forms a stable complex that prevents the bacteria from using iron, thus limiting bacterial growth [50,51]. In mammalian cells, Scn can bind to and transport iron within or across cells via catecholate siderophores [52-54].

Several studies have suggested that LCN2 may play a role in the development and progression of various diseases, including cancer, cardiovascular disease, and neurological disorders. These studies have suggested that LCN2 may promote tumor growth, metastasis, inflammation, oxidative stress, neuroinflammation, and neuronal damage, although the exact mechanisms are not fully understood. Preliminary studies believe that it may involve interactions through various signaling pathways, including the NF-κB and AKT pathways [55-57].

Studies have shown that Scn expression is increased in reactive astrocytes and microglia, indicating its potential involvement in glial activation [58-61]. Additionally, Scn upregulation has been observed in the substantia nigra of patients with Parkinson's disease (PD) and neurotoxin-treated animal models of PD. This upregulation has been proposed as a potential pathogenic mechanism of PD [62]. It may lead to disruption of the nigrostriatal dopaminergic system through neurotoxic iron accumulation and neuroinflammation, which could contribute to the progression of PD.

1.2 Animal models of Parkinson’s Disease

1.2.1 Reserpine

Reserpine is a well-known antipsychotic drug that has been widely used as an animal model for Parkinson's disease (PD) research and is known to cause dopamine depletion in the brain [63]. Reserpine causes long-lasting inhibition of the vesicular monoamine transporter, which leads to a depletion of vesicular stores of dopamine and in turn, induces PD-like symptoms in animals such as akinesia, rigidity, and tremors [64].

Reserpine-induced PD models have been used to study the underlying mechanisms of PD and to test the efficacy of potential therapeutic interventions [65]. Reserpine-induced PD models have also been used to investigate the role of various genes in the development of PD [66]. One such study used reserpine treatment to create a PD model in zebrafish and found that a mutation in the LRRK2 gene, which is associated with familial PD, increased the severity of the reserpine-induced PD phenotype [67].

Despite its usefulness as an animal model for PD research, reserpine has some limitations. Reserpine-induced PD models only mimic some aspects of PD pathology, and the pathology observed in reserpine-induced PD models may not entirely resemble the pathophysiology of human PD [68]. Furthermore, reserpine treatment can cause non-specific effects on the nervous system, making it difficult to interpret the results obtained from these models [69].

1.2.2 MPTP

MPTP (1-methyl-4-phenyl-1,2,3,6-tetrahydropyridine) is a neurotoxin that has been widely used to model PD in animal studies. MPTP is taken up into dopaminergic neurons by the dopamine transporter, where it is metabolized to MPP+ (1-methyl-4-phenylpyridinium), a potent mitochondrial toxin [70, 71].

MPTP-induced parkinsonism in humans and nonhuman primates closely resembles PD, with loss of dopaminergic neurons in the substantia nigra and the presence of Lewy body-like inclusions [72, 73]. Animal studies have provided important insights into the pathophysiology of PD and have been instrumental in the development of new treatments [74].

In mice, MPTP-induced toxicity is dose-dependent and leads to progressive neurodegeneration of dopaminergic neurons in the substantia nigra [75]. MPTP is also used in non-human primates to create a more complete and chronic model of PD, where the symptoms progress over time [76]. In addition, MPTP is used to investigate the potential of various therapies for PD, such as gene therapy, stem cell transplantation, and drug treatments [77, 78].

While MPTP is a useful tool for studying PD, it has limitations as a model of the disease. MPTP-induced parkinsonism does not fully replicate the complex neurodegenerative process of PD, which involves multiple neuronal populations and brain regions [79]. Nonetheless, MPTP remains a valuable tool for understanding the pathophysiology of PD and for evaluating potential therapeutic interventions.

2.1 Effects of Prenatal Stress

Exposure to intergenerational trauma can increase an individual's lifetime susceptibility to depression and is a significant risk factor for multiple neuropsychiatric disorders such as post-traumatic stress disorder (PTSD), autism spectrum disorder (ASD), and schizophrenia [80-83]. Major depressive disorder (MDD) affects millions of people globally, with stress being a major contributing factor in its development. While stress affects individuals worldwide, it is especially detrimental to vulnerable populations, such as pregnant women. The negative impact of stress during pregnancy is twofold, as it can affect both the mental health of the mothers and the development of the unborn offspring. Natural experiments involving human subjects provide evidence for the adverse health consequences in offspring resulting from exposure to existential and acute trauma during pregnancy, such as war and natural disasters [84-86].

It is unclear whether intergenerational trauma transmission and its negative effects result from disruptions to fetal neurodevelopment in utero or from poor maternal care by traumatized mothers. The complexity, superposition, and inseparability of prenatal and postnatal mechanisms make this ambiguity difficult to resolve. However, converging evidence from both human and animal studies supports the idea that exposure to stress during pregnancy can have negative effects on maternal behavior towards, and the care of, offspring [87-89]. Furthermore, maternal stress during pregnancy can affect offspring mental outcomes through prenatal programming, particularly through epigenetic mechanisms that cause permanent neuronal impairments and poor offspring outcomes that persist throughout life [90-92].

CHAPTER 2:

L-DOPA INDUCES LOCOMOTOR ACTIVITY IN RESERPINE-TREATED MICE IN THE ABSENCE OF DOPAMINE

ABSTRACT

L-DOPA has been recognized for its therapeutic properties in treating the motor symptoms of PD in numerous studies. However, only one study has explored the impact of blocking the enzyme responsible for converting L-DOPA to dopamine, aromatic amino acid decarboxylase, in combination with L-DOPA. The results showed a significant improvement in locomotor activity compared to the L-DOPA treatment alone. Here, we are able to replicate this phenomenon in reserpine-treated mice and investigate how varying the dosages of L-DOPA and NSD1015, the aromatic amino acid decarboxylase inhibitor, affects behavior. Interestingly, we discovered that the hyperactivity observed in the mice is not dopamine-related, as it cannot be blocked by a dopamine receptor D2 antagonist. Metabolomic data also suggests that ophthalmate or ophthalmic acid (OA) may be responsible for the observed phenomenon due to its drastic fold change increase in the hyperactive mice.

2.1 INTRODUCTION

L-DOPA, the precursor to dopamine, has been widely used for treating the motor symptoms of PD for many years. Due to the lack of dopamine in PD patients, there is a significant need for dopamine replacement therapies. Dopamine, however, itself cannot be used due to its inability to cross the blood-brain barrier. L-DOPA, its precursor, is used instead as it is able to cross the blood-brain barrier and increase dopamine levels in the brain, which in turn leads to improved motor function and reduced severity of the symptoms. In such treatment, L-DOPA is given with a peripheral dopa decarboxylase inhibitor, one that does not cross the blood-brain barrier, to prevent the conversion of L-DOPA to dopamine outside of the brain. In doing so, it is possible to ensure that a large quantity of the L-DOPA administered makes its way to the brain and is able to alleviate some of the motor symptoms in PD patients. Despite it being the gold standard when it comes to PD treatments, long-term L-DOPA usage can lead to a number of adverse effects, including dyskinesias, motor fluctuations, and psychiatric complications. Many studies have been done in an attempt to combine treatments with L-DOPA, such as with MAO-B inhibitors, in order to increase its efficacy. These combination therapies have proved successful in delaying the onset of the L-DOPA induced dyskinesias, but fail to prevent it.

One study investigating L-DOPA induced dyskinesia had looked at NSD1015, a peripheral dopa decarboxylase inhibitor, administered in combination with L-DOPA in reserpine-treated rats and had seen a delayed increase in locomotor activity that was vastly larger when compared to administering L-DOPA alone. This proved rather odd as giving both a peripheral and central acting dopa decarboxylase inhibitor ensures that L-DOPA would not be converted to dopamine anywhere in the animals, suggesting that what is inducing the locomotor activity would have to be unrelated to dopamine. That study had noticed the phenomenon and tested various antagonists and agonists to see if the hyperactivity could be blocked, but it was unable to be completely blocked by any D1, D2, or α_2 Adrenergic antagonists or a 5-HT agonist, further confirming the idea that the locomotor was induced by something unrelated to dopamine [93].

Here, we hypothesize that blocking the conversion of L-DOPA to dopamine in reserpine-treated mice will induce hyperactivity in the mice that is unrelated to the dopamine system. We report that the hyperactivity is unable to be blocked by a dopamine receptor D2 antagonist and by screening hundreds of metabolites, we found that there is little to no dopamine in the animals. We did see that there was one metabolite, ophthalmate (OA), that had a significant fold change in the hyperactive mice, making it a potential candidate for what may be responsible for the hyperactivity in the mice.

2.2 MATERIALS AND METHODS

2.2.1 Tissue Preparation for Harvesting

Adult male Swiss Webster mice, weighing approximately 20-30g, were sacrificed by asphyxiation. The brains were rapidly removed on a cold surface, frozen in isopentane at -40°C and then stored at -80°C.

2.2.2 Reserpine-treated Mouse Model of Parkinson's Disease

Adult male Swiss Webster mice were housed under controlled conditions and a 12-hr light/dark cycle. For the reserpine treatment, animals were lightly anesthetized and then injected subcutaneously with either reserpine (Sigma Aldrich) (1 mg/kg, dissolved in 1% (v/v) glacial acetic acid) or vehicle (1% (v/v) glacial acetic acid). 18 hours following the reserpine-treatment, the animals were either treated with saline or NSD1015 (20 mg/kg, Sigma) and 30 minutes after were given L-DOPA (100mg/kg, Sigma) in combination with benserazide (25 mg/kg, Sigma).

2.2.3 Animal and Treatment

Swiss Webster mice (8-10 weeks old) were obtained from Charles River Laboratories. Animals were group housed with a maximum of four animals per cage and acclimated to the vivarium for a week prior to treatments. Animals were kept in a normal 12:12 hour light/dark cycle with free access to food and water.

2.2.4 Assessment of Locomotor Activity

Mice were placed in a locomotor test chamber (40 x 40 x 38 cm^3) and the horizontal locomotor activity was monitored with a 16 x 16 photobeam array (San Diego Instruments, San Diego, CA) located 1.25 cm above the floor of the enclosure. Mice were transported to the activity chamber room at least 30 minutes prior to placement into the activity chambers. All mice were given time to acclimatize to the chamber prior to injections, and locomotor activity was recorded for 20-24 hours following drug administration. Mice were randomly distributed to each treatment group with all proper controls being run in parallel. Data was extracted first using the PAS Data Reporter software (San Diego Instruments, San Diego, CA) and the GraphPad Prism (GraphPad Software, Inc.) was used to further analyze data and produce figures.

2.2.5 Statistical Analysis

Statistical analyses of data were carried out using GraphPad Prism (GraphPad Software, Inc.). Data were presented as means ± standard error means (S.E.M.). Results were analyzed by unpaired student t-test, one-way, and two-way ANOVA followed by the appropriate post hoc comparisons, and $P < 0.05$ was considered statistically significant.

2.3 RESULTS

Reserpine treatment greatly inhibits locomotor activity in mice

After treating 8 week old Swiss Webster mice with reserpine, as described in Section 2.2.2, we were able to show that the reserpine treatment drastically reduces the locomotor activity in the mice and mimics the PD motor symptoms very well. The locomotor response seen in the saline treated group represents typical locomotor activity from the mice in a 12:12 hour light/dark cycle (Figure 2.1A). By calculating the area under the curve for the locomotor responses, we are able to quantify how much of the locomotor activity we were able to inhibit (263,403±27494 vs 26030±2978) ($P<0.0001$, Figure 2.1B).

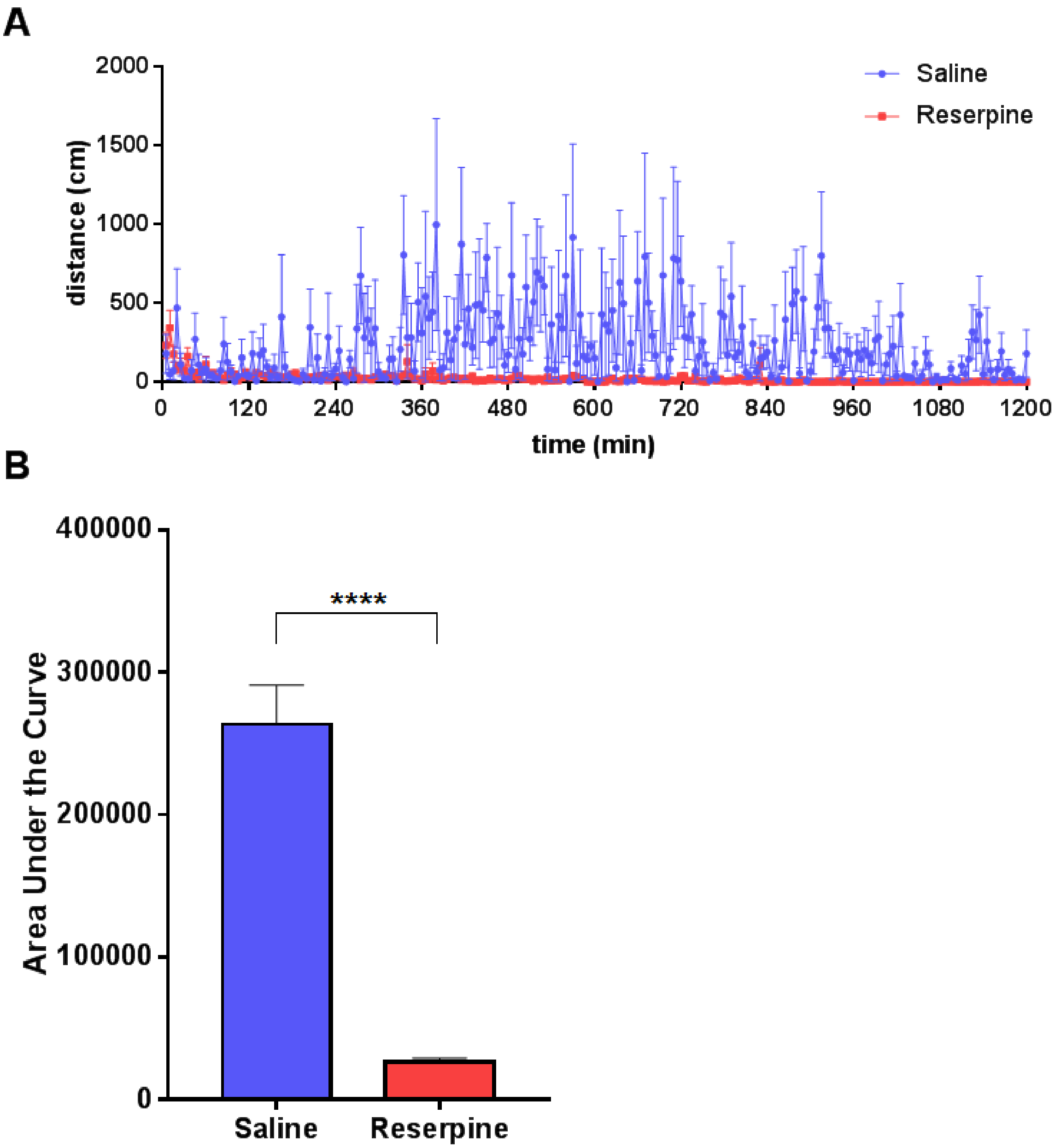

Figure 2.1. Effect of reserpine treatment on locomotor activity in mice

(A) Locomotor activity in mice after being given either saline or reserpine via subcutaneous (sq) injection and the (B) area under the curve (n = 8). Unpaired *t*-test (t = 8.583, P < 0.0001). Data are presented as means±S.E.M.

L-DOPA and NSD1015, in combination, induce hyperactivity in reserpine-treated mice

Based on the previous study investigating the cotreatment of L-DOPA and NSD1015 in rats, we hypothesized that we could induce hyperactivity in reserpine-treated mice. After treating mice with reserpine or saline, as described in Section 2.2.2, we treated mice with either saline or 20 mg/kg of NSD1015. 30 minutes later, the mice were given saline or 100 mg/kg of L-DOPA in combination with 25 mg/kg of benserazide, which on its own, has been shown previously to reverse the motor symptoms in reserpine-treated mice. In the non-reserpine treated mice, we can see that they do not display any abnormalities in their locomotor activity and behave similarly to the typical 12:12 hour light/dark cycle (Figure 2.2A). Quantitatively, the locomotor activity does not vary significantly among each of the groups with the area under the curve for each being 263403±27494, 231056±20644, 264653±21998, and 200725±19379 (saline, NSD1015, L-DOPA, and L-DOPA+NSD1015 respectively) ($P > 0.05$, Figure 2.2B). When looking at the reserpine-treated mice, however, the L-DOPA treatment was able to induce locomotor activity for a little over 4 hours and was able to bring the locomotor activity from its previous approximation of 26030±2978 to around 166238±14614. In the cotreatment of L-DOPA with NSD1015, there is a brief 3 hour delay where there is no locomotor activity, followed by a gradual increase that begins to decrease after the approximate 7 hour mark. The overall locomotor activity seems to spam an approximate 12 hours and quantitatively trumps the L-DOPA treatment by inducing almost 3 times as much locomotor activity (601576±34263 vs 166238±14614) ($P < 0.0001$, Figure 2.2C-D).

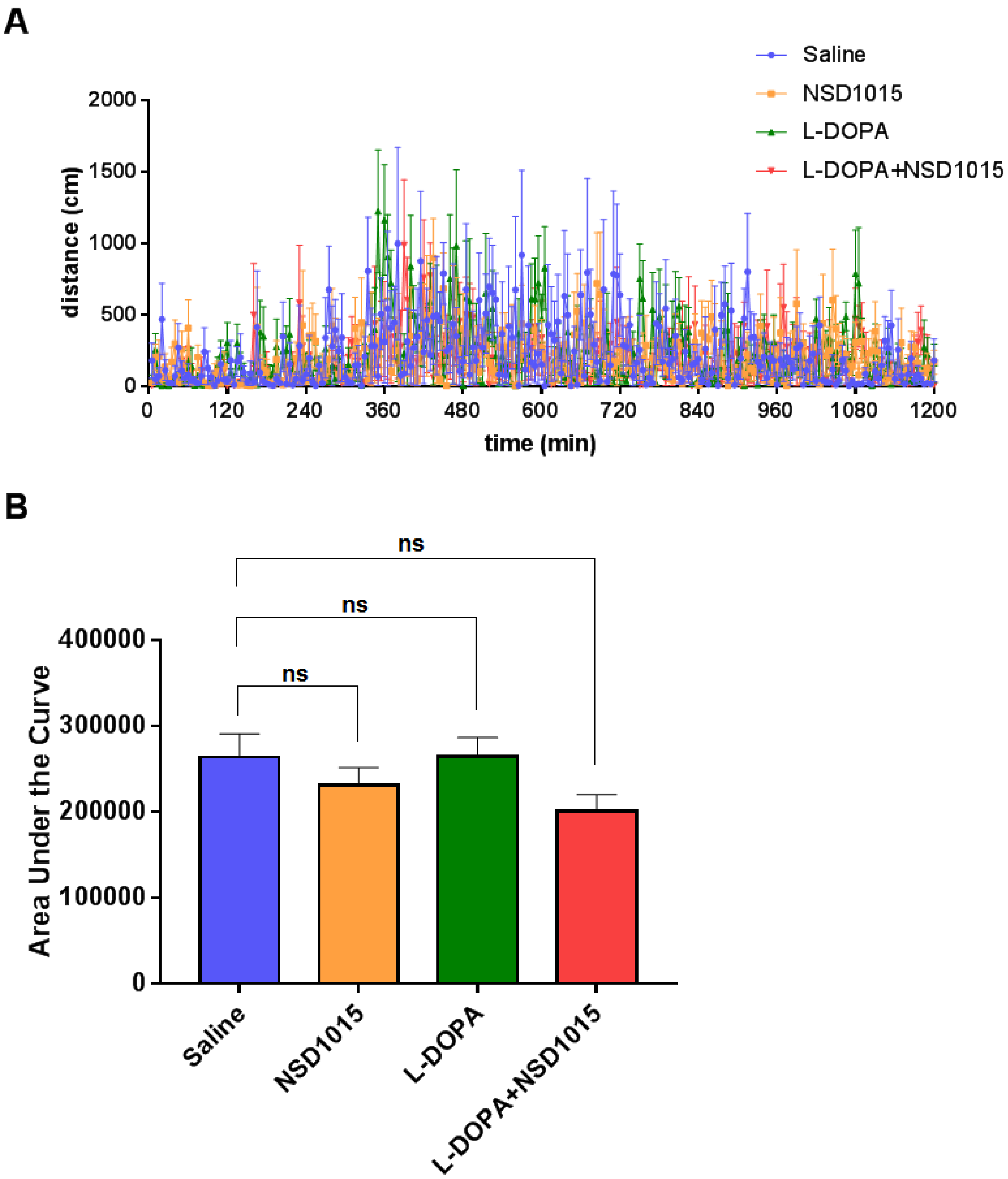
A
Saline
NSD1015
L-DOPA
L-DOPA+NSD1015
distance (cm)
2000
1500
1000
500
0
0
120
240
360
480
600
720
840
960
1080
1200
time (min)
B
Area Under the Curve
400000
300000
200000
100000
0
ns
ns
ns
Saline
NSD1015
L-DOPA
L-DOPA+NSD1015

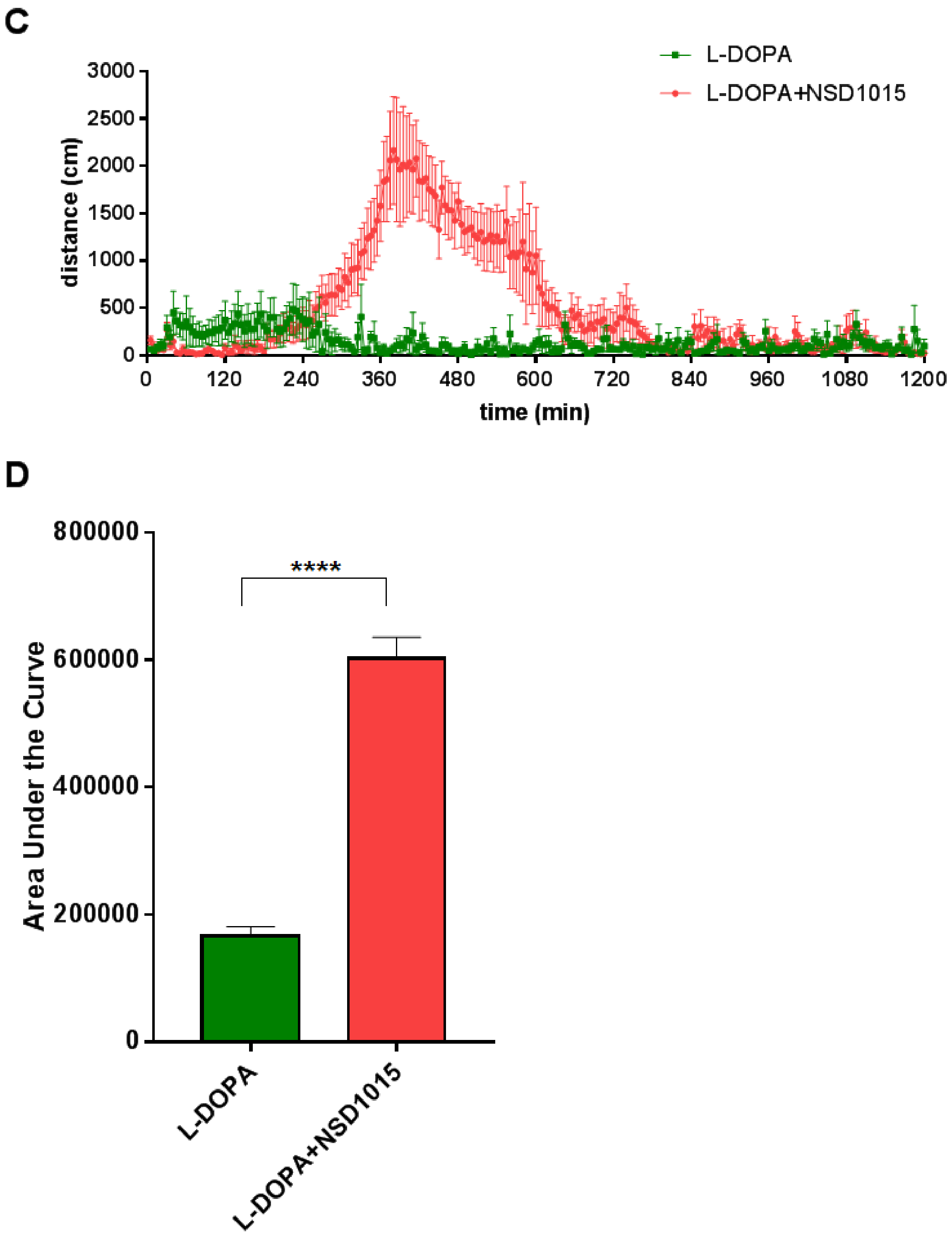

Figure 2.2 Effect of L-DOPA and NSD1015 on locomotor activity in reserpine-treated mice

(A) Locomotor activity in mice after being given saline, NSD1015, L-DOPA, or L-DOPA and NSD1015 via i.p. Injection and the (B) area under the curve (n = 8). One way ANOVA ($F_{3,28}$ = 1.814, P = 0.1675). (C) Locomotor activity in mice after being given reserpine via sq injection and then either NSD1015 or saline, followed by L-DOPA 30 minutes after and the (D) area under the curve (n = 8). Unpaired *t*-test (t = 11.69, P = 0.0388). Data are presented as means±S.E.M.

Haloperidol is unable to block the hyperactivity induced by L-DOPA and NSD1015

After treating the mice with reserpine, as described in Section 2.2.2, the mice were then treated with saline or NSD1015 and 30 minutes later were given L-DOPA with benserazide and haloperidol at 1 mg/kg, which has been shown to block the effects of L-DOPA previously. In the L-DOPA treated group with haloperidol, we see a delay in the locomotor response and a decrease in the overall locomotor activity, from 166238±14614 to 55918±6507. The L-DOPA and NSD1015 co-treatment group, however, displayed no changes in locomotor activity after given haloperidol (Figure 2.3A-B).

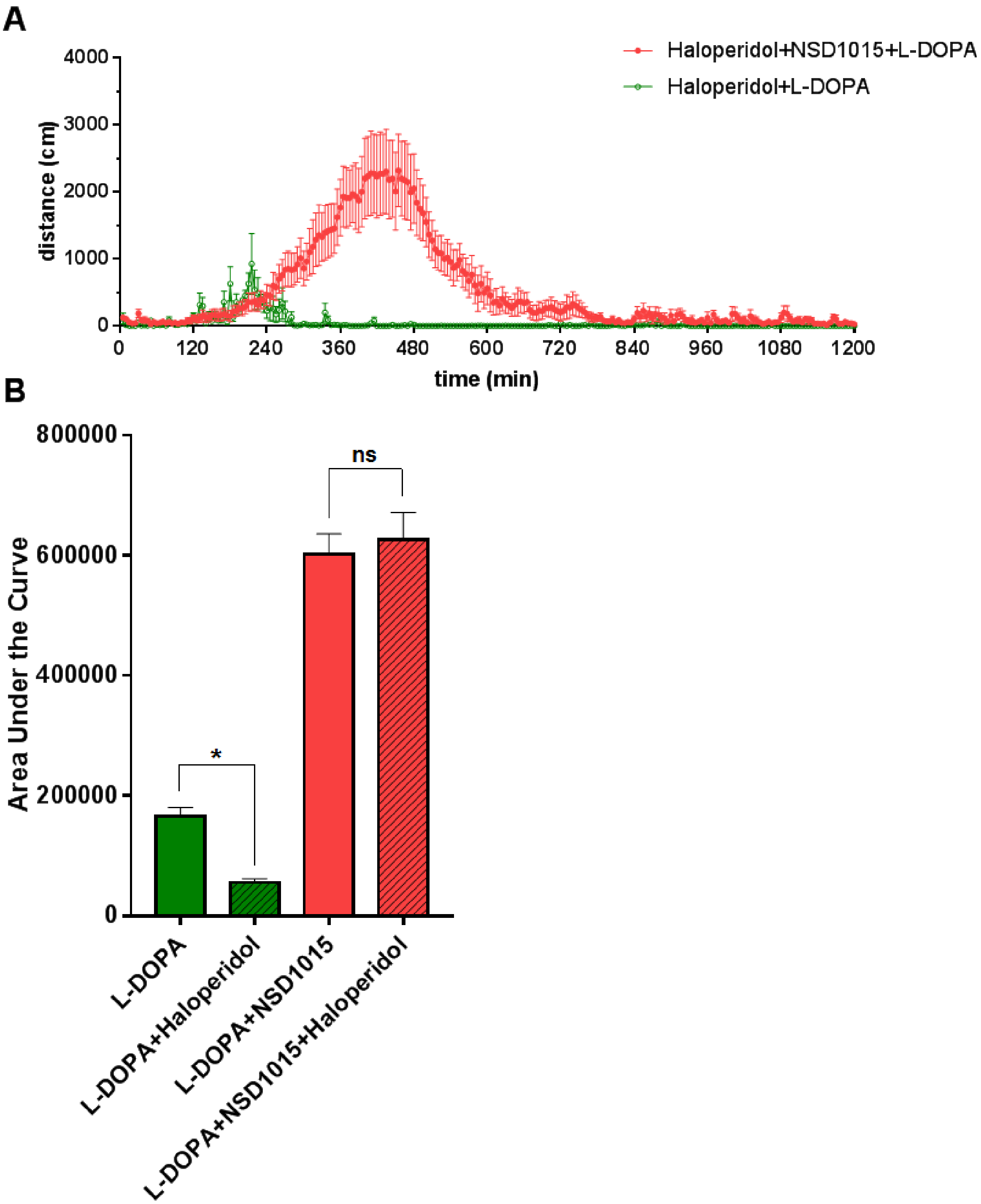

Figure 2.3 Effect of L-DOPA and NSD1015 in combination with haloperidol in reserpine-treated mice

(A) Locomotor activity in mice after being given reserpine via sq injection and then either NSD1015 or saline, followed by L-DOPA and haloperidol 30 minutes after and the (B) area under the curve (n = 8). One way ANOVA ($F_{3,28} = 100.9$, $P < 0.0001$) followed by the Tukey post hoc test, ****$P < 0.0001$, ns not significant. Data are presented as means±S.E.M.

Increasing the amount of L-DOPA in the co-treatment greatly increases the hyperactivity

After treating the mice with reserpine, as described in Section 2.2.2, the mice were then treated with varying doses of NSD1015 and L-DOPA, either half or two times the specified dose. Giving half the typical NSD1015 dose did not seem to be any different than the standard 20 mg/kg dose. Giving twice the standard dose, however, did seem to cause the locomotor activity to start quicker and the overall locomotor activity to increase (Figure 2.4A-B). Giving half the dose of L-DOPA severely decreased the locomotor activity seen in the animals compared to the typical dose, 166821±14250 vs 601576±34263, bringing the locomotor activity to a level similar to treating the animals with L-DOPA alone. Giving twice the dose of L-DOPA, however, cause the locomotor activity to start after only 2 hours and spanned approximately 14 hours at a significantly higher level than the typical dose, 1,126,037±50645 vs 601576±34263 (Figure 2.4C-D).

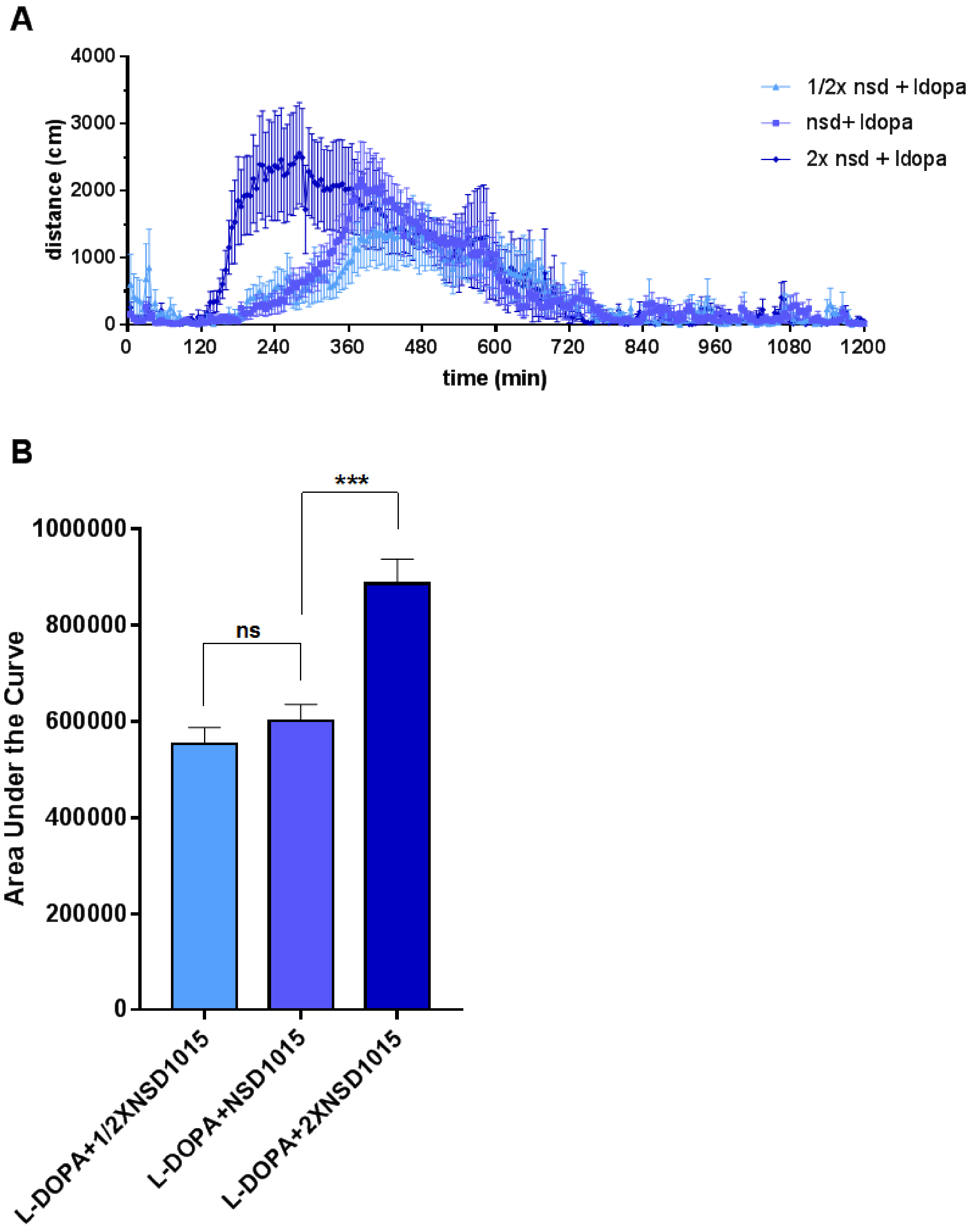
A
4000
3000
2000
1000
0
distance (cm)
0
120
240
360
480
600
720
840
960
1080
1200
time (min)
1/2x nsd + ldopa
nsd+ ldopa
2x nsd + ldopa
B
***
ns
1000000
800000
600000
400000
200000
0
Area Under the Curve
L-DOPA+1/2XNSD1015
L-DOPA+NSD1015
L-DOPA+2XNSD1015

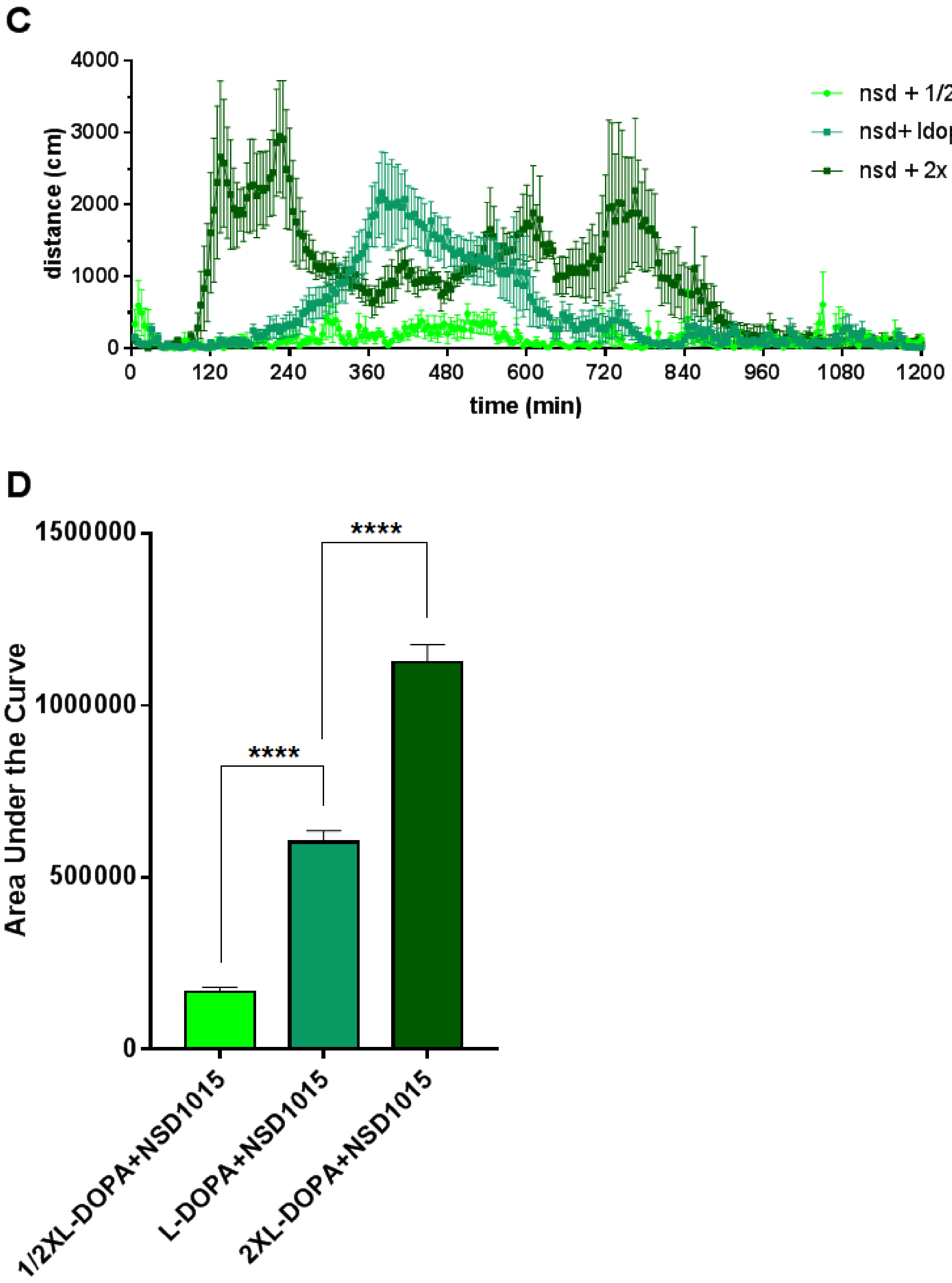

Figure 2.4 Effect of varying doses of L-DOPA and NSD1015 on locomotor activity in reserpine-treated mice

(A) Locomotor activity in mice after being given reserpine via sq injection and then either given 10, 20, or 40 mg/kg of NSD1015, followed by an L-DOPA injection 30 minutes after and the (B) area under the curve (n = 8). One way ANOVA ($F_{2,21} = 19.58$, $P < 0.0001$) followed by the Tukey post hoc test, ***$P < 0.001$, ns not significant. (C) Locomotor activity in mice after being given reserpine via sq injection and then given NSD1015, followed by either 50, 100, or 200 mg/kg of L-DOPA 30 minutes after and the (D) area under the curve (n = 8). One way ANOVA ($F_{2,21} = 175.6$, $P < 0.0001$) followed by the Tukey post hoc test, ****$P < 0.0001$, ns not significant. Data are presented as means±S.E.M.

L-DOPA and NSD1015 treatment causes elevated ophthalmic acid levels

After treating Swiss Webster mice (8 weeks old) with reserpine, as described in Section 2.2.2, the brains were harvested as described in Section 2.2.1, 2 and 7 hours after the L-DOPA injections (Figure 2.5a). The brains were then sent to Metabolon for analysis. Unsupervised principal component analysis (PCA) and hierarchical clustering analysis (HCA) was performed for the metabolites (Figure 2.5b,c). There were hundreds of significant changes between the various groups (Figure 2.5d). Here we specifically wanted to trace the amount of L-DOPA, NSD1015, and dopamine and see how these levels are changing amongst the different groups. Interestingly, there are no traces of L-DOPA or dopamine in the animals treated with L-DOPA and NSD1015 after 7 hours (Figure 2.5f). We also looked at the other metabolites downstream of dopamine and the tryptophan metabolic pathway and didn’t see changes that seemed abnormal (Figure 2.5g,h). We did, however, see a dramatic increase in the metabolite ophthalmate (ophthalmic acid, OA), as well as, other metabolite changes that were in line with the synthesis pathway of OA being upregulated (Figure 2.5i).

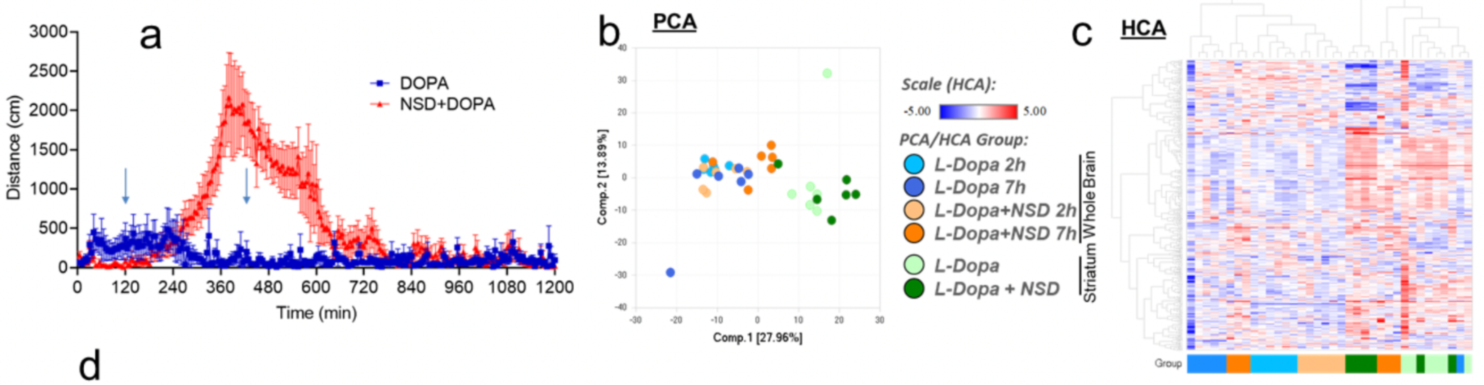

d

ANOVA Contrasts	Whole-Brain			
	L-DOPA + NSD1015 L-DOPA		7hr 2hr	
	2hr	7hr	L-DOPA	L-DOPA + NSD1015
Total biochemicals $p \leq 0.05$	54	134	87	132
Biochemicals (↑↓)	17 | 37	121 | 13	25 | 62	111 | 21
Total biochemicals $0.05 < p < 0.10$	40	65	25	51
Biochemicals (↑↓)	21 | 19	61 | 4	9 | 16	38 | 13

Statistical Comparisons

Welch's Two-Sample t-Test	Striatum 7hr
	L-DOPA + NSD1015 L-DOPA
Total biochemicals $p \leq 0.05$	93
Biochemicals (↑↓)	44 | 49
Total biochemicals $0.05 < p < 0.10$	32
Biochemicals (↑↓)	19 | 13

*From a total of **524** named and **49** unnamed biochemicals in **Whole Brain and Striatum***

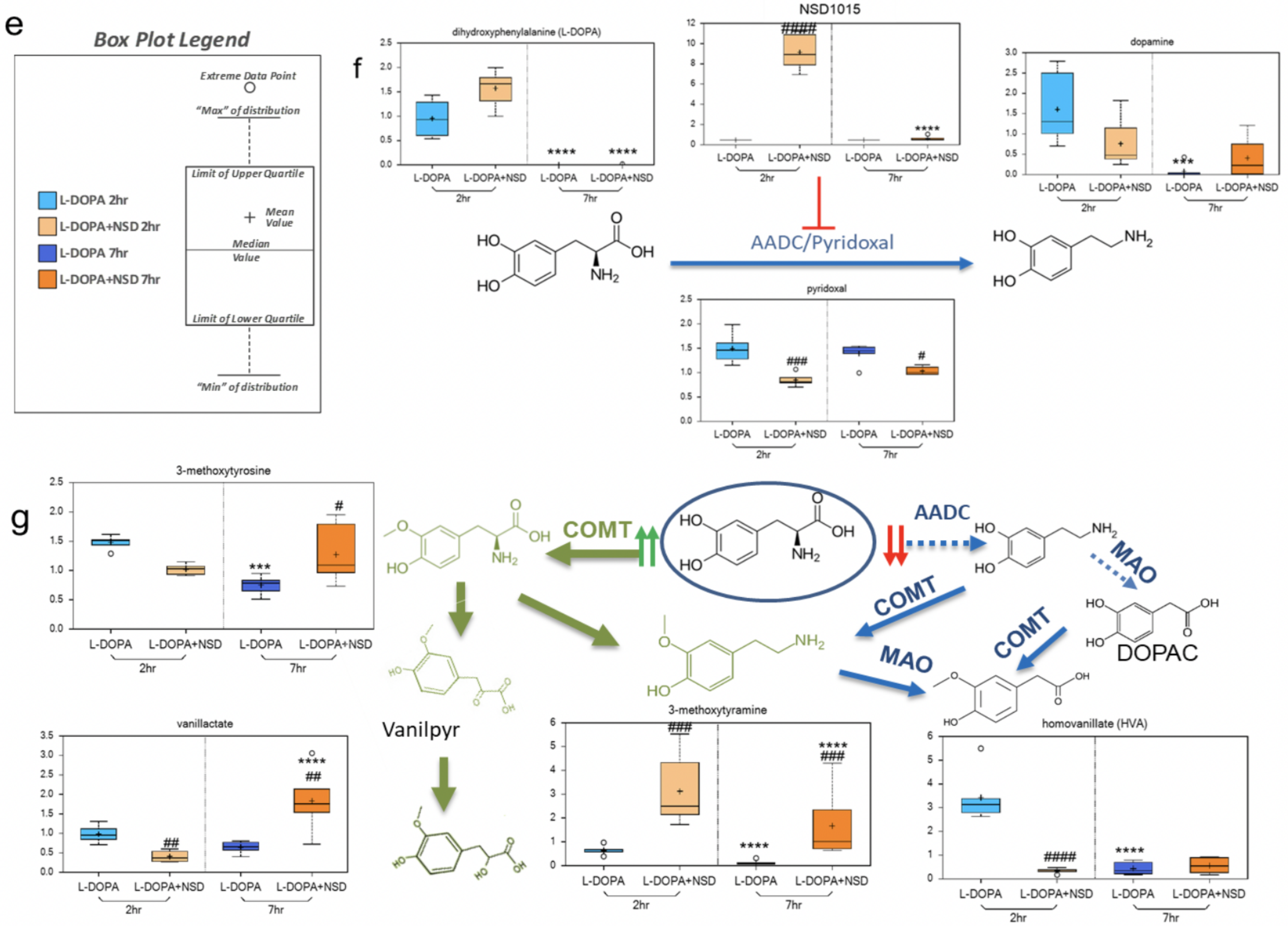

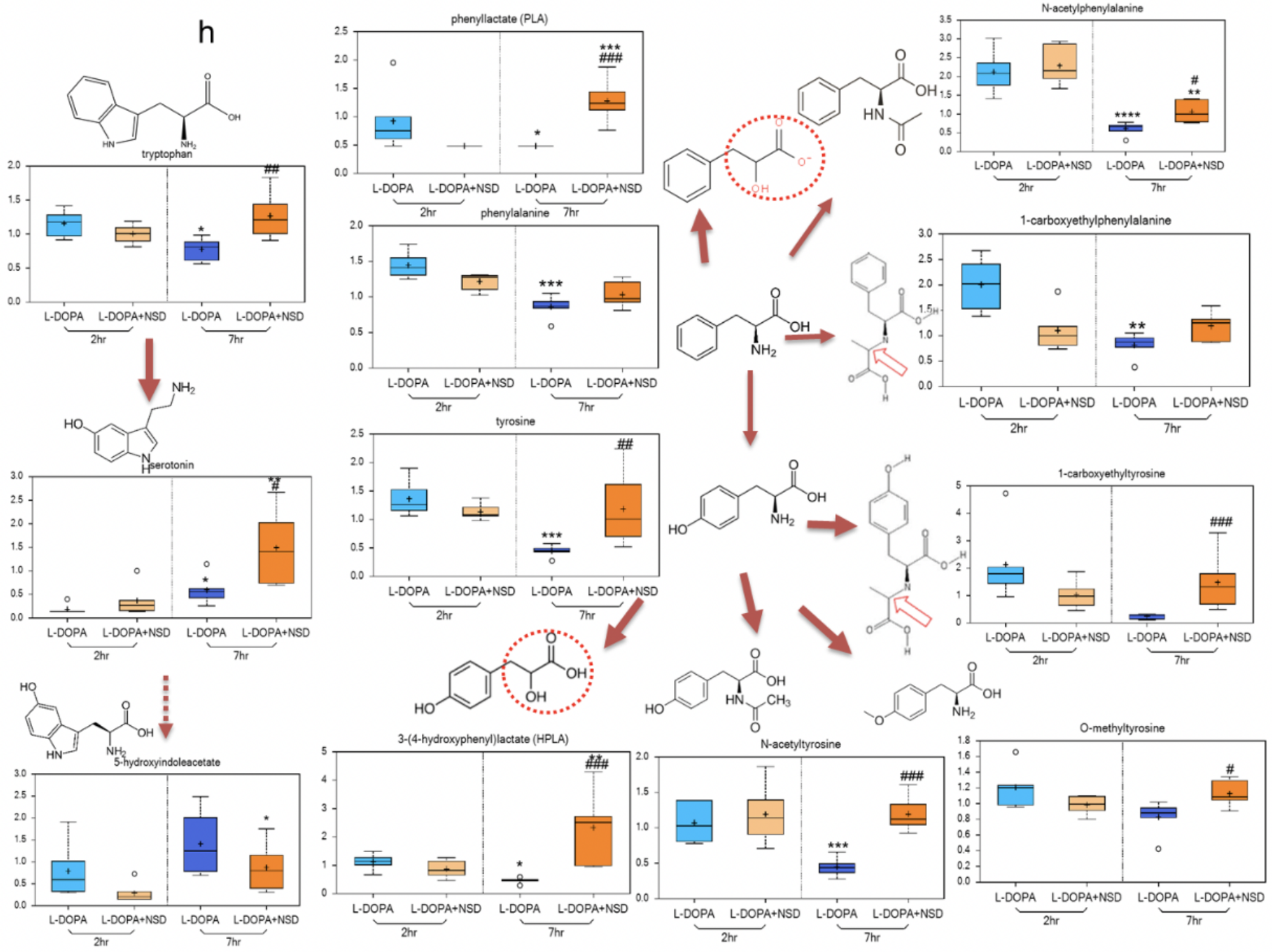
h
tryptophan
serotonin
5-hydroxyindoleacetate
phenyllactate (PLA)
phenylalanine
tyrosine
3-(4-hydroxyphenyl)lactate (HPLA)
N-acetyltyrosine
N-acetylphenylalanine
1-carboxyethylphenylalanine
1-carboxyethyltyrosine
O-methyltyrosine
L-DOPA
L-DOPA+NSD
L-DOPA
L-DOPA+NSD
2hr
7hr
*
**
***
****
#
##
###
HO
OH
NH2
HN
O
CH3

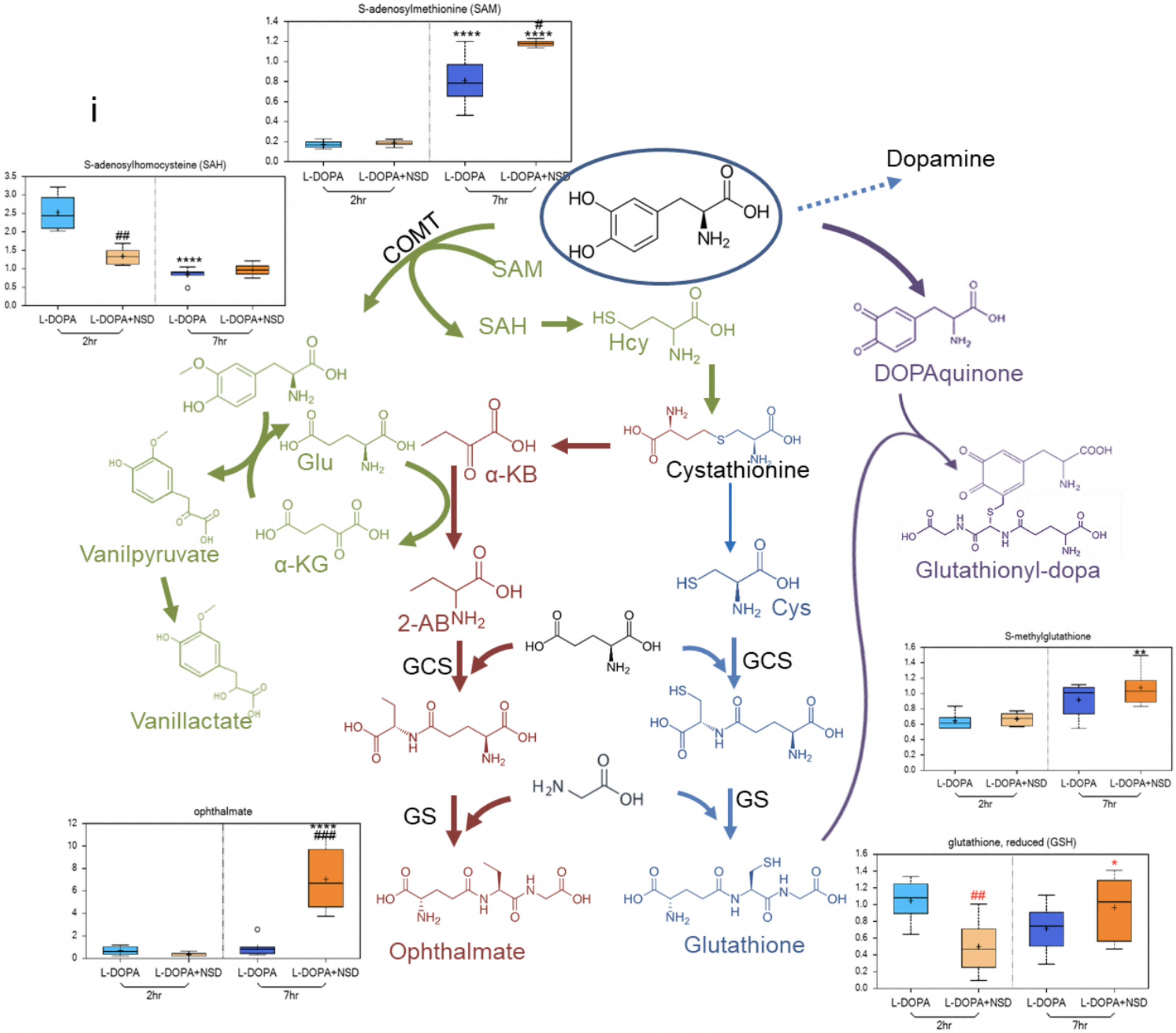

Figure 2.5 Effect of L-DOPA and NSD1015 treatment on reserpine-treated mice on various metabolites

(a) Experimental design for metabolomic study. Mice were injected (s.c.) with reserpine 1 mg/kg. After 18 hours, the mice were treated with NSD1015 or saline, followed by L-DOPA administration 30 minutes later. Brain tissues were collected from the two treatment groups at two time points (2 hours and 7 hours after L-DOPA administration). The brains were divided into two hemispheres, with one hemisphere homogenized entirely, and the other hemisphere's striatum was used to extract the striatum. (b) Unsupervised principal component analysis (PCA) of the metabolomics data of mouse brain and striatum from two treatment groups at the two time points, n=6 for each group. (c) Unsupervised hierarchical clustering analysis (HCA) of the differential metabolites of mouse brain and striatum from two treatment groups at two time points. (d) Table showing the count of altered metabolites in the (left) whole brain and (right) striatum. (e) Box plot legend showing the range, median, and quartiles. (f) The fold changes in the major components of the dopamine synthesis pathway after L-DOPA and NSD1015 administration. (g) The fold changes in the major L-DOPA metabolites that are not related to the dopamine pathway. (h) The fold changes in the major metabolites of the metabolic pathways for the aromatic amino acids: L-tryptophan, phenylalanine, and tyrosine. (i) The fold changes in ophthalmic acid and the key metabolites of the proposed pathways leading to its synthesis. The asterisk (*) is used to compare metabolite levels within the same group at the two different time points, whereas the hashtag (#) is used to compare metabolite levels between the two treatment groups at the same time point. * and # $P< 0.05$, ** and ## $P < 0.01$, *** and ### $P < 0.001$, and **** and #### $P < 0.0001$.

2.4 DISCUSSION

L-DOPA has been used in treating PD since its discovery many years ago. Despite it being the gold standard treatment, it is known to cause many motor complications as its use becomes more frequent in the patient [94]. Despite this, there has been a severe lack of research around alternatives that do not involve the dopamine system, as the system as a whole proves to be fairly complicated and difficult to maintain with treatments causing constant fluctuations in the amount of dopamine. Long-term treatment with L-DOPA and dopamine agonists can lead to motor fluctuations and dyskinesias due to the fluctuations in dopamine release [95]. So although L-DOPA and dopamine-related treatments are effective in treating the motor symptoms of Parkinson’s disease, they can be associated with a range of complications and limitations that may make them unsuitable for some patients and very poor long term solutions. Because of this, there is a significant demand for an alternative druggable system.

In the present study, when pretreating the mice with NSD1015 30 minutes prior to L-DOPA administration, there is a delay in locomotor activity of approximately 4 hours. This delay is then followed up by a dramatic increase in locomotor activity, an amount that greatly exceeds that of giving L-DOPA alone (Figure 2.3). The delay suggests that as long as NSD1015 is present, central dopa decarboxylase is actively being inhibited and preventing the enzymatic conversion of L-DOPA to dopamine, thus preventing any locomotor increases. However, after approximately 120 minutes, there is a gradual increase in locomotor activity over the next few hours that dramatically surpasses that of administering L-DOPA alone (Figure 2.3). If what is being seen is the effect of NSD1015 waning and L-DOPA is able to be converted to dopamine and exert its effect that way, then it would be assumed to have locomotor behavior similar to that of it being given in the absence of NSD1015 (Figure 2.2). This, however, is not the case and suggests that there must be an alternative mechanism at play.

As shown in this chapter, altering the dosing of L-DOPA or NSD1015 could have an effect on the locomotor response in the animals. When looking at altering the dosing of NSD1015, it becomes apparent that the dose of NSD1015 isn't necessarily important. What is important though, is that there is a minimum amount required to prevent the conversion of L-DOPA to dopamine. Although there is an increase in locomotor activity when using the higher dose of NSD1015, it may be by proxy of NSD1015 also acting as a peripheral dopa decarboxylase inhibitor, and thus you allow more L-DOPA to make its way to the brain (Figure 2.4A-B). That is important because it appears as though what is important in scaling the hyperactivity in the animals is related to how much L-DOPA makes its way to the brain. This is more evident when altering the doses of L-DOPA, which seem to follow in a more dose-dependent manner. When you lower the dose of L-DOPA by half, you see that there is a significant decrease in the locomotor activity, mainly due to the fact that you have less L-DOPA in the brain. On the contrary, when you have an increased dose of L-DOPA in the brain, you see a massive increase in the locomotor activity (Figure 2.4C-D), all of which suggests that L-DOPA plays a critical role after it has been accumulated in the brain.

The metabolomic data easily confirms that there is no dopamine in the animals at the peak of the locomotor activity, proving our hypothesis to be true that the hyperactivity seen in the animals is not due to dopamine. Interestingly, it also shows that there is no L-DOPA in the animals as well. This suggests two possibilities. The first is that L-DOPA is being converted to something and that is either directly, or indirectly, causing the increase in locomotor activity. The second possibility is that it may be binding to something, making us unable to detect it as

L-DOPA. There were also no significant changes in tyrosine metabolism further confirming that the dopamine system is uninvolved in the hyperactivity seen in the animals.There was however, significant fold changes in

Chapter 3:

SURFACE PLASMON RESONANCE IDENTIFIES HIGH-AFFINITY BINDING OF L-DOPA TO SIDEROCALIN/LIPOCALIN-2 THROUGH IRON-SIDEROPHORE ACTION: IMPLICATIONS FOR PARKINSON’S DISEASE TREATMENT

ACS Chem Neurosci. **Alhassen S**, Senel M, Alachkar A. Surface Plasmon Resonance Identifies High-Affinity Binding of l-DOPA to Siderocalin/Lipocalin-2 through Iron-Siderophore Action: Implications for Parkinson's Disease Treatment. ACS Chem Neurosci. 2022 Jan 5;13(1):158-165.

ABSTRACT

L-3,4-Dihydroxyphenylalanine (L-DOPA), the dopamine precursor, remains the frontline treatment for PD. With the treatment progress, L-DOPA efficacy decreases, necessitating higher and more frequent doses, with higher risks of dyskinesia. L-DOPA chelates iron through its catechol group, forming the L-DOPA:Fe complex; however, the fate of this complex is unknown. Catechol siderophore-like compounds are known to bind siderocalin (Scn)/lipocalin-2 to form stable siderophore:Fe:Scn complexes. Scn is upregulated in PD patients' substantia nigra and may play a role in PD pathophysiology. Therefore, in this study, we used the surface plasmon resonance (SPR) technique to examine the binding properties of L-DOPA to Scn. We found that L-DOPA formed a stable complex with Scn in the presence of Fe^{3+}. Our analysis of the binding properties of L-DOPA precursors and metabolites indicates that the catechol group is necessary but not sufficient to form a stable complex with Scn. Finally, the affinity constant (K_d) of DOPA:Fe^{3+}binding with Scn (0.8 μM) was lower than L-DOPA plasma peak concentrations in L-DOPA preparations in the past six decades. Our results speculate a significant role for the L-DOPA-Scn complex in the decreased bioavailability of L-DOPA with the progress of PD.

3.1 INTRODUCTION

Pharmacological strategies for treating Parkinson's disease (PD) depend mainly on replacing lost dopamine (DA) due to the degeneration of dopamine neurons in the substantia nigra compacta. Six decades after its initial use, l-3,4-dihydroxyphenylalanine (L-DOPA), the dopamine precursor, remains the gold standard frontline treatment for PD motor symptoms. L-DOPA can readily cross the blood-brain barrier (BBB) and is converted to dopamine by aromatic amino acid decarboxylase (AADC), presumably in the striatum [96]. The efficacy of L-DOPA as a treatment is increased when used in combination with peripheral decarboxylase inhibitors (e.g., benserazide and carbidopa), which prevent the formation of BBB-impermeable DA outside the central nervous system (CNS). This combination has been used to reduce the required doses of L-DOPA and to prevent systemic side effects such as nausea. While initially, L-DOPA successfully reverses parkinsonian symptoms, as the treatment progresses, its effectiveness decreases, and dyskinesia, fluctuations in mobility, and freezing episodes occur [97,98]. Paradoxically, the exact L-DOPA therapy that has improved the quality of life of tens of thousands of PD patients is the one that contributes to the rapid decline in quality of life as the treatment progresses [99,100].

With the treatment progress, the dose of L-DOPA required to induce dyskinesia gradually decreases, whereas the dose of L-DOPA required to alleviate parkinsonian symptoms increases, resulting in a narrow therapeutic window [101]. Further, L-DOPA has been proposed to accelerate disease progression through neurotoxic mechanisms that are not very well understood. L-DOPA toxicity might be related to its potentiation of oxidative stress by increasing the available DA pool for Fe-catalyzed oxidation to form neurotoxic DA quinones [102-107]. In addition, L-DOPA itself seems to act as a siderophore because it chelates iron with high affinity through its catechol group, forming the L-DOPA:Fe complex [103,108]. Thus, while peripheral AADC inhibition increases L-DOPA available for the brain, it also increases the peripheral L-DOPA pool available to chelate iron in the blood and peripheral organs.

Further, AADC activity and expression are known to decrease in the SNc, caudate, and putamen of PD patients, [109,110] increasing the amount of L-DOPA that binds Fe. Fe has multiple well-established roles in normal DA metabolism and neurotoxic oxidation [103,111,112]. Reports have shown that increasing brain Fe accumulation via early-life dietary overexposure is sufficient to induce age-related nigrostriatal damage and parkinsonism, evidenced by a specific loss of TH-positive neurons, increased oxidative stress, and locomotor deficits [113,114]. The fate of DOPA:Fe is unknown, although some reports provided evidence for incorporating DOPA:Fe into neuromelanin and synuclein [115-120]. Whether the DOPA:Fe complex binds to or interacts with other proteins is not known.

Siderocalin (Scn), a member of the heterogeneous secretory protein family of lipocalins, is known for its interaction with bacterial and mammalian catechol siderophores. Scn, also known as lipocalin-2 (Lcn2), neutrophil gelatinase-associated lipocalin, and 24p3, [121] forms a stable complex with bacterial siderophores, thus sequestering iron and preventing its use by bacteria, which limits bacterial growth [122,123]. In mammalian cells, Scn can bind to and use catecholate siderophores to shuttle iron within or across cells [124-126] Scn has been implicated in glial activation, and its expression is increased in reactive astrocytes and microglia [127-130]. Scn upregulation was found in the substantia nigra of patients with PD and neurotoxin-treated animal models of PD [131]. The upregulation of Scn has been suggested as a potential pathogenic mechanism of PD, resulting in disruption of the nigrostriatal dopaminergic system through neurotoxic iron accumulation and neuroinflammation [131]. Whether L-DOPA binds to Scn directly or through its siderophore action has not been examined. Therefore, the current study aims to examine the binding properties of L-DOPA to Scn in the presence and absence of iron cations, using surface plasmon resonance (SPR) analysis.

3.2 MATERIALS AND METHODS

3.2.1 Chemicals

The following chemicals used in the experiments were purchased from Sigma-Aldrich: iron(III) chloride, iron(II) sulfate heptahydrate, calcium chloride, copper(I) chloride, zinc chloride, magnesium chloride, 3,4-dihydroxy-l-phenylalanine (L-DOPA), L-DOPA methyl ester, 3,4-dihydroxyphenethylamine (dopamine), l-tyrosine, 3,4-dihydroxyphenylacetic acid (DOPAC), and 3-methoxytyramine (3-MT).

3.2.2 Immobilization of Scn

The binding properties of L-DOPA and other compounds to Scn were analyzed using surface plasmon resonance (SPR) (Biacore 3000 Instrument, GE Healthcare, Sweden) as described previously with some modifications [132]. We used the CM5 chip (GE Healthcare, Sweden), a standard general-purpose chip that allows for binding to the surface due to the matrix of carboxymethylated dextran covalently attached to the gold surface. Prior to the immobilization, the surface of the CM5 chip was activated with freshly prepared 1-ethyl-3-(3-dimethylaminopropyl) carbodiimide hydrochloride (EDC, 0.4 M) and *N*-hydroxysuccinimide (NHS, 0.1 M). An EDC/NHS 1:1 mixture was run over the sensor chip for 10 min, followed by 50 µg/mL of the recombinant Scn protein (R&D systems #1757-LC-050) in HBS-EP buffer (GE Healthcare, Sweden) at pH 7.4 for 30 min. After the protein immobilization, ethanolamine (1 M, pH 8.5) was added to quench unreacted carboxyl groups.

3.2.3 SPR Experimental Design

To monitor the binding to immobilized Scn, all procedures were standardized and implemented to create repetitive sample injections (10 µL injections at a flow rate of 5 µL/min).

The surface was regenerated using NaOH (50 mM), recommended by instructional guidelines. All analytes were dissolved in the running buffer (50 μM), and their bindings to Scn were quantified and represented as the difference between the response units (RUs) after sample injection and the baseline before sample injection (ΔRU).

L-DOPA (and its metabolites) and Fe^{3+} or Fe^{2+} and other cations were added in three different orders of injection: (1) L-DOPA followed by the cation, (2) the cation followed by L-DOPA, and (3) the L-DOPA/cation mixture. Cations tested included calcium (Ca), copper (Cu), zinc (Zn), and magnesium (Mg). In addition, the bindings of L-DOPA precursors (tyrosine and L-DOPA methyl ester) and metabolites (dopamine, 3-MT, and DOPAC) to Scn in the presence of Fe^{3+} were examined similar to that of L-DOPA.

GraphPad was used to perform statistical analyses. One-way ANOVA followed by the Tukey post hoc test was used to analyze ΔRU in different conditions.

To identify the affinity of the binding between Scn, Fe^{3+}, and L-DOPA, Scn was immobilized onto the surface, and a mixture of Fe^{3+} and L-DOPA, at varying concentrations of L-DOPA (0.1-50 μM) and a fixed concentration of Fe^{3+} (50 μM), was allowed to run through the channel. The specific binding was quantified by ΔRU. The binding data were fitted into nonlinear regression one site binding using GraphPad prism, and the dissociation constant (K_d) was calculated (in μM) using eq 1 where B_{max} is the maximum specific binding.

$$\text{binding} = \frac{B_{\text{max}} \times [\text{L} - \text{DOPA}]}{K_{\text{d}} + [\text{L} - \text{DOPA}]}$$

3.3 RESULTS AND DISCUSSION

In this study, we report for the first time that L-DOPA can bind to Scn through acting as an Fe^{3+} siderophore. Using the SPR technology, we investigated the interactions in real time between Scn and L-DOPA. We show that this interaction occurs through chelating Fe^{3+} but not Fe^{2+}. We also demonstrate that the catechol structure in L-DOPA is essential but not sufficient for binding.

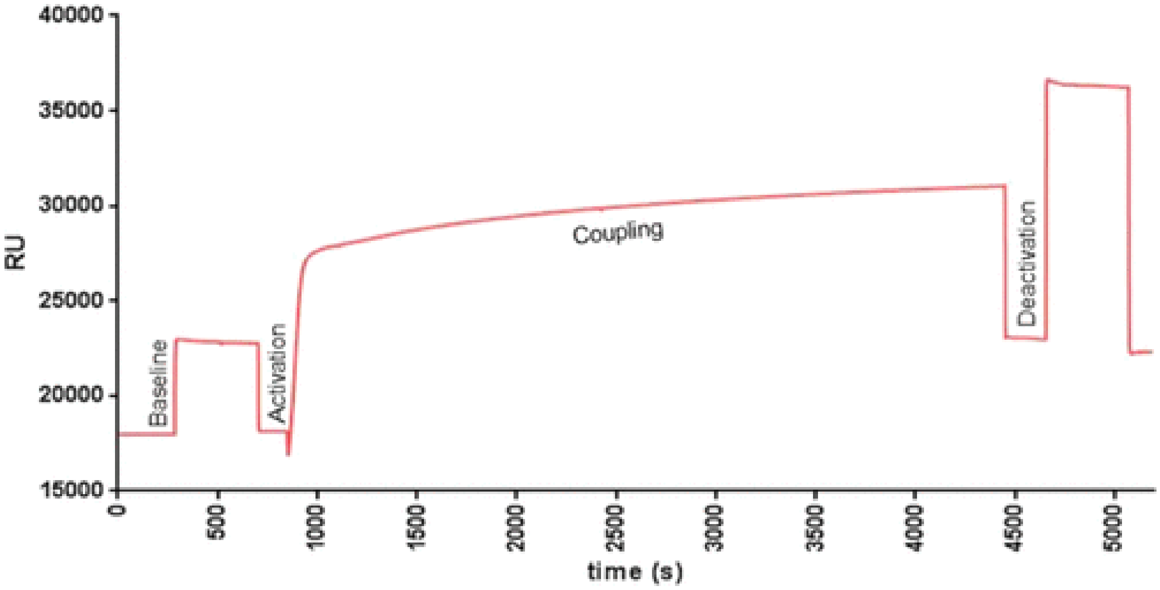

Figure 3.1. Sensorgram showing the immobilization of recombinant Scn on a CM5 chip (Biacore)

The surface of the CM5 chip was activated with EDC and NHS (0-840 s), followed by an injection of recombinant Scn (841-4450 s). Lastly, an injection of ethanolamine (4451-5200 s) was performed to block the remaining active sites.

L-DOPA Interaction with Scn is Fe^{3+}-Dependent

Most known Scn-bound siderophores contain catechol moieties in their structures. Examples of Scn-bound siderophores are bacterial enterochelin, bacillibactin, and carboxymycobactins. Mammalian catechols such as catechol, 3-methylcatechol, 4-methylcatechol, and pyrogallol were also found to act as siderophores that form ternary Scn:catechols:Fe complexes.

L-DOPA contains catechol groups in its structure and is known for its Fe-chelating properties [101,106]. Therefore, it is reasonable to speculate that L-DOPA may act as a siderophore that forms a ternary DOPA:Fe:Scn complex. To test this hypothesis, we first verified whether Fe^{3+} and/or Fe^{2+} bind to Scn. We found that the ΔRU value of the binding of Fe^{3+} to Scn was approximately 16, whereas Fe^{2+} displayed a ΔRU of approximately 5 (basal ΔRU values for buffer are around 1). We then characterized the binding of L-DOPA to Scn in the absence and presence of metal ions. We found that in the absence of any ion, the SPR response to L-DOPA-Scn binding was trivial (ΔRU ~ 2), indicating a very low interaction between L-DOPA and Scn (Figure 2A-C).

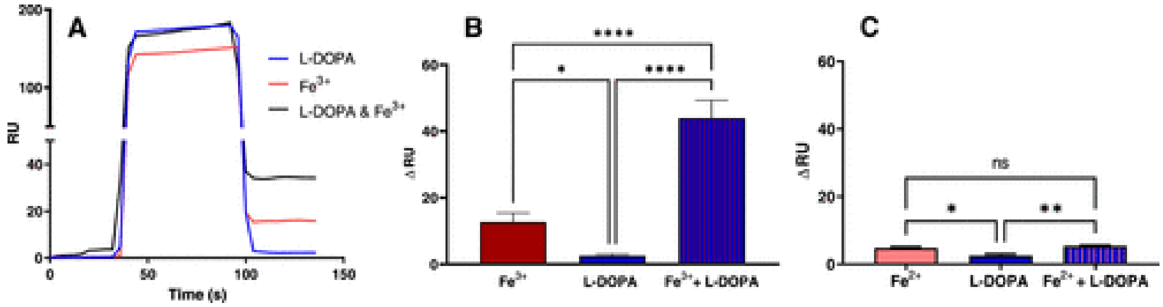

Figure 3.2. SPR sensor responses to Scn interactions with Fe^{3+}, Fe^{2+}, and L-DOPA

(A) Sensorgram reading for the injection of Fe^{3+} and L-DOPA separately and in a mixture (0-135 s) on a CM5 chip with recombinant Scn immobilized on the surface. (B) Bar plot of the reflectivity change for Scn and Fe^{3+} and L-DOPA separately and in the mixture. After recombinant Scn was immobilized on the CM5 chip, L-DOPA, Fe^{3+}, or a mixture of Fe^{3+} and L-DOPA was injected, and the response was measured. The response was measured as the difference between the baseline prior to injection and after the injection by one-way analysis of variance (ANOVA) followed by the Tukey post hoc test ($F = 35.73$, $P < 0.0001$). (C) Bar plot of the reflectivity change for Scn and Fe^{2+} and L-DOPA separately and in the mixture. After recombinant Scn was immobilized on the CM5 chip, L-DOPA, Fe^{2+}, or a mixture of Fe^{2+} and L-DOPA was injected, and the response was measured by one-way ANOVA followed by the Tukey post hoc test ($F = 4.79$, $P = 0.0093$). The response was measured as the difference between the baseline prior to injection and after the injection. *$P < 0.05$, **$P < 0.01$, ****$P < 0.0001$.

However, when Fe cations and L-DOPA were run as mixtures, the L-DOPA:Fe^{3+} mixture displayed a higher SPR response (ΔRU = 44) than L-DOPA and Fe^{3+} when administered separately ($P < 0.0001$, Figure 2A-C). The SPR response to L-DOPA:Fe^{2+} was relatively very low (ΔRU = 5) and not different from that of Fe^{2+} alone ($P > 0.05$, Figure 2A-C).

Since L-DOPA binds other metal cations (M) such as calcium (Ca), copper (Cu), zinc (Zn), and magnesium (Mg), we asked whether DOPA:M complexes interact with Scn. Different metal cations were tested for their capacity to interact with Scn individually and with L-DOPA. When tested separately, none of the metal cations other than Fe^{3+} displayed any interaction with Scn; ΔRU for Fe^{3+} was 14 compared to around 1 for the other metal ions. These metal cations were then tested in the presence of L-DOPA, either with the metal cation being injected onto the surface first, followed by L-DOPA, or L-DOPA being injected onto the surface first, followed by the metal. In both cases, all metal ions other than Fe^{3+} displayed low to no interaction with Scn, reflected by the very low ΔRU values (around 1). ΔRU values for the interactions with Scn were significantly higher for L-DOPA injected after or before Fe^{3+} compared with any other metals ($P < 0.05$, Figure 3A-D). Similarly, Fe^{3+} in a mixture with L-DOPA still showed the highest level of interaction with Scn (ΔRU = 44; Figure 3E,F).

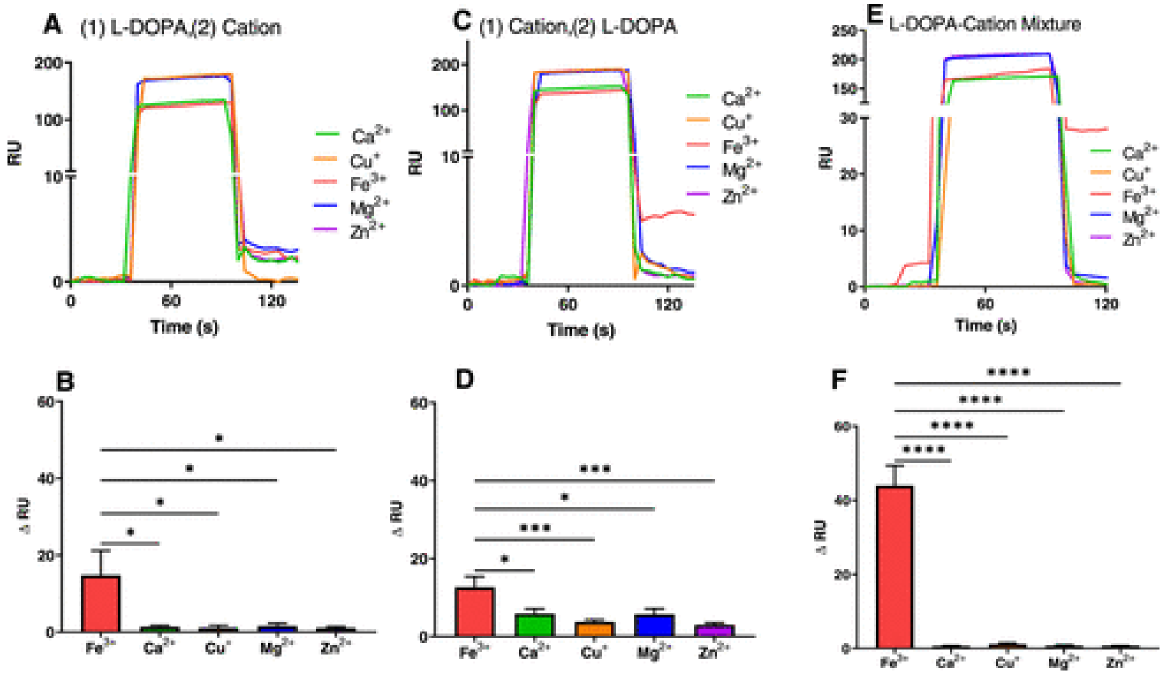

Figure 3.3. SPR sensor responses to Scn interactions with different cations and L-DOPA

SPR analyses were conducted on a CM5 chip with immobilized recombinant Scn on its surface. (A) Sensorgram reading for the injection of L-DOPA, followed by the injection of different cations (0-135 s). (B) Bar plot of the reflectivity change for Scn, L-DOPA, and different cations. L-DOPA was injected, followed by different cations, and the response was measured by one-way ANOVA followed by the Tukey post hoc test ($F = 4.318$, $P = 0.016$). (C) Sensorgram reading for the injection of a mixture of L-DOPA with different cations (0-135 s). (D) Bar plot of the reflectivity change for Scn, different cations, and L-DOPA. Cations were injected, followed by L-DOPA, and the response was then measured by one-way ANOVA followed by the Tukey post hoc test ($F = 6.262$, $P = 0.0002$). (E) Sensorgram reading for the injection of a mixture of L-DOPA with different cations (0-135 s). (F) Bar plot of the reflectivity change for Scn and a mixture of L-DOPA and different cations. A mixture of L-DOPA and different cations was injected, and the response was measured. The responses in (B), (D), and (F) were measured as the difference between the baseline prior to injection and after the injection (ΔRU). $^{*}P < 0.05$, $^{**}P < 0.01$, $^{***}P < 0.001$, and $^{****}P < 0.0001$. Data represent mean ± standard error mean (SEM) of at least three experiments and five replicates in each experiment.

Altogether, these results demonstrate that L-DOPA itself does not bind to Scn in the absence of Fe. Furthermore, the results reveal that the interaction between L-DOPA and Scn is Fe^{3+}-dependent, as combinations of L-DOPA with Fe^{2+} did not lead to any interaction with Scn. However, our results also indicate that the binding capacity of Fe^{3+} with Scn in the absence of L-DOPA is lower than the preformed L-DOPA:Fe^{3+} complex.

Catechol Group Is Necessary But Not Sufficient for the Binding to Scn

Since some L-DOPA metabolites such as dopamine and 3,4-dihydroxyphenylacetic acid (DOPAC) contain catechol moieties, we asked whether these catecholamines act as siderophores and bind to Scn.

To answer this question and determine the key structural components of L-DOPA that facilitated the binding to Fe^{3+} and Scn, different L-DOPA precursors and metabolites were tested in mixtures containing Fe^{3+}. Of these metabolites, those containing catechols in their structures showed an interaction with Fe^{3+} and Scn with variable levels of ΔRU (Figure 4). Thus, mixtures of Fe^{3+} with dopamine, which lacks the L-DOPA carboxyl moiety, showed some degree of interaction with Scn, though to a lesser degree than L-DOPA (ΔRU = 11, $P < 0.05$ compared to ΔRU of L-DOPA binding, Figure 4). Tyrosine, a non-catechol L-DOPA precursor, exhibited a significantly lower SPR response than L-DOPA (ΔRU = 4, Figure 4). Similarly, the metabolite 3-methoxytyramine (3-MT), in which one hydroxyl of the catechol group is methylated, showed no interaction with Scn in the presence of Fe^{3+} (ΔRU < 1, Figure 4). These results suggest that the catechol structure is necessary for the interaction to occur. However, DOPAC, an oxidation metabolite of dopamine that results from oxidative deamination of dopamine, showed low interaction with Scn upon combining it with Fe^{3+}, albeit its structure contains a catechol moiety (ΔRU = 2, Figure 4). On the other hand, L-DOPA methyl ester, in which the carboxyl group is substituted with the methyl ester group, was able to form a complex with Fe^{3+} and bound Scn (ΔRU around 24). These results indicate that the binding properties of L-DOPA and its metabolites to Scn are related to specific structural features, including the catechol, amino, and carboxyl moieties. Based on these findings, it can be concluded that the catechol moiety is necessary but not sufficient for complexation with Scn.

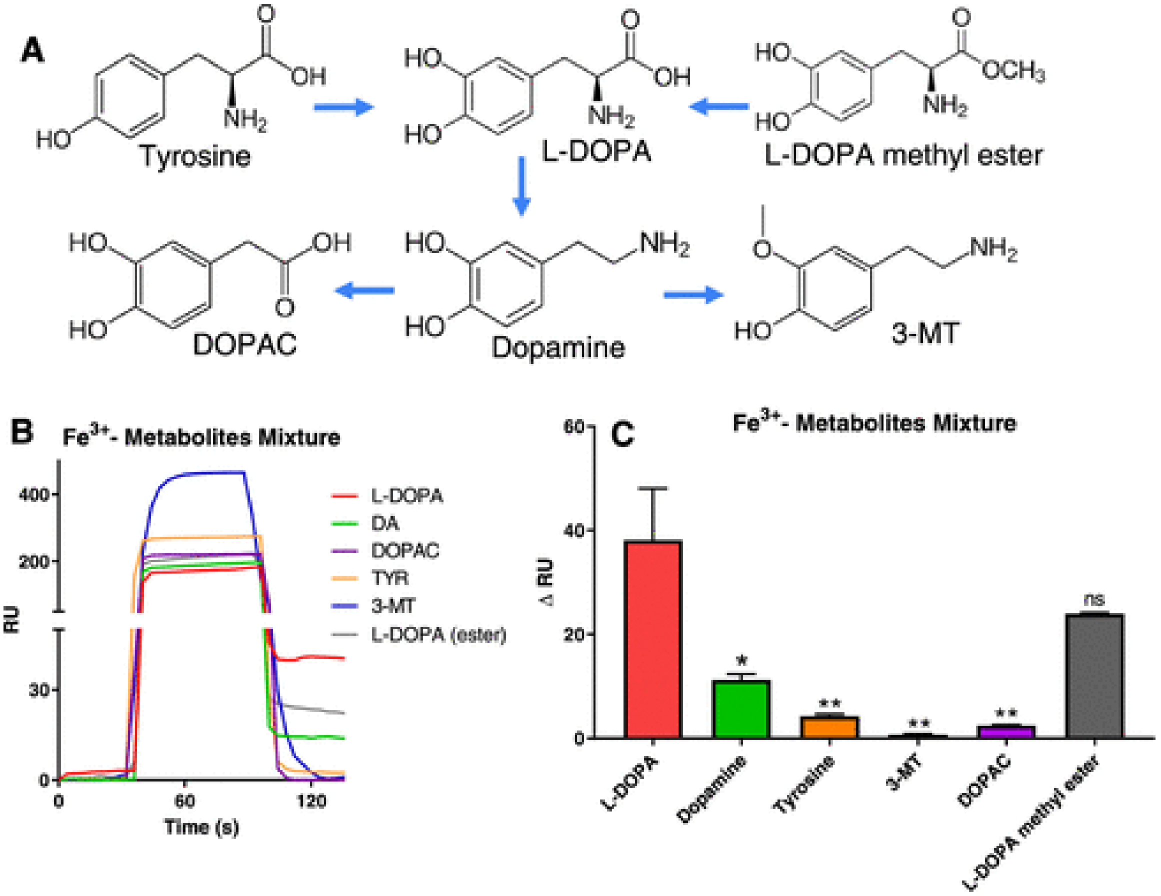

Figure 3.4. SPR sensor responses to Scn interactions with L-DOPA precursors and metabolites

(A) Schematic of L-DOPA synthesis and metabolic pathways; (B) sensorgram reading for the injection of a mixture of iron and different catechols (0-135 s) on a CM5 chip with recombinant Scn immobilized on the surface; and (C) bar plot of the reflectivity change for Scn and a mixture of iron and different catechols. After recombinant Scn was immobilized on the CM5 chip, a mixture of iron and different catechols was injected, and the response was measured. The response was measured as the difference between the baseline prior to injection and after the injection by one-way ANOVA followed by the Tukey post hoc test ($F = 13.09$, $P = 0.0035$; * $P < 0.05$ and ** $P < 0.01$; ns: nonsignificant). Data represent mean ± SEM of at least three experiments and five replicates in each experiment.

Affinity of L-DOPA Binding to Scn and Its Physiopathological Relevance

We then analyzed the affinity of the binding of L-DOPA:Fe^{3+} to Scn by measuring the dissociation constant (K_d) after fitting the dose-response curve data into the nonlinear regression-specific binding (one site). K_d calculated from two separate experiments was 0.86 ± 0.43 μM (Figure 5).

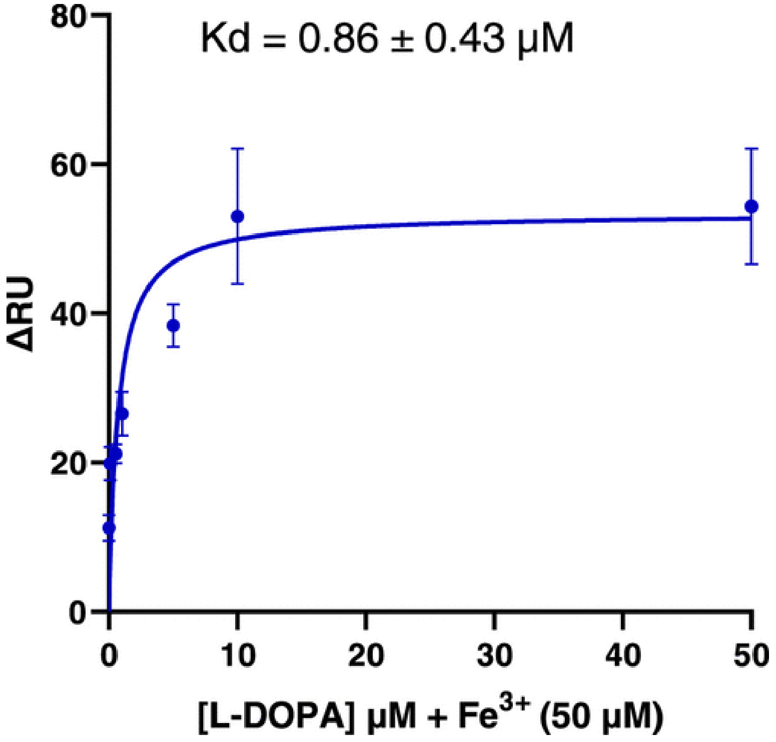

Figure 3.5. Determination of binding constant (K_d) of the Fe^{3+}-L-DOPA interaction with Scn

The dose-response curve for Scn binding to a mixture of L-DOPA and Fe at varying doses of L-DOPA and a fixed dose of Fe^{3+}. Recombinant Scn was immobilized, and a mixture of L-DOPA and iron was added at varying concentrations of L-DOPA. The response was measured as the difference between the baseline prior to injection and after the injection. Data were fitted in nonlinear regression one site specific binding using the GraphPad program. K_d = 0.86 ± 0.43 μM.

To determine the physiological relevance of our findings, we reviewed L-DOPA pharmacokinetics studies. We found that throughout its use in the last six decades, L-DOPA reached plasma concentrations that were higher than the K_d of its binding with Scn in the presence of Fe^{3+} (Table 1) [133-137]. However, these results should be interpreted with caution. First, since L-DOPA can form complexes with other metal ions than iron, and these complexes do not bind with Scn, it is reasonable to expect that not all L-DOPA doses will bind with iron in vivo and be available for the formation of the L-DOPA:Fe^{3+}:Scn complex. Similarly, Scn can bind other iron-siderophore complexes in vivo that do not contain L-DOPA.

Table 3.1. Examples of Pharmacokinetics Studies on L-DOPA Showing Its Maximum Concentrations (C_{max})[a]

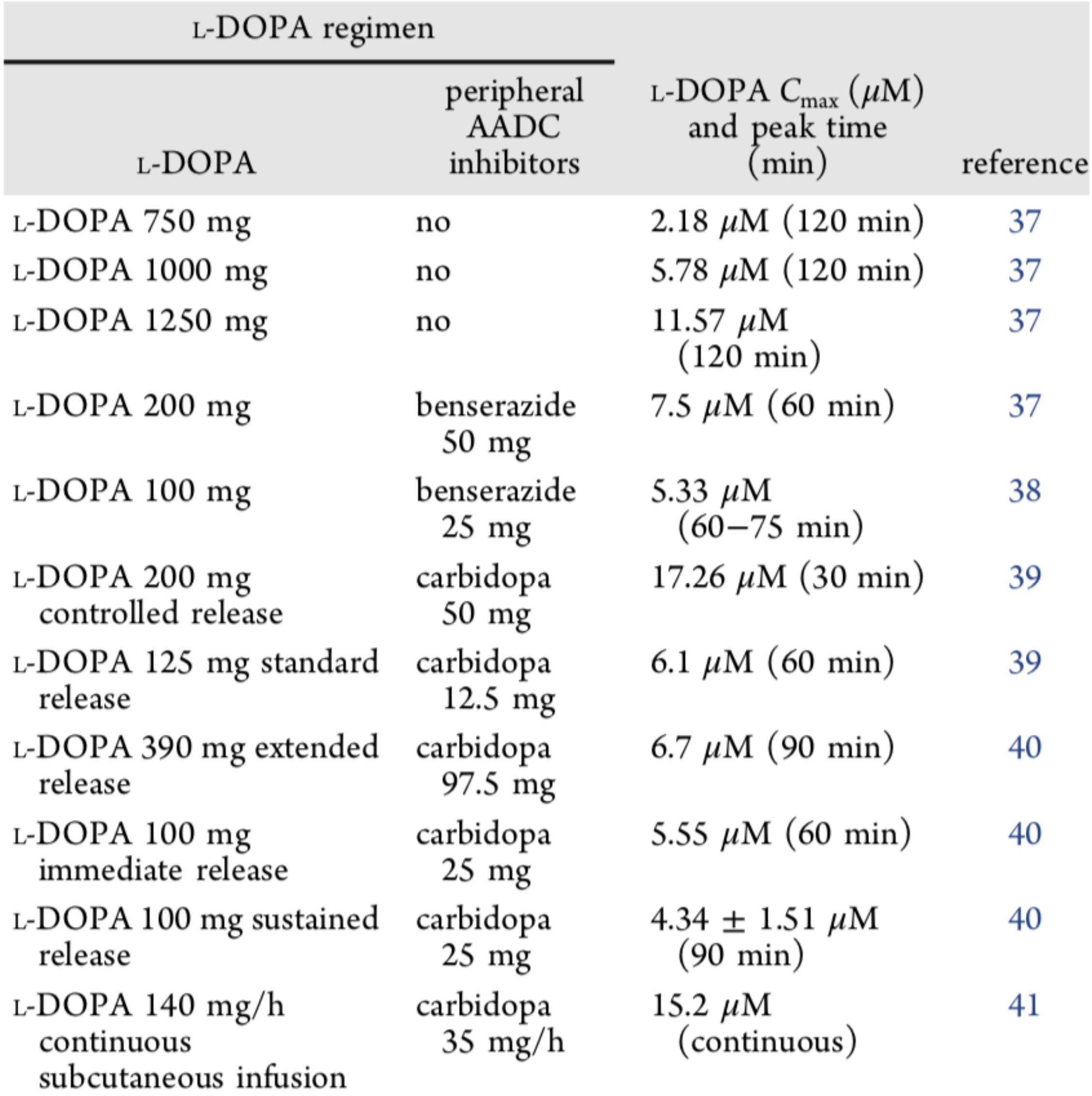

L-DOPA regimen			
L-DOPA	peripheral AADC inhibitors	L-DOPA C_{max} (μM) and peak time (min)	reference
L-DOPA 750 mg	no	2.18 μM (120 min)	37
L-DOPA 1000 mg	no	5.78 μM (120 min)	37
L-DOPA 1250 mg	no	11.57 μM (120 min)	37
L-DOPA 200 mg	benserazide 50 mg	7.5 μM (60 min)	37
L-DOPA 100 mg	benserazide 25 mg	5.33 μM (60–75 min)	38
L-DOPA 200 mg controlled release	carbidopa 50 mg	17.26 μM (30 min)	39
L-DOPA 125 mg standard release	carbidopa 12.5 mg	6.1 μM (60 min)	39
L-DOPA 390 mg extended release	carbidopa 97.5 mg	6.7 μM (90 min)	40
L-DOPA 100 mg immediate release	carbidopa 25 mg	5.55 μM (60 min)	40
L-DOPA 100 mg sustained release	carbidopa 25 mg	4.34 ± 1.51 μM (90 min)	40
L-DOPA 140 mg/h continuous subcutaneous infusion	carbidopa 35 mg/h	15.2 μM (continuous)	41

[a] All L-DOPA preparations in the last five decades produce C_{max} values higher than the K_d of L-DOPA: Fe binding to Scn.

Our results may have significant physiological and pathophysiological implications. First, considering the high affinity of the L-DOPA:Fe complex to Scn, our results indicate that L-DOPA:Fe can readily form a stable complex with Scn in the blood and brain environments, wherein Fe is abundant. This complex may facilitate the cellular uptake of Fe through endosomes, causing cellular iron overload. Although catechol chelator affinities for iron might not be sufficient to outcompete transferrin, the primary iron transporter [116], their iron trafficking efficiency is known to be increased by Scn, which increases the stability of iron complexation [116]. Accordingly, we speculate that Scn-mediated iron transport using the L-DOPA siderophore may contribute to iron-mediated oxidative stress and neuroinflammation in the substantia nigra [138]. Previous studies proposed the role of Scn accumulation as a potential pathogenic mechanism of PD [139]. Indeed, Scn is upregulated in the substantia nigra of PD patients and neurotoxin-treated animal PD models [130]. Further, a case-control study found increased plasma levels of Scn in PD patients compared to age-matched healthy individuals [134], albeit these results were not confirmed by a more recent study [137]. Catechol siderophores transport iron within or across cells, either by themselves or upon interaction with Scn [122,140].

Our results may also have important implications for both acute and chronic treatment with L-DOPA. While peripheral AADC inhibitors increase the amount of L-DOPA available for the brain, they may increase the peripheral L-DOPA pool available to chelate iron and facilitate the formation of L-DOPA:Fe:Scn complexes in the plasma and peripheral organs. There is evidence that Scn can cross the BBB [141,142], but whether the L-DOPA:Fe:Scn complex, formed peripherally, can cross BBB needs investigations. Given the decrease in the activity and expression of AADC in the brain of PD patients [111,112], it is possible that exogenous L-DOPA that reaches the brain can also chelate Fe in the basal ganglia, causing an increase in the formation of DOPA:Fe:Scn complexes and contributing to the toxicity of L-DOPA continuous treatment in PD patients. With L-DOPA continuous treatment, the dose of L-DOPA required to alleviate parkinsonian symptoms increases. It is tempting to speculate that the formation of L-DOPA:Fe:Scn complexes may play a role in reducing L-DOPA efficacy with the disease's progress by reducing the amount of free L-DOPA available for decarboxylation to dopamine.

Chapter 4:

OPHTHALMIC ACID INDUCES LOCOMOTOR ACTIVITY IN MPTP-TREATED MICE

Abstract

Using MPTP as a model for PD in mice is more representative of the etiology of PD. We were able to induce this model in our animals by deleting dopaminergic neurons to a sufficient degree to cause motor deficits, as measured by locomotor activity. Furthermore, we found that we could induce hyperactivity in the animals through treatment with L-DOPA and NSD1015, suggesting that this hyperactivity is not dependent on the specific PD model used. In the previous chapter, we identified OA as showing the highest fold increase at the peak of hyperactivity in the L-DOPA and NSD1015-treated mice. However, very little is known about OA, particularly with respect to its relationship to movement or motor control. In this study, we found that OA is unable to cross the blood-brain barrier, and thus had no effect on locomotion when injected i.p. However, when administered ICV, OA was able to induce locomotor activity in a dose-dependent manner. This suggests that the hyperactivity observed in the animals treated with L-DOPA and NSD1015 may be attributed to the elevated levels of OA.

4.1 INTRODUCTION

From the previous metabolomic study that was performed, we were given a list of hundreds of metabolites and how they changed in the hyperactive mice. As mentioned briefly earlier, ophthalmic acid (OA) was the metabolite that showed the largest fold increase. Because of this, we chose to pursue it because the high fold increase could mean that it is directly responsible for the hyperactivity seen in the animals, which would make testing it fairly easy to do. The alternative is that it is not directly responsible, but rather, indirectly responsible, which at the very least could point us in the direction of what metabolite is truly responsible for the dramatic increase in locomotor activity.

Ophthalmic acid, or, (OA) is a tripeptide analog of glutathione in which the cysteine group is replaced by L-2-aminobutyrate. It was first discovered when researchers were studying tryptophan metabolism and discovered that when tryptophan was metabolized in the lens of the eye, OA was produced. OA was observed to accumulate in the lens of the eye and that its levels were higher in people with cataracts, thus it was hypothesized to play a role in forming protein aggregates that would eventually cloud the lens and impair vision [143-145].

Aside from its role in the eye, very little is known about OA. Some more recent studies have shown that it may serve as a potential oxidative stress biomarker in patients with schizophrenia [146]. Studies have also shown that it is present in the gut microbiome and may play a role in gut-microme signaling [147]. In this chapter, we will investigate what the locomotor effects of OA are on the mice and if we are able to reproduce the hyperactivity induced by L-DOPA and NSD1015.

4.2 MATERIALS AND METHODS

4.2.1 Tissue Preparation for Liquid Chromatography with Tandem Mass Spectrometry (LC-MS-MS)

Adult male Swiss Webster mice, weighing approximately 20-30g, were sacrificed by asphyxiation. After decapitation, the blood was collected and the brains were rapidly removed on a cold surface, frozen in isopentane at -40°C and then stored at -80°C. The protocol for metabolite extraction from the brain tissue and serum was adapted from a previously reported protocol [148]. Frozen tissue was immediately plunged into methanol (1 ml) containing internal standards and homogenized for 1 minute to inactivate enzymes. 500 µl of deionized water was added and 300 µl of the solution was transferred to another tube and 200 µl of chloroform was added and mixed thoroughly. The solution was centrifuged at 12,000 x g for 15 minutes at 4°C. The upper aqueous layer was filtered and the filtrate was lyophilized and dissolved in 50 µl of methanol. For the serum, 200 µl of serum was plunged into 1.8 ml of methanol. 800 µl of deionized water was added and an additional 2 ml of chloroform was added as well. The solution was centrifuged at 2,500 x g for 5 minutes at 4°C. The upper aqueous layer was filtered, lyophilized and dissolved in 50 µl of methanol. All LC-MS-MS experiments were performed using a TSQ Quantum Ultra Mass Spectrometer (Thermo Finnigan, San Jose, CA)

4.2.2 MPTP-treated Mouse Model of Parkinson's Disease

Adult male Swiss Webster mice were housed under controlled conditions and a 12-hr light/dark cycle. For the MPTP treatment, mice were injected intraperitoneally once per day for 3 days with either MPTP (Sigma) (20 mg/kg) or saline. MPTP is a neurotoxin that works by being converted into MPP+ by MAO-B. MPP+ is then taken up into dopaminergic neurons in the substantia nigra, where it inhibits complex I of the electron transport chain. This inhibition leads to a decrease in the production of ATP and an increase in reactive oxygen species which eventually leads to damage to the mitochondria and cell death. The loss of dopaminergic neurons in the substantia nigra through MPTP is ideal to model PD as it mimics the most key feature of the disease.

4.2.3 Animal and Treatment

Swiss Webster mice (8-10 weeks old) were obtained from Charles River Laboratories. Animals were group housed with a maximum of four animals per cage and acclimated to the vivarium for a week prior to treatments. Animals were kept in a normal 12:12 hour light/dark cycle with free access to food and water.

4.2.4 Cannulation Surgery

Swiss Webster mice were anesthetized with isoflurane (5% for induction; 1-3% to sustain). Once anesthetized, each mouse was placed on the stereotaxic device and implanted with a stainless-steel cannula (20G, 2.5 mm length) into the brain ventricle (0.2 mm posterior and 1 mm lateral to bregma and 2.3 mm below the surface of the skull). Mice were allowed to recover for 7 days.

4.2.5 Assessment of Locomotor Activity

Mice were placed in a locomotor test chamber (40 x 40 x 38 cm3) and the horizontal locomotor activity was monitored with a 16 x 16 photobeam array (San Diego Instruments, San Diego, CA) located 1.25 cm above the floor of the enclosure. Mice were transported to the activity chamber room at least 30 minutes prior to placement into the activity chambers. All mice were given time to acclimatize to the chamber prior to injections, and locomotor activity was recorded for 20-24 hours following drug administration. Mice were randomly distributed to each treatment group with all proper controls being run in parallel. Data was extracted first using the

PAS Data Reporter software (San Diego Instruments, San Diego, CA) and the GraphPad Prism (GraphPad Software, Inc.) was used to further analyze data and produce figures.

4.2.5 Statistical Analysis

Statistical analyses of data were carried out using GraphPad Prism (GraphPad Software, Inc.). Data were presented as means ± standard error means (S.E.M.). Results were analyzed by unpaired student t-test, one-way, and two-way ANOVA followed by the appropriate post hoc comparisons, and $P < 0.05$ was considered statistically significant.

4.2.6 Immunohistochemistry

Immunohistochemistry methods to examine the tyrosine hydroxylase (TH) positive neurons. Mice were perfused under isoflurane anesthesia with 4% paraformaldehyde (PFA), and brains were removed, post-fixed in 4% PFA for overnight at 4 °C, and stored in 30% sucrose. Coronal sections were cut at 20 μm thickness, and three sections were used from each region of interest. Sections were blocked with 4% normal goat serum in PBS with 0.3% Triton X-100 for 1 h, and were then incubated in the blocking buffer that contains the primary antibodies (TH 1:500, Sigma). The sections were then washed with PBS, incubated with the secondary antibody (1:500) for 1 h, then with 4′,6-diamidino-2-phenylindole (DAPI) (Sigma) for 5 min, and were then mounted on slides. Imaging was carried out using Leica Sp8 TCS confocal microscope (UCI optical biology core facility). TH positive neurons were counted in the bilateral areas of each section, and the mean counts of three non-consecutive sections per brain of 3–5 brains were calculated. Cell counts were performed using ImageJ and confirmed manually.

4.2.7 Synthesis of d5-Ophthalmate

The synthesis of d_5-OA as a mixture of isomers was accomplished with standard peptide coupling reagents. Glycine benzyl ester was first coupled with racemic tert-butyloxycarbonyl protected d_5-2-aminobutyrate. This dipeptide was deprotected and N-carbobenzyloxy-L-glutamate 1-methyl ester (Z-L-Glu-OMe) was added. Two deprotection steps (hydrolysis of the methyl ester and hydrogenolysis of the benzyl ester and the N-carbobenzyloxy groups) gave the acetate salt of d_5-OA.

4.3 RESULTS

MPTP treatment greatly inhibits locomotor activity in mice

After treating 8 week old Swiss Webster mice with MPTP, as described in Section 4.2.2, we were able to show that the MPTP treatment drastically reduces the locomotor activity in the mice. The locomotor response seen in the saline treated group closely resembles that of typical locomotor activity from mice in a 12:12 hour light/dark cycle (Figure 4.1A). By calculating the area under the curve, we are able to quantify how much of the locomotor activity we were able to inhibit (263403±27494 vs 16153±1914) ($P < 0.0001$, Figure 4.1B).

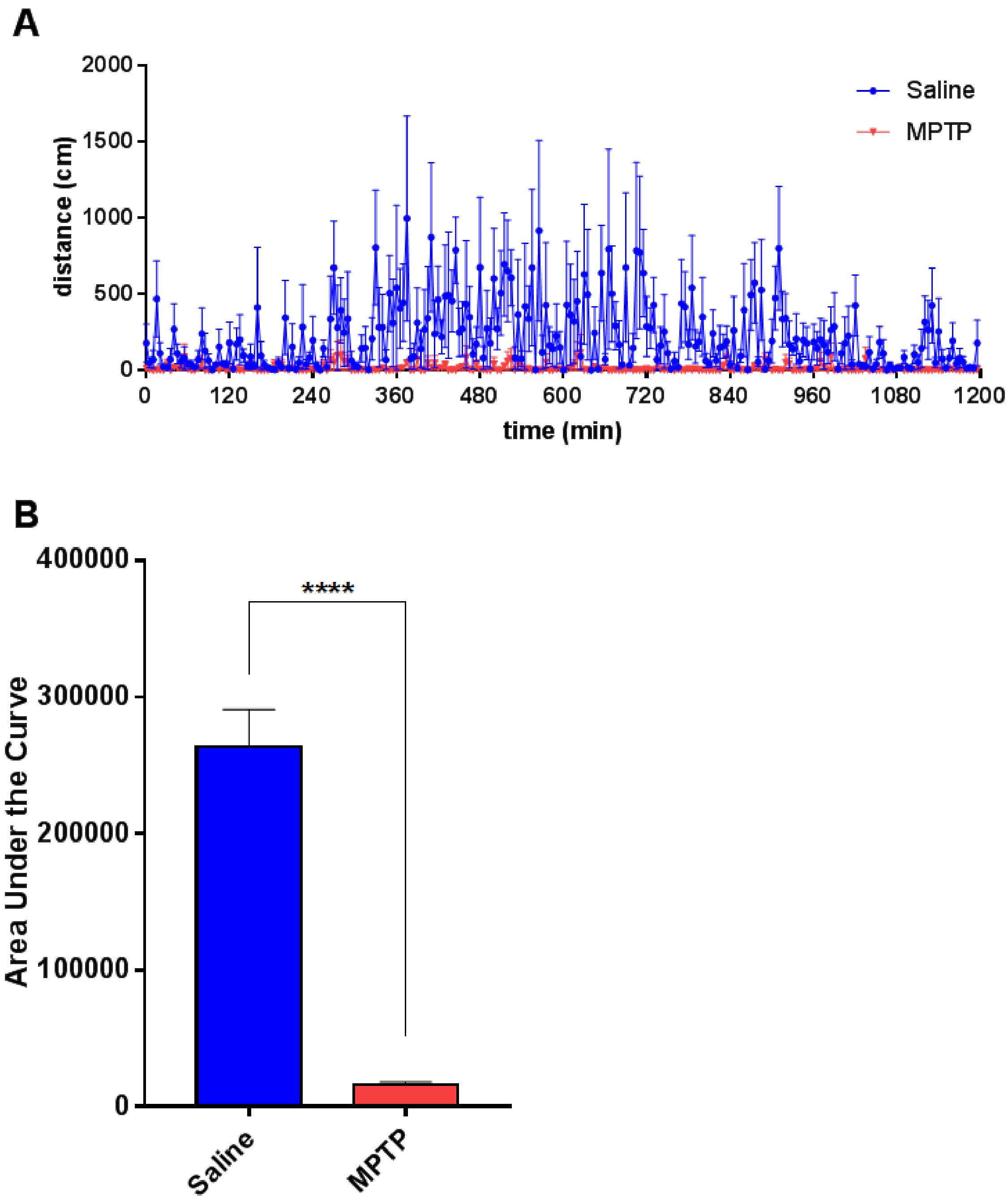

Figure 4.1. Effect of MPTP treatment on locomotor activity in mice

(A) Locomotor activity in mice after being given either saline or MPTP once a day for 3 days and the (B) area under the curve (n = 8). Unpaired t-test (t = 10.09, $P < 0.0001$). Data are presented as means±S.E.M.

MPTP treatment induces severe dopamine neuron loss in the SNc

After treating 8 week old Swiss Webster mice with MPTP, as described in Section 4.2.2, their brains were perfused and immunohistochemistry was run, as described in Section 4.2.6. Tyrosine hydroxylase (TH) is stained (green) as a marker for dopaminergic neurons and DAPI (blue) is used to identify the number of cells by staining the cell nuclei. All MPTP treated mice had their brains extracted and stained for TH to demonstrate a sufficient amount (~90%) of dopamine neurons were deleted. Any animals that failed to show at least 90% deletion were removed. Here we demonstrate what a normal baseline level of TH would be (Figure 4.2A) and what the TH levels look like after MPTP treatment (Figure 4.2B).

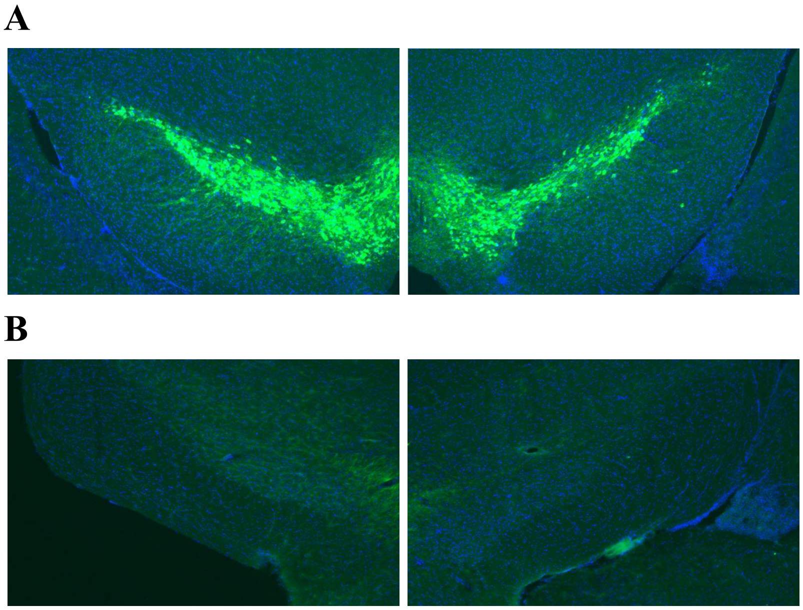

Figure 4.2. Effect of MPTP on dopamine neuronal loss in the substantia nigra

Representative immunostaining of TH and DAPI in (A) saline and (B) MPTP-treated mice.

Co-treatment of L-DOPA and NSD1015 induce hyperactivity in MPTP-treated mice

After treating mice with MPTP once a day for three days, as described in Section 4.2.2, we treated mice with either saline or NSD1015. 30 minutes later, the mice were given L-DOPA in combination with benserazide. Treating the mice with only L-DOPA was able to bring the animals baseline activity to a level that is more in line to a normal animal. When treated with NSD1015 and L-DOPA, however, we once again see the same delayed, large peak spanning many hours, similar to what was seen in the reserpine-treated mice (Figure 4.3A). Quantitatively, we are able to see just how much more locomotor activity is induced by L-DOPA alone compared to giving L-DOPA with NSD1015 ($P < 0.0001$, Figure 4.3B).

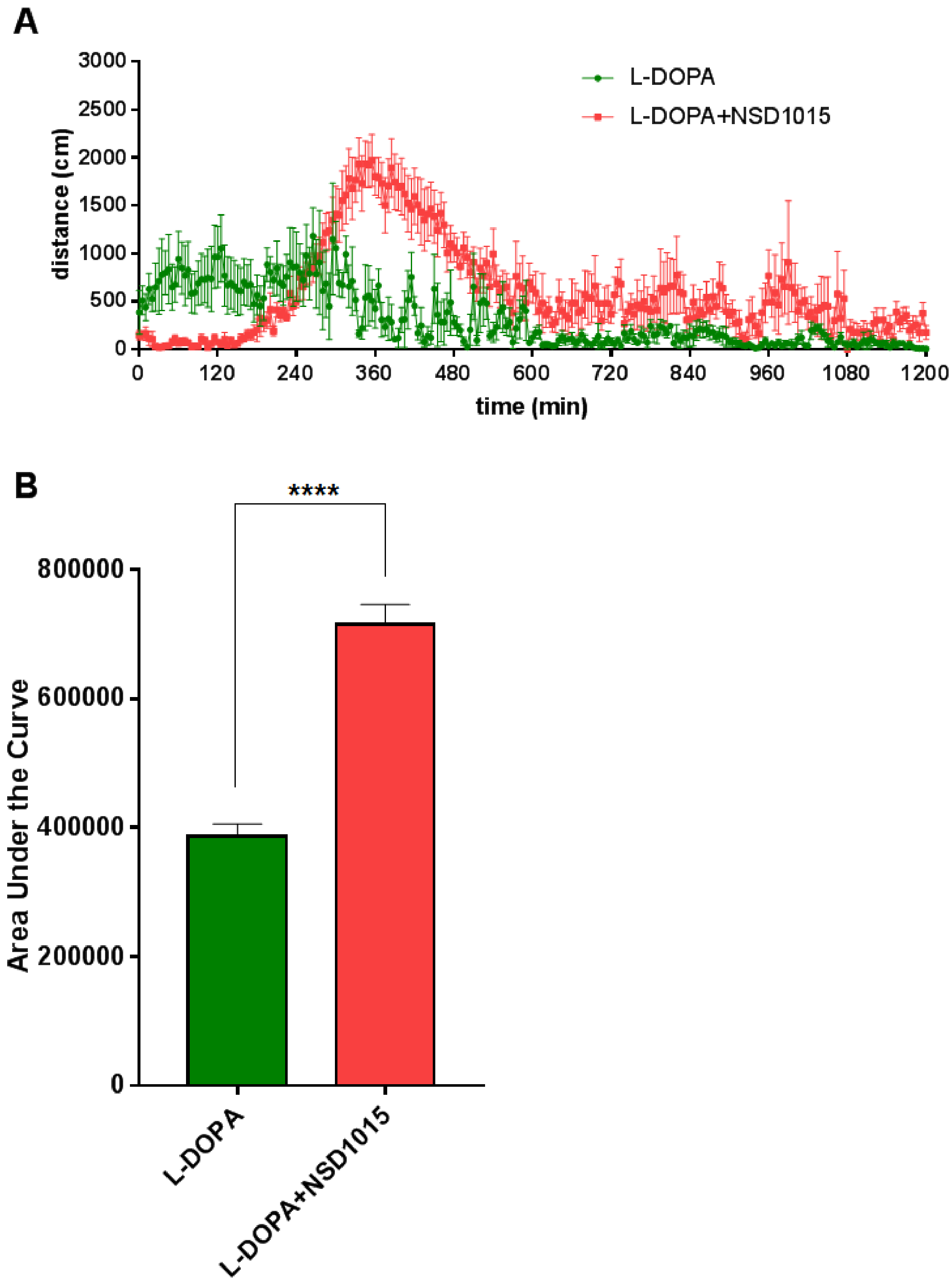
A
3000
2500
2000
1500
1000
500
0
distance (cm)
0
120
240
360
480
600
720
840
960
1080
1200
time (min)
L-DOPA
L-DOPA+NSD1015
B
****
800000
600000
400000
200000
0
Area Under the Curve
L-DOPA
L-DOPA+NSD1015

Figure 4.3. Effect of L-DOPA and NSD1015 on locomotor activity in MPTP-treated mice

Mice were injected with MPTP once a day for 3 days. (A) Locomotor activity in mice after being given either saline or NSD1015 followed by L-DOPA 30 minutes after and the (B) area under the curve (n = 8). Unpaired t-test (t = 8.93, P < 0.0001). Data are presented as means±S.E.M.

OA injected peripherally has no effect on MPTP-treated mice

After treating 8 week old Swiss Webster mice with MPTP, as described in Section 4.2.2, we injected the animals with either saline or 100, 50, 100 mg/kg of OA. The locomotor response seen in the animals treated with OA is extremely similar to that of the saline treated group (Figure 4.4A). Quantitatively, the locomotor activity amongst the groups don't seem to vary much at all (P > 0.05, Figure 4.4B)

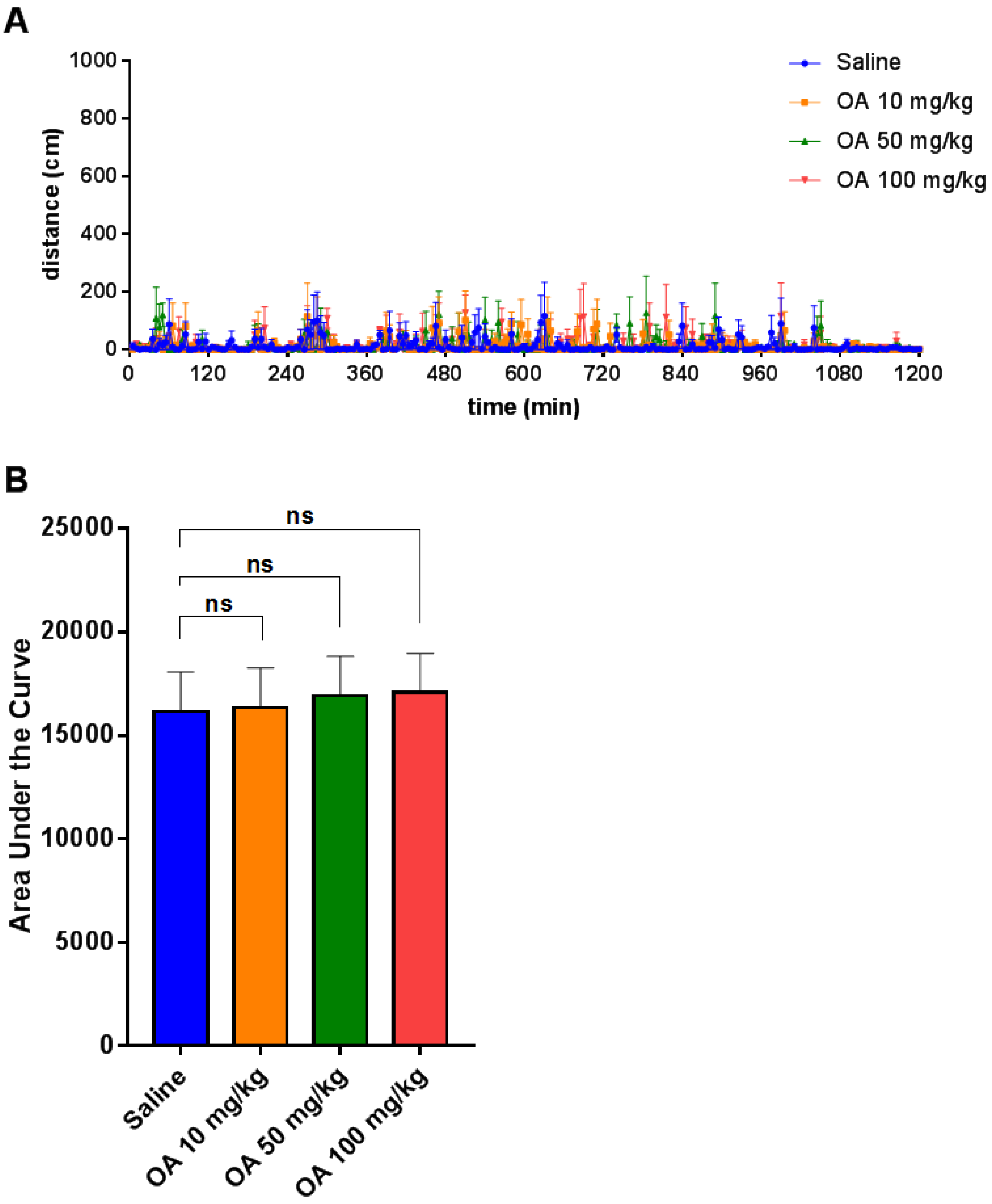

Figure 4.4. Effect of i.p. injection of OA on MPTP-treated mice

Mice were injected with MPTP once a day for 3 days. (A) Locomotor activity in mice after being given either saline or OA at 10, 50, and 100 mg/kg and the (B) area under the curve (n = 8). One way ANOVA ($F_{3,28}$ = 0.05262, P = 0.9837). Data are presented as means±S.E.M.

OA does not appear to cross the blood-brain barrier

Deuterated OA was synthesized to be used as a tracer in the LC-MS-MS. Animals were injected with 20 mg/kg of d_5-OA i.p. The animals were then promptly sacrificed 15 minutes post injection and the brain and blood was collected. The brain tissue and blood were then prepared as described in Section 4.2.1. Once ready, the samples, alongside a standard curve, were run on the machine and the concentration oa d_5-OA in the brain and blood was interpolated based on the standard curve. Some traces of the deuterated OA had made its way to the blood in the blood (~2 µm), however, none had made its way to the brain, suggesting that OA may be unable to cross the blood-brain barrier (Figure 4.5).

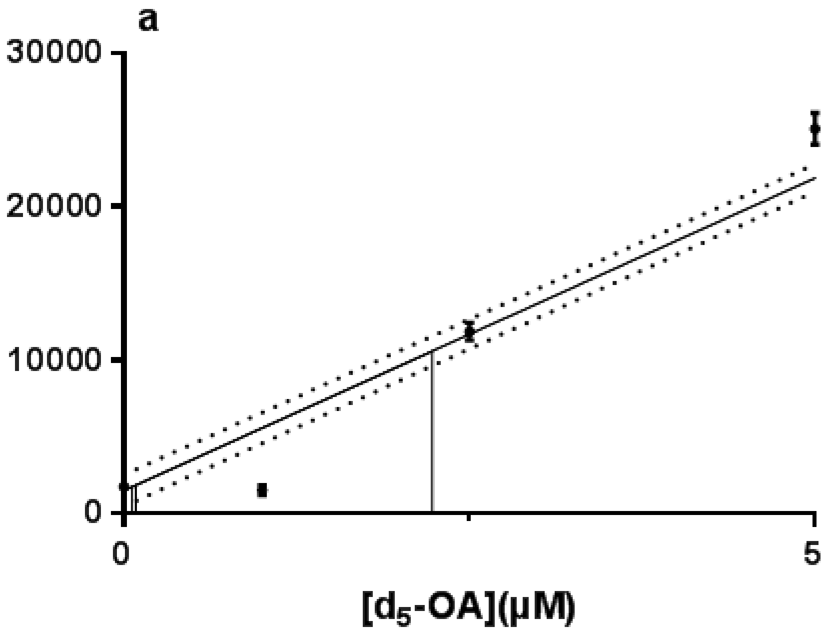

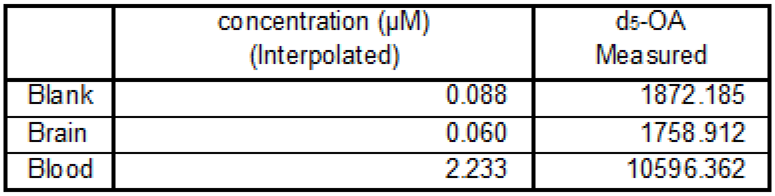

	concentration (μM) (Interpolated)	d_5-OA Measured
Blank	0.088	1872.185
Brain	0.060	1758.912
Blood	2.233	10596.362

B

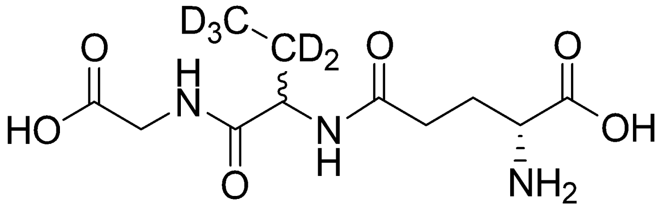

Figure 4.5. Structure and standard curve of d_5-OA and interpolated concentrations of d_5-OA in the mice

(a) Mice were injected with d_5-OA and the brain and blood were collected 10 minutes after injection as described in Section 4.2.1. The brain and blood samples were prepared and cleaned and injected into the LC-MS-MS system, as well as a standard curve. Data represents the interpolated concentration of d_5-OA in the blood and brain. Values are expressed as mean±S.E.M. n=4 for each group. (b) Structure of the synthesized deuterated OA.

OA induces hyperactivity in ICV injection

Mice were anesthetized and underwent surgery where a cannula was implanted for future intracerebroventricular (ICV) injections as described in Section 4.2.4. Following recovery, the mice were injected (i.p.) with either saline or MPTP 20 mg/kg for three days as described in Section 4.2.2. The following day, mice were injected ICV with either saline or OA at four different doses. Treating the non-MPTP-treated mice with OA via ICV injection did not seem to have an impact on the locomotor activity ($P > 0.05$, Figure 4.6B). The locomotor activity seen seems to reflect that of typical locomotor activity from mice in a 12:12 hour light/dark cycle (Figure 4.6A). In the MPTP-treated mice, however, there was a dose-dependent increase in locomotor activity from the ICV OA injections ($P < 0.0001$, Figure 4.6C-D).

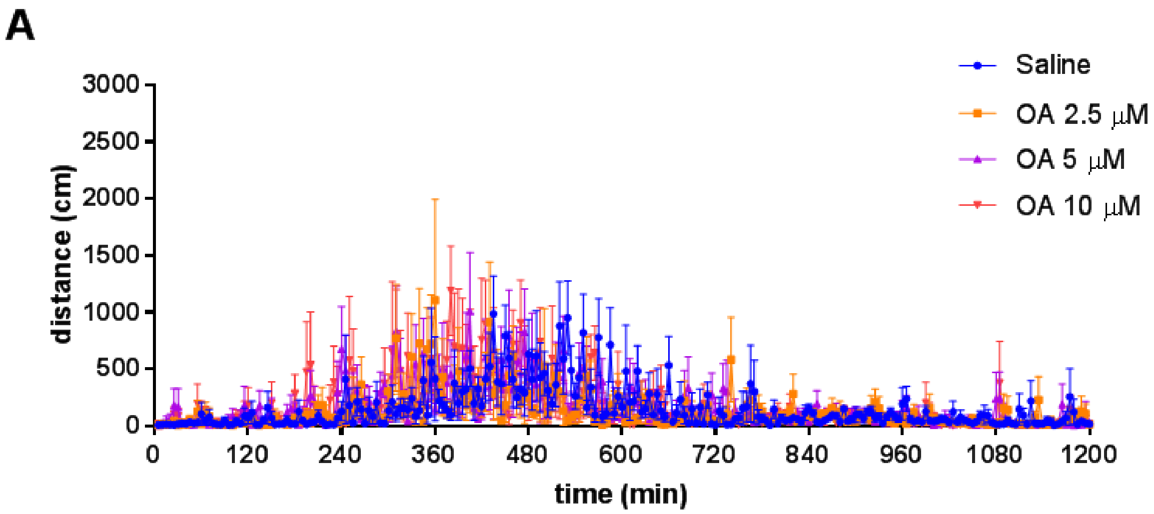
A
Saline
OA 2.5 µM
OA 5 µM
OA 10 µM
distance (cm)
3000
2500
2000
1500
1000
500
0
0
120
240
360
480
600
720
840
960
1080
1200
time (min)

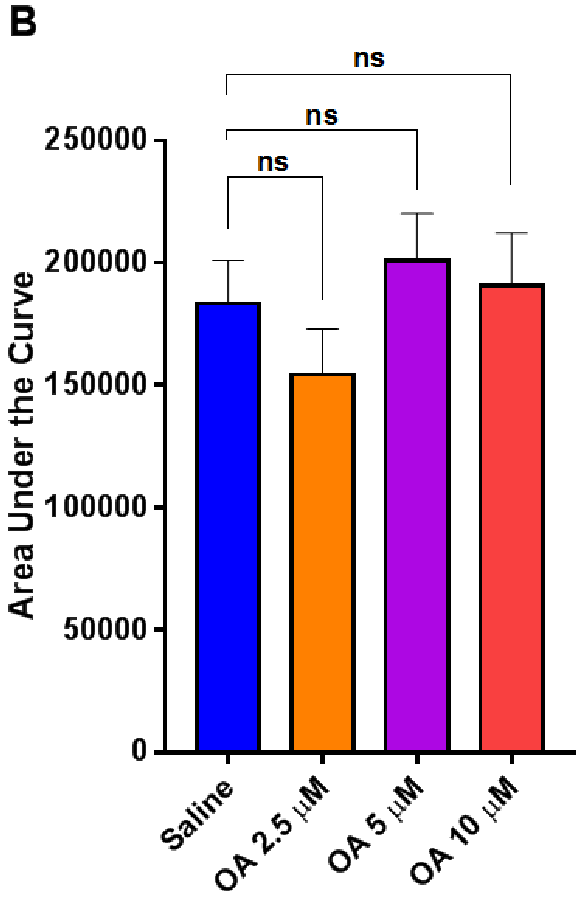
B
ns
ns
ns
Area Under the Curve
250000
200000
150000
100000
50000
0
Saline
OA 2.5 µM
OA 5 µM
OA 10 µM

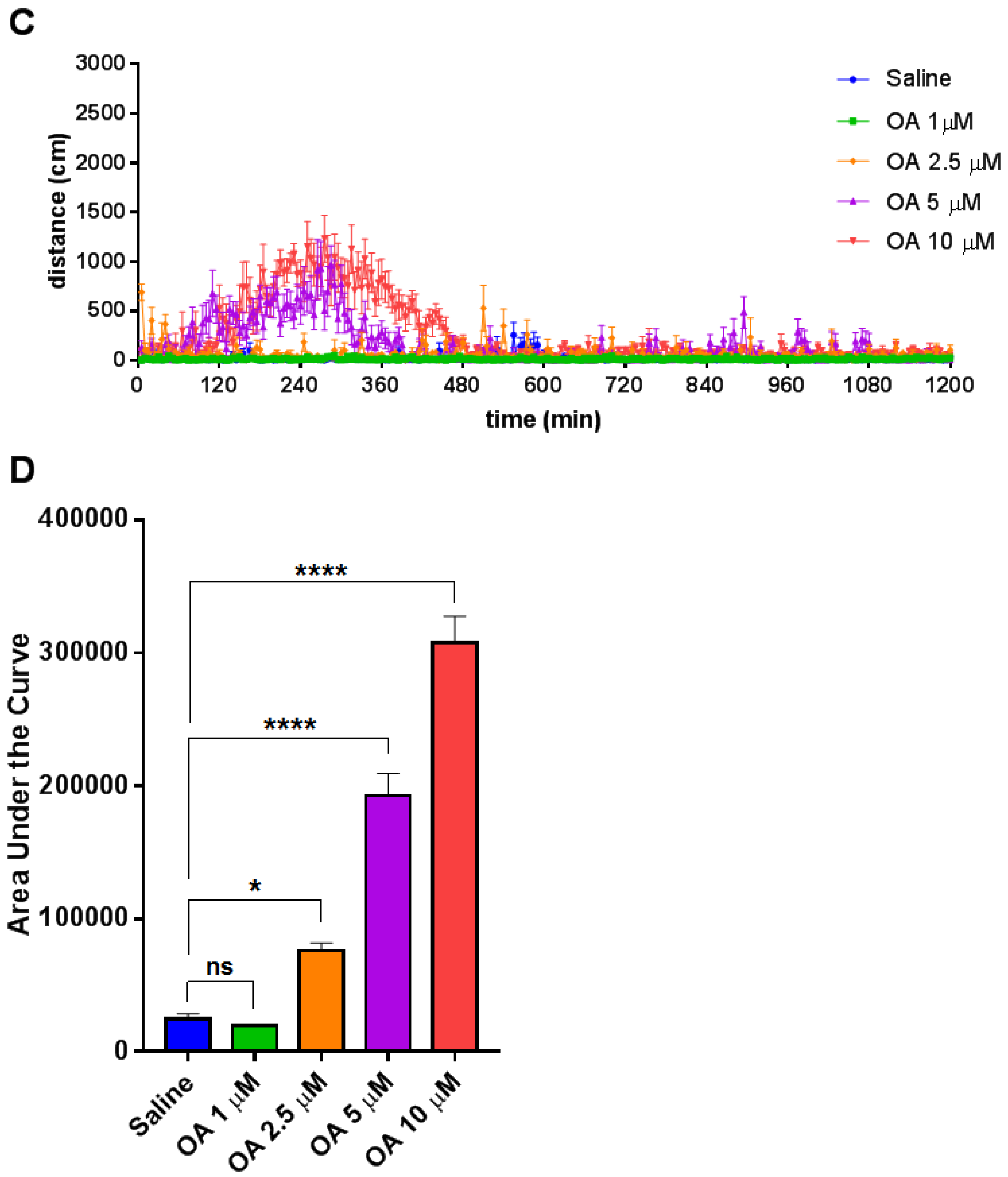

Figure 4.6. Effect of ICV injection of OA on MPTP-treated mice

Mice were anesthetized and underwent surgery where a cannula was implanted for future intracerebroventricular (ICV) injections as described in Section 4.2.4. Following recovery, the mice were injected (i.p.) with either saline or MPTP 20 mg/kg for three days as described in Section 4.2.2. The following day, mice were injected ICV with either saline or OA at four different doses. (A) Locomotor activity in mice after being given an ICV injection of saline or 2.5, 5, or 10 µm of OA and the (B) area under the curve (n = 8). One way ANOVA ($F_{3,28} = 1.064$, P = 0.3802) followed by the Tukey post hoc test, ns not significant. Data are presented as means±S.E.M. (C) Locomotor activity in MPTP-treated mice after being given an ICV injection of saline or 1, 2.5, 5, or 10 µm of OA and the (D) area under the curve (n = 8). One way ANOVA ($F_{4,35} = 104.4$, $P < 0.0001$) followed by the Tukey post hoc test, ****$P < 0.0001$, ns not significant. Data are presented as means±S.E.M.

4.4 DISCUSSION

We wanted to explore an alternative PD model to determine if we would still observe hyperactivity induced by L-DOPA and NSD1015. The MPTP treatment closely mimics the disease's etiology and is persistent, unlike reserpine. Our research successfully induced this model in mice, as evidenced by the decrease in locomotor activity (Figure 4.1) and the significant decrease in TH staining, indicating a considerable reduction in dopaminergic neurons in the SNc (Figure 4.2). Going forward, any mouse treated with MPTP was perfused and subjected to immunohistochemistry as described in Section 4.2.6 after completing their locomotor activity, and any animal that did not exhibit at least a 90% reduction was excluded. Furthermore, our findings demonstrate that hyperactivity is replicable in this mouse model of PD (Figure 4.3).

After noticing a significant increase in OA levels in the metabolomic data, it became our prime suspect as the cause of hyperactivity in the mice. However, when we administered OA i.p. to the MPTP-treated mice, the response was comparable to that of saline ($P > 0.05$, Figure 4.4). This outcome raised two possibilities: either OA cannot penetrate the blood-brain barrier, rendering it ineffective, or it is not responsible for the hyperactivity resulting from treatment with NSD1015 and L-DOPA.

In order to investigate whether OA could cross the blood-brain barrier, we synthesized d5-OA as a tracer for detecting OA in animals via liquid chromatography coupled with tandem mass spectrometry (LC-MS-MS). By administering d5-OA to the animals, we were able to track the deuterated OA and examine whether it crossed the blood-brain barrier through collecting and preparing tissue and blood samples. Our findings showed that only a small amount of d5-OA was present in the blood, with negligible amounts detected in the brain (Figure 4.5). These results strongly suggest that OA is incapable of crossing the blood-brain barrier, and hence, a central injection would be required for it to have any observable effects on the brain.

The mice were anesthetized and underwent surgery to have a cannula implanted for future ICV injections, following the protocol outlined in Section 4.2.4. After a recovery period of one week, the mice were given three i.p. injections of MPTP over three days as detailed in Section 4.2.2, and the experiment was conducted the following day. The mice were administered varying doses of OA ICV, and their locomotor activity was observed to respond in a dose-dependent manner ($P < 0.0001$, Figure 4.6D). This finding is highly significant as it confirms that OA is indeed responsible, either alone or in combination with other factors, for directly inducing hyperactivity in the animals.

Chapter 5:
OPHTHALMIC ACID INDUCES LOCOMOTOR ACTIVITY THROUGH THE CALCIUM SENSING RECEPTOR

ABSTRACT

Through previous research, it has been demonstrated that OA has the ability to bind to the CaSR, which has been seen to be expressed in regions related to movement regulation. This chapter provides further evidence of this binding, with a significant affinity observed through the radioligand binding assay. Interestingly, OA was unable to be displaced by other agonists or antagonists, indicating a specific interaction with the CaSR. Furthermore, our results show that OA not only binds to the CaSR but also activates it. This was observed through cAMP binding assays, which revealed a micromolar affinity for the receptor, similar to values estimated from the radioligand binding assay. When looking at the effects of OA and L-DOPA in the cAMP assay, when given together, L-DOPA seems to have a positive effect on OA binding to the CaSR when it is present. This suggests that the accumulation of L-DOPA may also promote and enhance the binding of OA to the CaSR. Based on these findings, we propose that OA is the mechanism behind the hyperactivity induced in animals treated with L-DOPA and NSD1015. To support this hypothesis, we utilized NPS2143, a CaSR antagonist, and were able to block the hyperactivity induced in animals treated with NSD1015 and L-DOPA, as well as in those receiving OA via ICV injection. These findings provide additional evidence that hyperactivity is a result of CaSR activation and suggest a promising non-dopaminergic system as a potential target for treating motor symptoms of PD.

5.1 INTRODUCTION

Despite the function and role of OA not being studied extensively, a few studies have shown that gamma-glutamyl peptides, such as OA, can activate the calcium sensing receptor (CaSR) [145]. The CaSR is a G protein-coupled receptor (GPCR) that is primarily expressed in parathyroid cells, thyroid C-cells, and renal tubular cells. The CaSR plays a critical role in regulating systemic calcium homeostasis by sensing and responding to changes in extracellular calcium levels. When extracellular calcium levels increase, the CaSR is activated and initiates a signaling cascade that inhibits the secretion of parathyroid hormone (PTH), a hormone that increases blood calcium levels. Conversely, when extracellular calcium levels decrease, the CaSR is deactivated, leading to an increase in PTH secretion and subsequent calcium mobilization from bone and increased calcium reabsorption from the kidneys [146-149].

The structure of the CaSR has been studied using a variety of techniques, including X-ray crystallography and cryo-electron microscopy. The receptor is a homodimeric protein consisting of a large extracellular domain (ECD), a seven-transmembrane domain (7TMD), and a short intracellular domain [150,151]. The ECD is responsible for binding extracellular calcium ions and contains a large, globular Venus flytrap-like domain that undergoes a conformational change upon calcium binding to activate the receptor [147,152]. The 7TMD domain contains seven transmembrane helices that are connected by extracellular and intracellular loops, and is responsible for coupling to downstream signaling pathways [153].

Upon calcium binding to the ECD, the 7TMD domain undergoes a conformational change that leads to the activation of heterotrimeric G proteins, such as Gαq/11, Gαi, and Gαs. This results in the activation of multiple downstream signaling pathways, including phospholipase C (PLC), mitogen-activated protein kinase (MAPK), and protein kinase A (PKA).

The specific signaling pathways activated by the CaSR depend on the cell type and the ligands that bind to the receptor [154]. When an extracellular ligand binds to a GPCR, it causes a conformational change in the receptor that allows it to interact with and activate a nearby G protein. In the case of a Gs-coupled receptor, the activated Gs protein binds to and activates the enzyme adenylyl cyclase, which catalyzes the conversion of ATP to cyclic adenosine monophosphate (cAMP). The increase in cAMP levels leads to the activation of protein kinase A (PKA) and other downstream signaling pathways, which ultimately produce the cellular response to the extracellular stimulus. On the other hand, when a GPCR is coupled to a Gi protein, as is the CaSR, the activated Gi protein binds to and inhibits adenylyl cyclase, which reduces cAMP production. This decrease in cAMP levels leads to the inhibition of PKA and other downstream signaling pathways, resulting in a different cellular response. These changes in cAMP levels can be measured by using specific antibodies that recognize and bind to cAMP. Typically these antibodies are labeled with an enzyme or fluorescent molecules which allows for future detection of the bound antibody.

In addition to regulating calcium homeostasis, the CaSR is also involved in a variety of other physiological processes, including magnesium and amino acid metabolism, and is implicated in the pathogenesis of several diseases, including familial hypocalciuric hypercalcemia (FHH) and neonatal severe hyperparathyroidism (NSHPT). The structure and function of the CaSR continue to be an active area of research, with new insights into the receptor's regulation and pharmacology continually emerging [149,154].

In the brain, the CaSR is also expressed in regions involved in the regulation of movement, such as the cerebellum and the basal ganglia. Studies have shown that activation of the CaSR in these regions can modulate locomotor activity in animal models. The authors saw that activation of the CaSR in the basal ganglia increased locomotor activity in mice, while inhibition of the CaSR decreased activity [155]. Another study also found that activation of the CaSR in the cerebellum increased locomotor activity in rats [156,157].

5.2 MATERIALS AND METHODS

5.2.1 Tissue Preparation

Adult male Swiss Webster mice, weighing approximately 20-30g, were sacrificed by asphyxiation. The brains were rapidly removed on a cold surface, frozen in isopentane at -40°C and then stored at -80°C. 20 μm coronal sections of the brain were cut on the cryostat at the levels of the striatum, lateral globus pallidus, substantia nigra, and hippocampus. The slices were then thaw-mounted on gelatin-coated glass slides and stored at -80°C.

5.2.2 Protocol for Radioligand Binding Assay

Sections were pre-incubated in buffer (50mM Tris, 1.5mM EDTA), PH 7.4 for 30 minutes at 4°C. Total binding was determined by incubating sections in buffer containing varying concentrations of [^{3}H]-OA (Moravek Inc.) for 60 minutes at room temperature. Non-specific binding of [^{3}H]-OA was defined by that seen in the presence of 10μM NPS-2143 (Tocris Bioscience). The incubation was terminated by washing the sections in an ice-cold (4°C) incubation buffer for 10 minutes. The sections were then dipped in ice-cold distilled water and dried in a stream of cold air. Sections were scraped off of the slides and placed into vials containing 4.5 ml of scintillation fluid and were subsequently measured at a scintillation counter.

5.2.3 Protocol for Transient Transfection

Human embryonic kidney 203 (HEK293T) cells were grown in DMEM adjusted to contain 10% fetal bovine serum (FBS) (Sigma), 1% penicillin and streptomycin (SIgma) at 5-10% CO2 and 37°C.

HEK293T cells were transiently transfected to express both the pGloSensor-22F cAMP plasmid (Promega Corporation) and a CaSR plasmid (Addgene). Cells were transfected using the jetPRIME transfection reagent using the standard conditions of 5 μg of each plasmid and 20 μl of the reagent (Polyplus). After an overnight incubation in 37°C with 5-10% CO2, the cells were then ready to be used.

5.2.4 Protocol for GloSensor cAMP Assay

The GloSensor cAMP assay is a bioluminescent assay that uses a genetically encoded biosensor to detect changes in intracellular cAMP levels in real time. The assay is based on the fact that cAMP binding to the regulatory subunit of protein kinase A (PKA) results in the release of the catalytic subunit of PKA, which can then phosphorylate a target protein, resulting in a cellular response. The assay uses genetically encoded biosensor variants with cAMP-binding domains fused to mutant forms of photinus pyralis luciferase. On binding to cAMP, this enzyme undergoes conformational changes, leading to increased bioluminescence. This means that cells expressing the GloSensor plasmid can be used to evaluate cAMP levels in living cells in real time, rather than having to lyse the cells. The biosensor used in the GloSensor assay is a modified form of the PKA regulatory subunit that is fused to a circularly permuted form of green fluorescent protein (GFP). When cAMP binds to the regulatory subunit, it causes a conformational change that brings the two halves of the GFP together, resulting in an increase in fluorescence. This increase in fluorescence can be measured using a luminometer, allowing real-time monitoring of changes in cAMP levels [158].

Cells are washed with PBS and detached using 0.05% trypsin. The cells are then pelleted and resuspended in CO_2-independent media (Thermo Fisher Scientific), 10% FBS, and the GloSensor cAMP reagent (Promega Corporation). The cells are incubated at room temperature for 2 hours and are gently mixed every 15 minutes to prevent the cells from settling. The cells are then transferred to a 96-well plate and luminescence was measured using the MicroBeta2

2450 Microplate counter (PerkinElmer). Basal luminescence level is recorded and another recording is done after the addition of forskolin to increase the basal luminescence level.

5.2.5 MPTP-treated Mouse Model of Parkinson's Disease

Adult male Swiss Webster mice were housed under controlled conditions and a 12-hr light/dark cycle. For the MPTP treatment, mice were injected intraperitoneally once per day for 3 days with either MPTP (20 mg/kg) or saline. MPTP is a neurotoxin that works by being converted into MPP+ by MAO-B. MPP+ is then taken up into dopaminergic neurons in the substantia nigra, where it inhibits complex I of the electron transport chain. This inhibition leads to a decrease in the production of ATP and an increase in reactive oxygen species which eventually leads to damage to the mitochondria and cell death. The loss of dopaminergic neurons in the substantia nigra through MPTP is ideal to model PD as it mimics the most key feature of the disease.

5.2.6 Animal and Treatment

Swiss Webster mice (8-10 weeks old) were obtained from Charles River Laboratories. Animals were group housed with a maximum of four animals per cage and acclimated to the vivarium for a week prior to treatments. Animals were kept in a normal 12:12 hour light/dark cycle with free access to food and water.

5.2.7 Cannulation Surgery

Swiss Webster mice were anesthetized with isoflurane (5% for induction; 1-3% to sustain). Once anesthetized, each mouse was placed on the stereotaxic device and implanted with a stainless-steel cannula (20G, 2.5 mm length) into the brain ventricle (0.2 mm posterior and 1 mm lateral to bregma and 2.3 mm below the surface of the skull). Mice were allowed to recover for 7 days.

5.2.8 Assessment of Locomotor Activity

Mice were placed in a locomotor test chamber (40 x 40 x 38 cm3) and the horizontal locomotor activity was monitored with a 16 x 16 photobeam array (San Diego Instruments, San Diego, CA) located 1.25 cm above the floor of the enclosure. Mice were transported to the activity chamber room at least 30 minutes prior to placement into the activity chambers. All mice were given time to acclimatize to the chamber prior to injections, and locomotor activity was recorded for 20-24 hours following drug administration. Mice were randomly distributed to each treatment group with all proper controls being run in parallel. Data was extracted first using the PAS Data Reporter software (San Diego Instruments, San Diego, CA) and the GraphPad Prism (GraphPad Software, Inc.) was used to further analyze data and produce figures.

5.2.9 Statistical Analysis

Statistical analyses of data were carried out using GraphPad Prism (GraphPad Software, Inc.). Data were presented as means ± standard error means (S.E.M.). Results were analyzed by unpaired student t-test, one-way, and two-way ANOVA followed by the appropriate post hoc comparisons, and $P < 0.05$ was considered statistically significant.

5.3 RESULTS

[^{3}H]-OA is able to be displaced by NPS2143

The radioligand binding assay was run as described in Section 5.2.2. Brain sections were incubated with [^{3}H]-OA and were displaced by a larger concentration of unlabeled OA (Figure 5.1A). [^{3}H]-OA was also able to be displaced by a CaSR agonist, calcium, and antagonist, NPS2143 (Figure 5.1B-C). Lastly, [^{3}H]-OA was able to be displaced in the presence of L-DOPA, suggesting that L-DOPA and OA bind to similar receptors in the brain (Figure 5.1D).

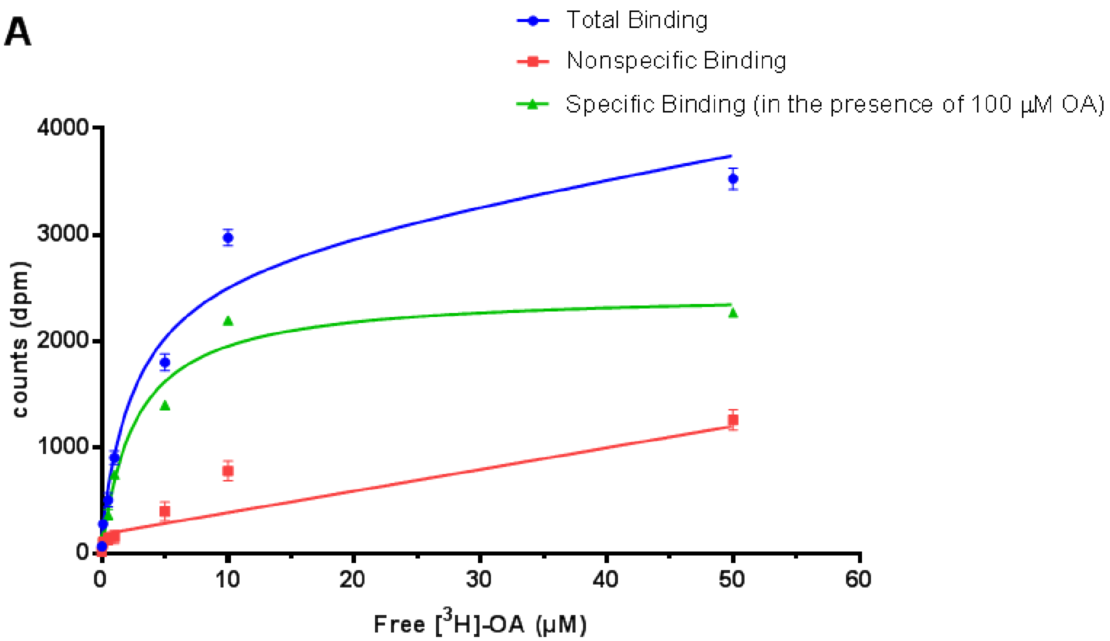
A
Total Binding
Nonspecific Binding
Specific Binding (in the presence of 100 μM OA)
counts (dpm)
4000
3000
2000
1000
0
0
10
20
30
40
50
60
Free [^{3}H]-OA (μM)

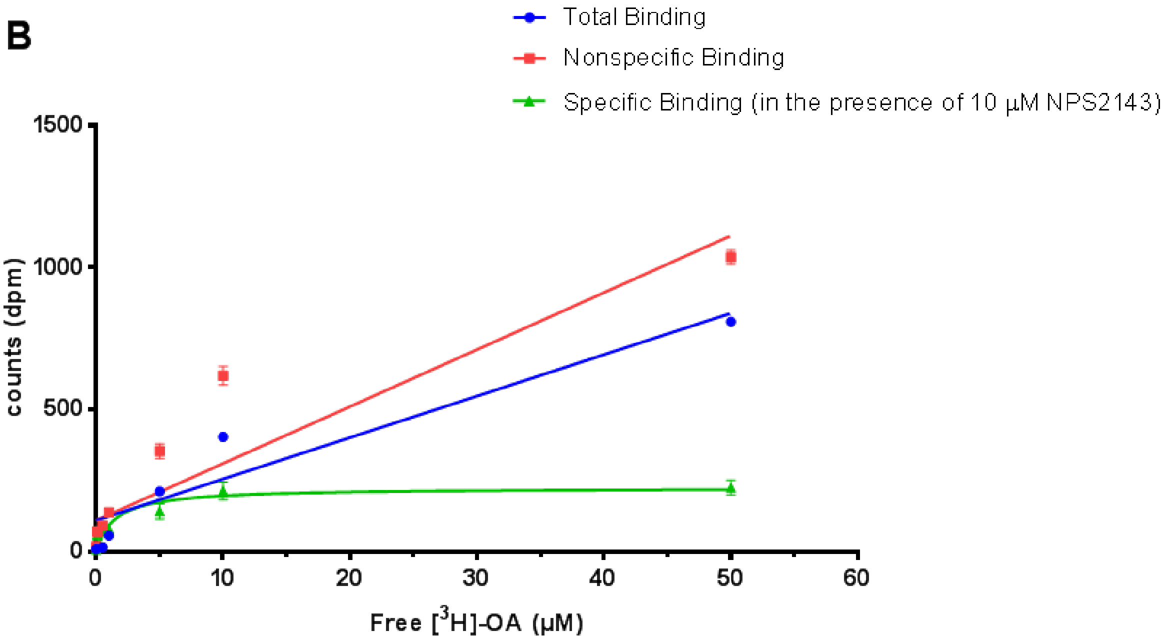
B
Total Binding
Nonspecific Binding
Specific Binding (in the presence of 10 μM NPS2143)
counts (dpm)
1500
1000
500
0
0
10
20
30
40
50
60
Free [^{3}H]-OA (μM)

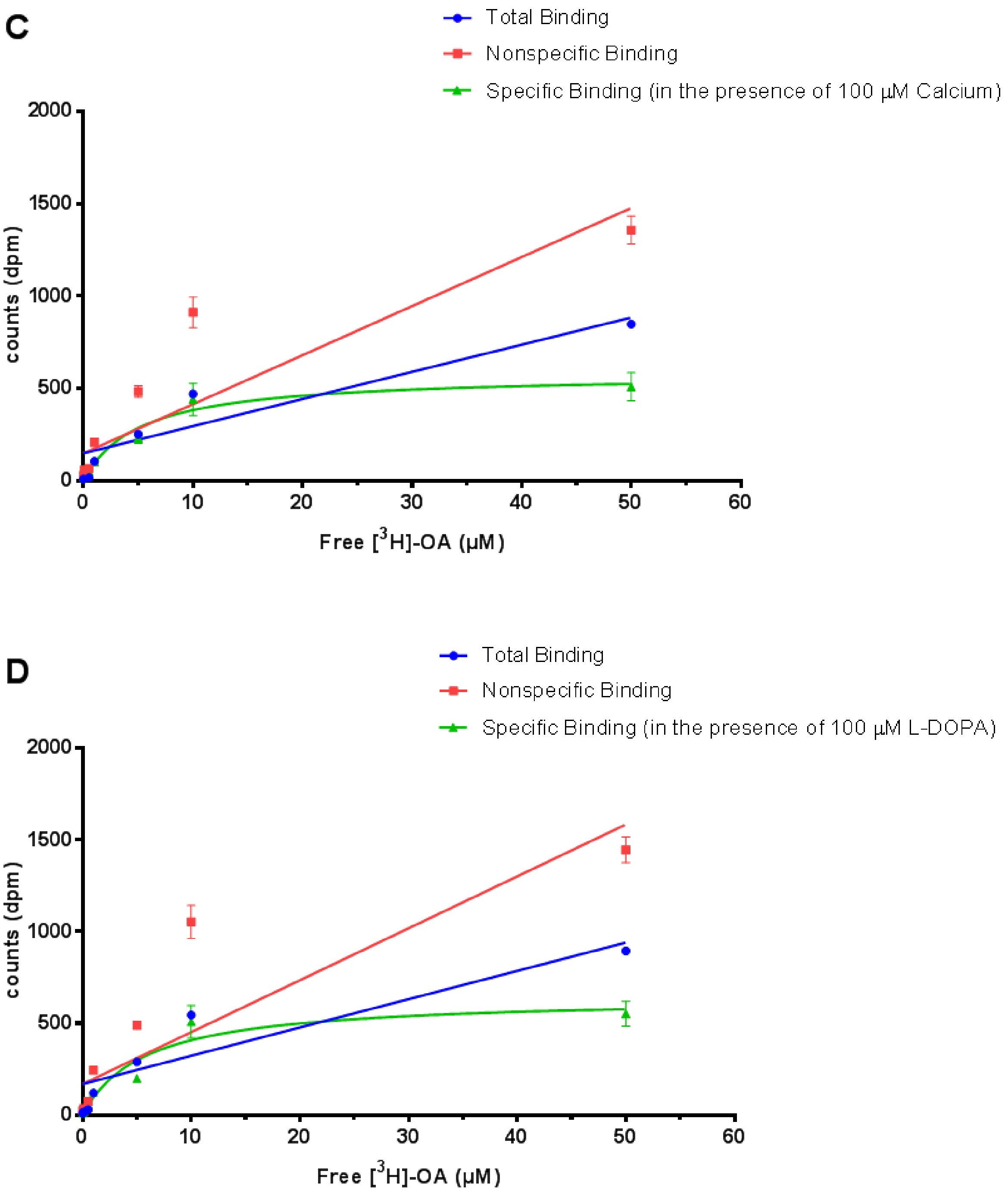

Figure 5.1. Saturation curve of [^{3}H]-OA binding to mouse brain sections in the presence of unlabelled OA, NPS2143, calcium, and L-DOPA

[^{3}H]-OA binding was carried out as described in Section 5.2.2. Non-specific binding was defined as the degree of [^{3}H]-OA binding in the presence of (a) 100 µm unlabelled OA (Kd = 2.612±0.3613 µm), (b) 10 µm NPS2143 (Kd = 1.437±0.4932 µm), (c) 100 µm calcium (Kd = 5.111±1.755 µm), and (d) 100 µm L-DOPA (Kd = 5.797±1.806 µm). The degree of binding is expressed in disintegrations per minute (dpm). Data represents binding from three experiments averaged together (36 sections for total and 36 sections for non-specific binding for each point). Data are presented as means±S.E.M.

[^{3}H]-OA is unable to be displaced by haloperidol or SKF-82958

To further confirm the specificity of the [^{3}H]-OA binding to the CaSR, agonists and antagonists for other receptors were tested. [^{3}H]-OA was unable to be displaced by SKF-82958, a dopamine receptor D1 agonist (Figure 5.2A). In the presence of haloperidol, [^{3}H]-OA was also unable to be displaced (Figure 5.2B). These negative controls, alongside the positive controls in Figure 5.1 suggest that the [^{3}H]-OA binding to the CaSR is specific.

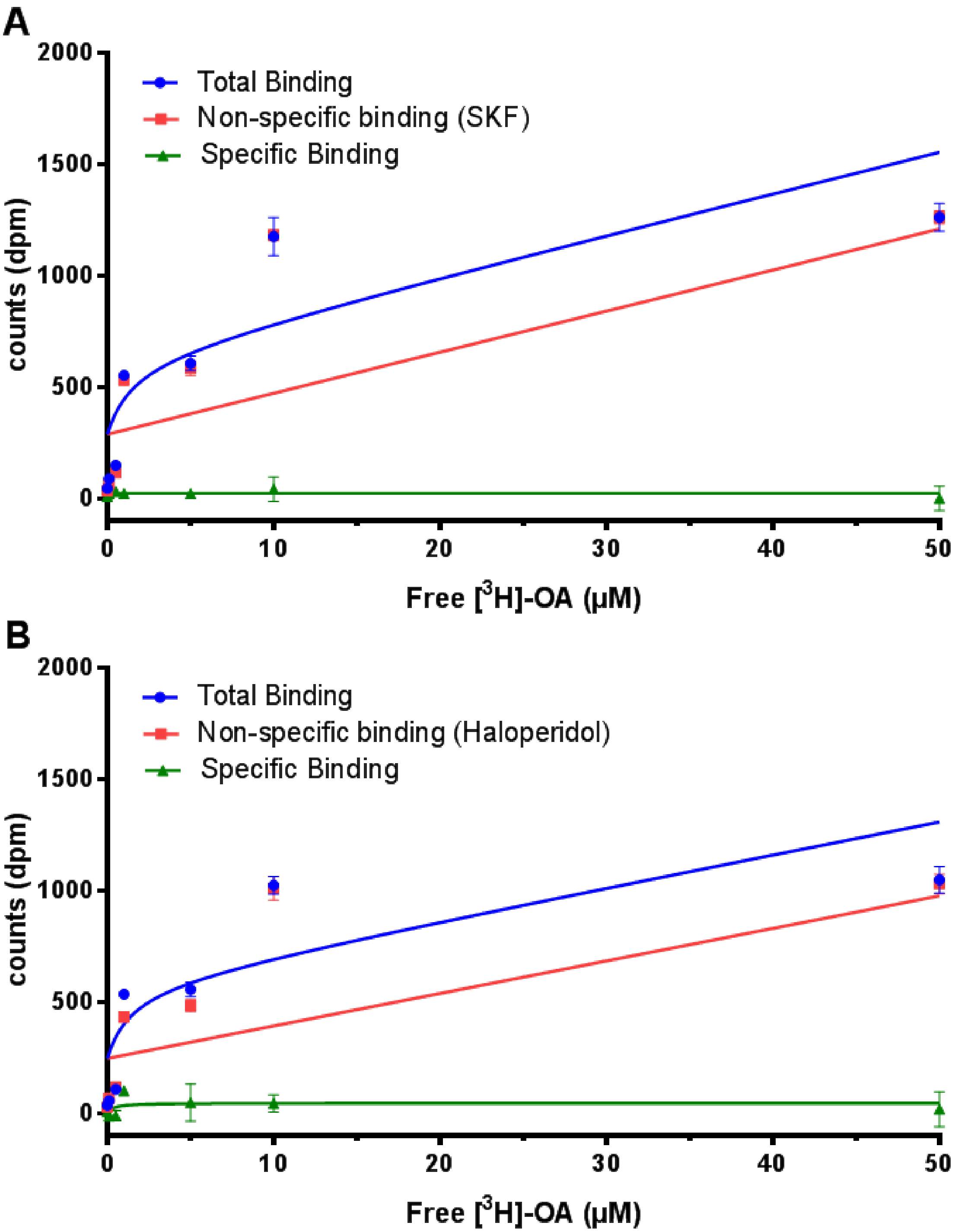

Figure 5.2. Saturation curve of [^{3}H]-OA binding to mouse brain sections in the presence of SKF-82958 and haloperidol

[^{3}H]-OA binding was carried out as described in Section 5.2.2. Non-specific binding was defined as the degree of [^{3}H]-OA binding in the presence of (a) 1µm SKF-82958 and (b) 10 µm haloperidol. The degree of binding is expressed in disintegrations per minute (dpm). Data represents binding from three experiments averaged together (36 sections for total and 36 sections for non-specific binding for each point).

Calcium, OA, and L-DOPA bind to the CaSR and decrease cAMP levels

HEK293T cells are cultured and grown in DMEM containing 10% FBS and 1% penicillin and streptomycin. After cells reach approximately 70% confluency, they are transiently transfected with the GloSensor plasmid and the CaSR plasmid. The cells are left in an incubator containing 5-10% CO_2 and 37°C for 24 hours. The following day, the cells are prepared as described in Section 5.2.4. After the cells are incubated with the GloSensor cAMP reagent for 2 hours, they are plated in a 96-well plate and then treated with calcium, OA, or L-DOPA and with or without the addition of a CaSR antagonist, NPS2143 (Figure 5.3). This demonstrates that calcium, OA, and L-DOPA are able to bind to the CaSR and activate the receptor at varying degrees of success. The addition of NPS2143 proves that the response is due to the binding of these agonists to the CaSR and not any non-specific binding.

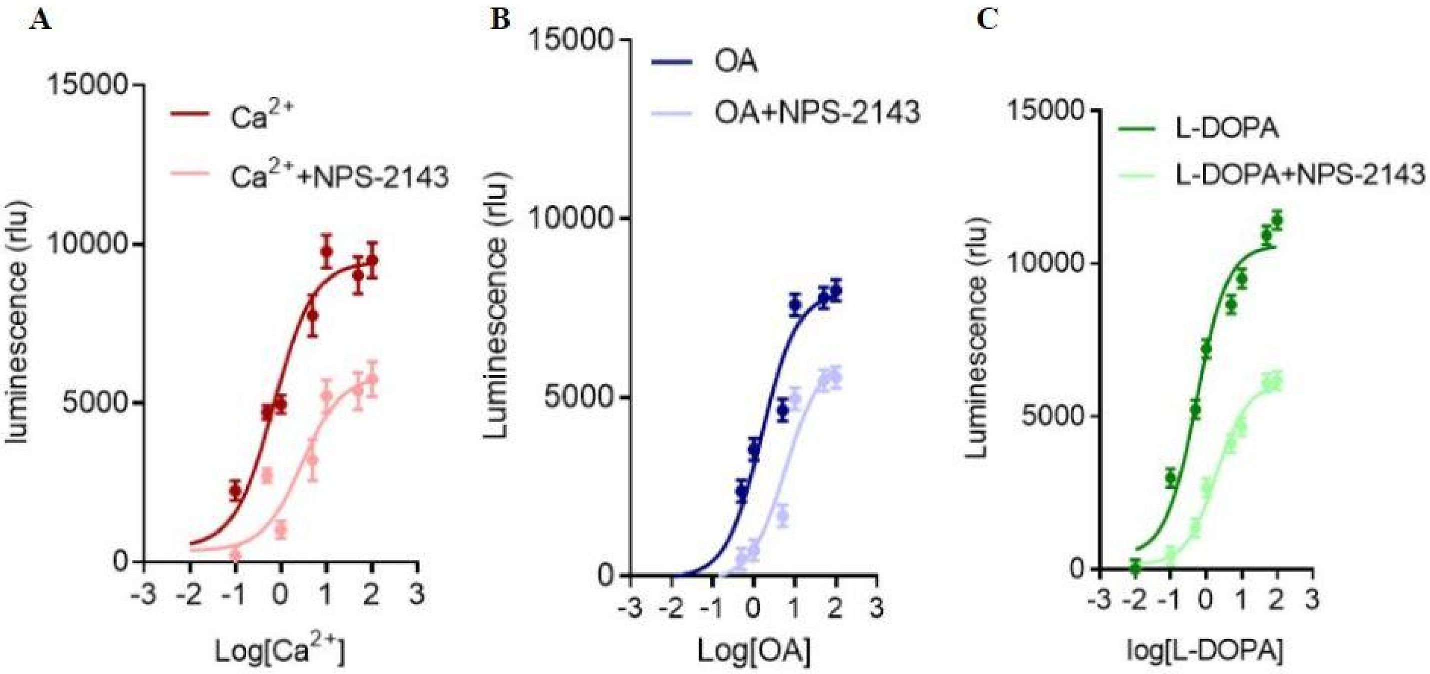

Figure 5.3. cAMP activation by OA, L-DOPA, and calcium and inhibition by NPS2143

HEK293T cells transiently transfected with the Glosensor cAMP biosensor and the CaSR plasmid show concentration-dependent increases cAMP levels, which is correlated to Relative Light Units (R.L.U.), when treated with increasing concentrations of (a) calcium (EC_{50} ~ 0.7076 μm), (b) OA (EC_{50} ~ 1.546 μm), and (c) L-DOPA (EC_{50} ~ 0.5312 μm) and decrease when treated with 10 μm NPS2143 (EC_{50} ~ 2.935 μm, 5.976 μm, 1.935 μm for calcium with NPS2143, OA with NPS2143 and L-DOPA with NPS2143 respectively). Values are expressed as mean±S.E.M. of at least three independent experiments.

L-DOPA promotes and enhances the binding of OA and calcium

HEK293T cells transiently expressing both the GloSensor and CaSR plasmids, were used to measure cAMP levels after the addition of calcium, OA, L-DOPA, and various combinations of the three. Individually, all three compounds showed similar affinities to the CaSR.

Interestingly, similar to tryptophan, it appears as though adding L-DOPA with either calcium or OA increases the efficacy of the agonists to the receptor. Adding both calcium and OA does seem to increase the potency slightly, but we hypothesize that is because what we are seeing is a compounding effect (Figure 5.4).

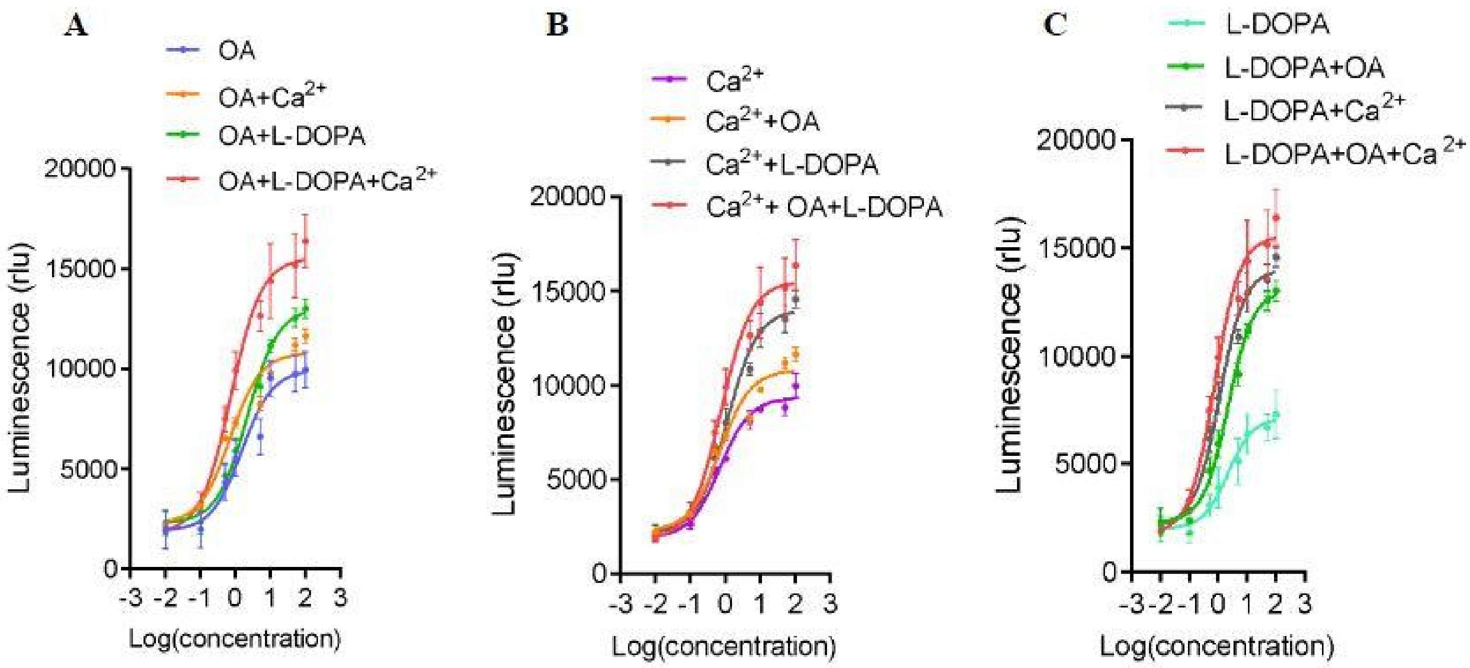

Figure 5.4. Effects of calcium, OA, and L-DOPA when given individually and in combination on cAMP levels

HEK293T cells transiently transfected with the Glosensor cAMP biosensor and the CaSR plasmid show concentration-dependent increases in cAMP levels (correlated to R.L.U.) when treated with OA, L-DOPA, calcium, and varying combinations of each. Values are expressed as mean±S.E.M. of at least three independent experiments.

NPS2143 inhibits the hyperactivity induced by L-DOPA and NSD1015

Mice were injected with MPTP, as described in Section 5.2.5. Following the MPTP treatment, the animals were injected i.p. with NSD1015, followed by either L-DOPA or L-DOPA and 5 mg/kg of NPS2143. Looking at the locomotor activity, it's clear that we no longer have the large and gradual peak that is always present after L-DOPA and NSD1015 treatment (Figure 5.5A). In fact, quantitatively, approximately half of the locomotor activity is inhibited in the group treated with NPS2143 ($P < 0.0001$, Figure 5.5B). This suggests that the CaSR, at least in part, is responsible for inducing locomotor activity.

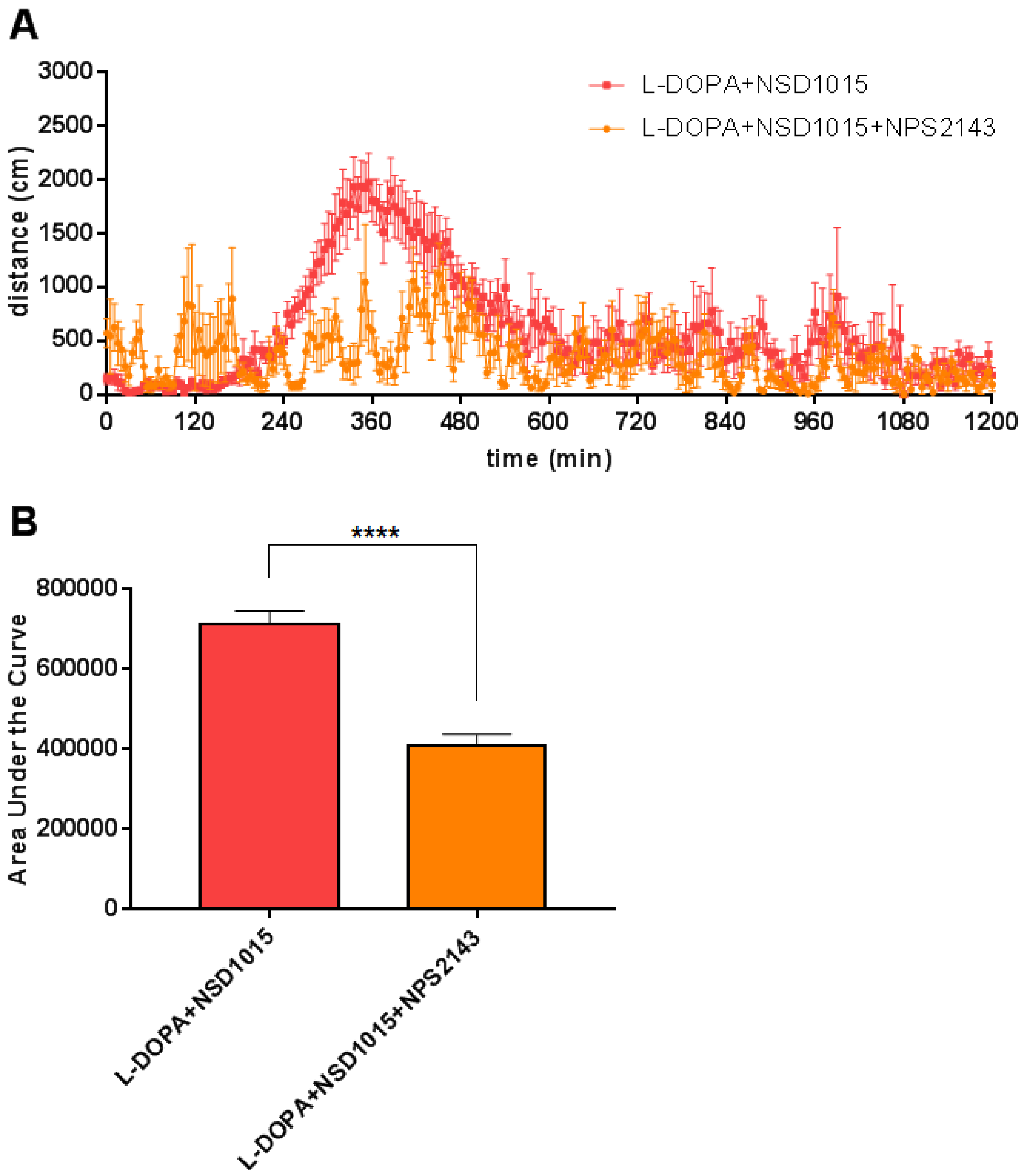

Figure 5.5. Effect of NPS2143 on locomotor activity following L-DOPA and NSD1015 treatment on MPTP-treated mice

Mice were injected with MPTP once a day for three days. (A) Locomotor activity in mice after being given NSD1015 followed by L-DOPA or L-DOPA and NPS2143 30 minutes after and the

(B) area under the curve (n = 8). Unpaired t-test (t = 7.229, $P < 0.0001$). Data are presented as means±S.E.M.

NPS2143 inhibits the locomotor activity induced by ICV OA injections in a dose-dependent manner

Mice were anesthetized and underwent surgery where a cannula was implanted for future ICV injections as described in Section 5.2.7. Following recovery, the mice were injected (i.p.) with either saline or MPTP 20 mg/kg for three days as described in Section 5.2.5. The following day, mice were injected ICV with either saline or OA at either 5 or 10 µm. Some mice were also given 10 or 20 µm of NPS2143. What we observed was that OA at 5 and 10 µm effectively stimulated locomotor activity in MPTP-treated mice, as previously demonstrated, but we also found that NPS2143 significantly inhibited this locomotor activity at both administered doses ($P < 0.0001$, Figure 5.6).

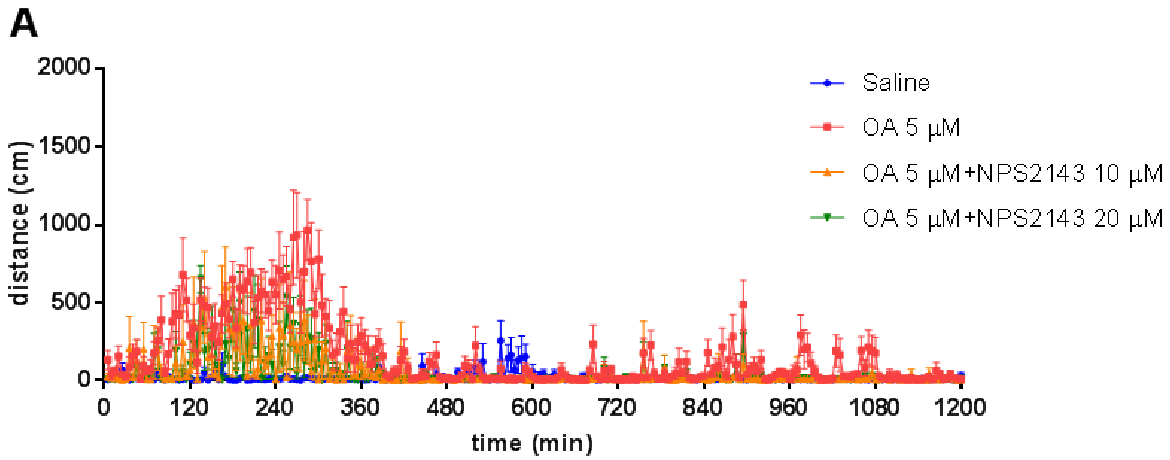
A
2000
1500
1000
500
0
distance (cm)
0
120
240
360
480
600
720
840
960
1080
1200
time (min)
Saline
OA 5 μM
OA 5 μM+NPS2143 10 μM
OA 5 μM+NPS2143 20 μM

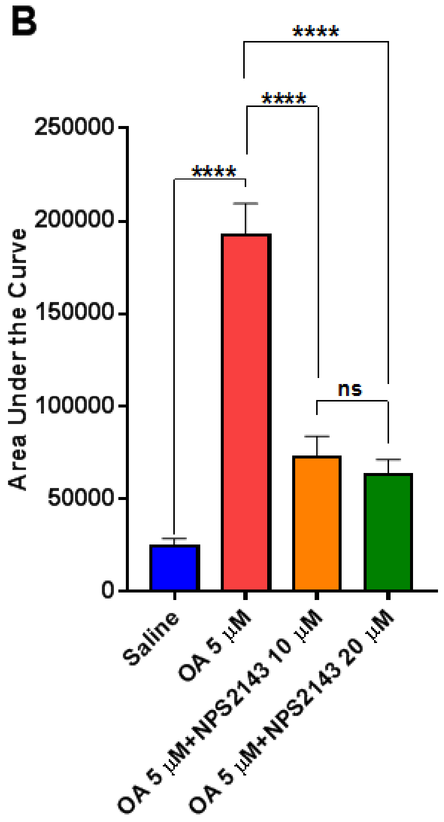
B
****
****
****
ns
250000
200000
150000
100000
50000
0
Area Under the Curve
Saline
OA 5 μM
OA 5 μM+NPS2143 10 μM
OA 5 μM+NPS2143 20 μM

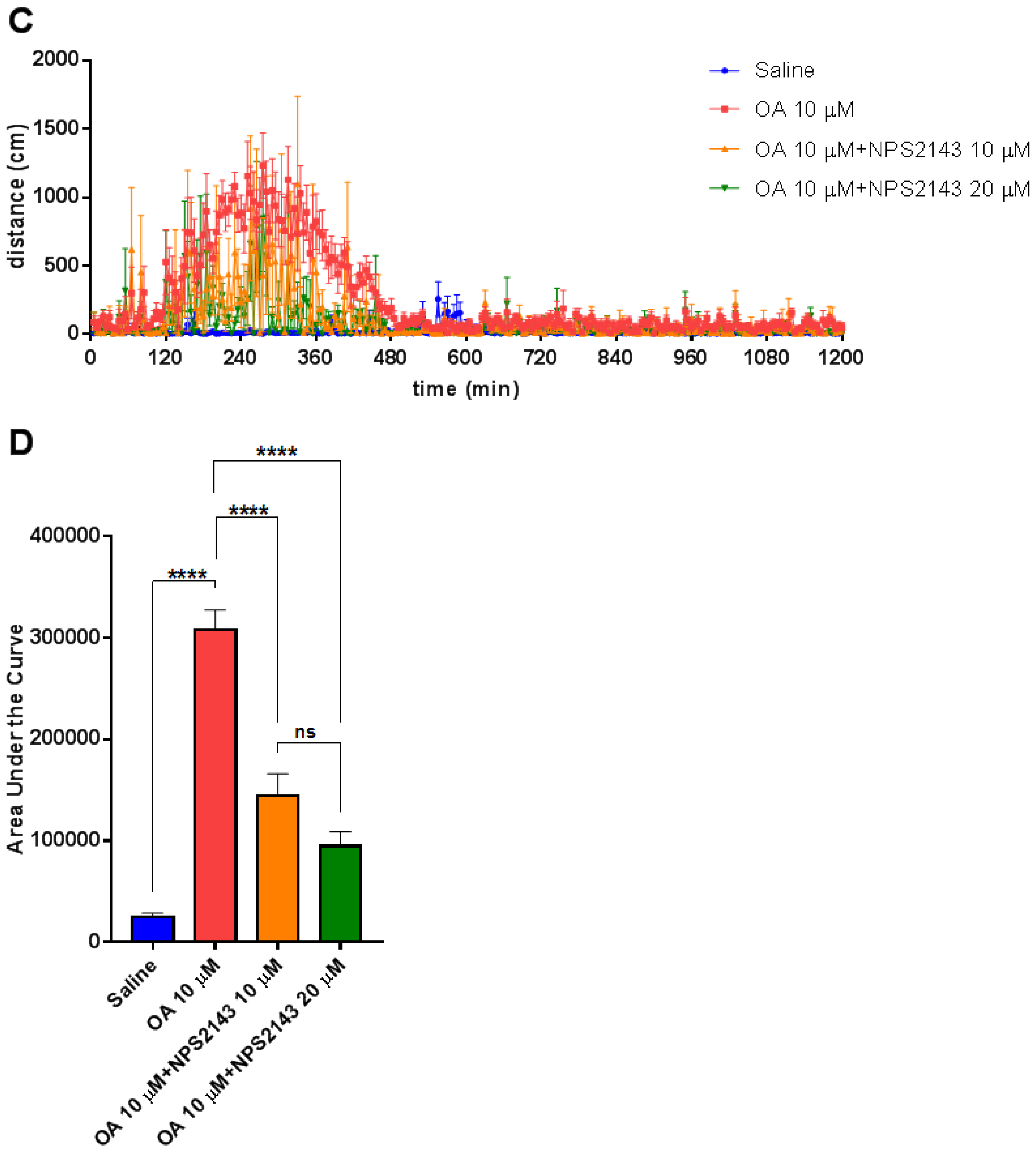

Figure 5.6. Effect of NPS2143 on locomotor activity following OA treatment on MPTP-treated mice

Mice were anesthetized and underwent surgery where a cannula was implanted for future ICV injections as described in Section 5.2.7. Following recovery, the mice were injected (i.p.) with either saline or MPTP 20 mg/kg for three days as described in Section 5.2.5. The following day, mice were injected ICV with either saline or OA at four different doses. (A) Locomotor activity in mice after being given an ICV injection of 5 µm of OA or 5 µm of OA with either 10 or 20 µm of NPS2143 and the (B) area under the curve (n = 8). One way ANOVA ($F_{3,28} = 42.09$, $P < 0.0001$) followed by the Tukey post hoc test, ****$P < 0.0001$, ns not significant. Data are presented as means±S.E.M. (C) Locomotor activity in mice after being given an ICV injection of 5 µm of OA or 5 µm of OA with either 10 or 20 µm of NPS2143 and the (D) area under the curve (n = 8). One way ANOVA ($F_{3,28} = 53.74$, $P < 0.0001$) followed by the Tukey post hoc test, ****$P < 0.0001$, ns not significant. Data are presented as means±S.E.M.

5.4 DISCUSSION

Radioligand binding is a commonly used technique to study the interactions between a ligand and a receptor. The principle behind radioligand binding is that you have a radiolabeled form of your ligand and it is allowed to interact with the receptor. The labeled ligand then competes with other agonists or antagonists for the same receptor in order to better understand the receptor-ligand binding affinities. The radiolabeled ligand can be detected and quantified and by measuring the amount of ligand that binds to the receptor we are able to determine specific properties of the ligand, such as affinity and specificity for the receptor.

Total binding refers to the amount of radiolabeled ligand that binds to the sample in the absence of any competing or displacing ligands. This includes both specific and non-specific binding. Total binding is proportional to the total amount of radiolabeled ligand added to the sample. Non-specific binding refers to the binding of a radiolabeled ligand to any other component in the sample that is not the target receptor. This binding is not saturable and cannot be displaced by a competing ligand or specific receptor antagonists. Non-specific binding is independent of the number of receptors in the sample and is typically measured in the presence of an excess of an unlabeled, non-binding ligand. By subtracting the non-specific binding from the total binding, we can calculate the specific binding. Specific binding refers to the binding of a radiolabeled ligand to a particular receptor in a sample that is specific and saturable. This binding can be displaced by the addition of a competing ligand or by specific receptor antagonists. Specific binding is proportional to the number of receptors in the sample and reflects the affinity of the ligand for the receptor.

First ran radioligand binding using [^{3}H]-OA and unlabeled OA to see if OA would bind anywhere in the brain. Because it is able to be displaced by the unlabeled OA, that means that

OA does indeed bind to somewhere in the brain (Figure 5.1A). To be more specific, we used a CaSR agonist, calcium, and antagonist, NPS2143 and we were able to see that those displace the [^{3}H]-OA as well, suggesting that the binding site of OA is indeed on the CaSR (Figure 5.1B-C). Lastly, studies have shown that L-tryptophan and calcium act as co-agonists to induce receptor activation on the CaSR. The study also showed that other tryptophan derivatives and other aromatic L-amino acids are also able to do the same thing [150]. Because of this, we decided to test L-DOPA to see if it had any affinity to the CaSR. What we saw was that it was indeed able to displace [^{3}H]-OA, suggesting that it does have some affinity to the CaSR (Figure 5.1D).

To further confirm the specificity of [^{3}H]-OA binding to the CaSR, we attempted to displace it via other receptor agonists and antagonists. This included a D1 agonist, SKF-82958, and a D2 antagonist, haloperidol, both of which failed to displace [^{3}H]-OA, suggesting that [^{3}H]-OA binding is specific to the CaSR and is not displaced by any compound (Figure 5.2).

The cAMP assay was in congruence with our radioligand binding data, suggesting that not only does OA bind to the CaSR, but it also activates the receptor. The GloSensor cAMP assay employs a bioluminescent technique that utilizes a genetically encoded biosensor to instantly detect fluctuations in intracellular cAMP levels. The assay is based on the principle that when cAMP binds to the regulatory subunit of protein kinase A (PKA), the catalytic subunit of PKA is released and triggers the phosphorylation of a target protein, which elicits a cellular response. The assay utilizes genetically engineered biosensor variants fused with cAMP-binding domains and mutated forms of photinus pyralis luciferase. Upon binding with cAMP, the luciferase enzyme undergoes changes in its structure, resulting in an upsurge in bioluminescence. As a result, cells that express the GloSensor plasmid can be used to gauge cAMP levels in real-time, without the need to disrupt the cells. The biosensor utilized in the GloSensor assay is a modified version of the PKA regulatory subunit, fused with a circularly permuted form of GFP. The binding of cAMP to the regulatory subunit triggers a conformational change, which brings together the two halves of the GFP, leading to an increase in fluorescence. The increase in fluorescence can be quantified using a luminometer, enabling the real-time tracking of variations in cAMP levels. Cells are transfected to express the GloSensor plasmid, as well as, a CaSR plasmid, so they will transiently express both. When an agonist binds to the CaSR, because it is Gi coupled, the activation of the Gi subunit leads to the inhibition of adenylyl cyclase, which in turn reduces the production of cAMP from ATP. This decrease in cAMP levels can lead to downstream effects such as the inhibition of protein kinase A, decreased activation of ion channels, and ultimately a reduction in cellular activity. Because of this, we use forskolin, which increases the levels of cAMP in cells, to increase the baseline, so after we add our agonist, we can see a decrease in the cAMP levels.

What we observed was that all of calcium, OA, and L-DOPA were able to individually bind and activate the CaSR and were all able to be blocked by the CaSR antagonist, NPS2143 (Figure 5.3). As mentioned previously, L-tryptophan and calcium act as co-agonists and different aromatic L-amino acids can enhance the binding of different agonists to the CaSR. This led us to try administering L-DOPA with calcium or with OA to see if it would behave in a similar way. When administered together we see that L-DOPA does seem to increase the efficacy of both, suggesting that L-DOPA may be enhancing or promoting OA binding to the CaSR similar to L-tryptophan and calcium.

Now that the mechanism of action has been somewhat identified, we looked to test our hypothesis in the mice. After injecting mice with MPTP for three days, the animals were injected with NSD1015 and 30 minutes later were given either L-DOPA or L-DOPA and NPS2143. The locomotor activity was recorded and we saw that the animals that were given the CaSR antagonist showed a dramatic decrease in locomotor activity (Figure 5.5B). This dramatic decrease can be attributed to NPS2143 blocking the effect of the OA that is produced in these animals as NPS2143 on its own does not affect locomotor activity (not shown).

Finally, we wanted to confirm if NPS2143 could block the OA induced locomotor activity that we showed previously. Mice were anesthetized and underwent surgery where a cannula was implanted for ICV injections as described in Section 5.2.7. Following their recovery, they were injected with MPTP as described in Section 5.2.5. The animals were then injected ICV with either saline, 5 or 10 µm of OA, and either with or without 10 or 20 µm of NPS2143. Unsurprisingly, we saw that OA induced locomotor activity in a dose dependent manner and that locomotor activity was subsequently able to be blocked by both doses of NPS2143 (Figure 5.6). This fully confirms that OA is what is inducing the hyperactivity in the L-DOPA and NSD1015 treated animals and does so by acting on the CaSR.

CHAPTER 6:

INTERGENERATIONAL TRAUMA TRANSMISSION IS ASSOCIATED WITH BRAIN METABOTRANSCRIPTOME REMODELING AND MITOCHONDRIAL DYSFUNCTION

Commun Biol. 2021, **Alhassen S**, Chen S, Alhassen L, Phan A, Khoudari M, De Silva A, Barhoosh H, Wang Z, Parrocha C, Shapiro E, Henrich C, Wang Z, Mutesa L, Baldi P, Abbott GW, Alachkar A. Intergenerational trauma transmission is associated with brain metabotranscriptome remodeling and mitochondrial dysfunction. Commun Biol. 2021 Jun 24;4(1):783

ABSTRACT

Intergenerational trauma increases lifetime susceptibility to depression and other psychiatric disorders. Whether intergenerational trauma transmission is a consequence of in-utero neurodevelopmental disruptions versus early-life mother–infant interaction is unknown. Here, we demonstrate that trauma exposure during pregnancy induces in mouse offspring social deficits and depressive-like behavior. Normal pups raised by traumatized mothers exhibited similar behavioral deficits to those induced in pups raised by their biological traumatized mothers. Good caregiving by normal mothers did not reverse prenatal trauma-induced behaviors, indicating a two-hit stress mechanism comprising both in-utero abnormalities and early-life poor parenting. The behavioral deficits were associated with profound changes in the brain metabotranscriptome. Striking increases in the mitochondrial hypoxia marker and epigenetic modifier 2-hydroxyglutaric acid in the brains of neonates and adults exposed prenatally to trauma indicated mitochondrial dysfunction and epigenetic mechanisms. Bioinformatic analyses revealed stress- and hypoxia-response metabolic pathways in the neonates, which produced long-lasting alterations in mitochondrial energy metabolism and epigenetic processes (DNA and chromatin modifications). Most strikingly, early pharmacological interventions with acetyl-L-carnitine (ALCAR) supplementation produced long-lasting protection against intergenerational trauma-induced depression.

6.1 INTRODUCTION

Intergenerational trauma increases lifetime susceptibility to depression and is a major risk factor for developing multiple neuropsychiatric disorders such as post-traumatic stress disorder (PTSD), autism spectrum disorder (ASD), and schizophrenia [160-163]. Major depressive disorder (MDD) affects millions of people globally who have been subject to stress and trauma at some times of their lives. While stress deleteriously impacts humans worldwide and attacks all segments of societies at this moment in human history, it is disproportionately devastating to individuals in vulnerable situations such as pregnant women. Unlike other vulnerable conditions, the deleterious impacts of stress during pregnancy are doubled as they affect the mental health of the mothers and the unborn offspring. Human natural experiments provide evidence for the devastating health consequences in offspring as a result of exposure during pregnancy to existential and acute trauma such as war and natural disasters [164-166].

Whether intergenerational trauma transmission and its negative outcomes are a consequence of in utero fetal neurodevelopment disruptions or from poor maternal care by traumatized mothers is still largely ambiguous. This ambiguity is mainly due to the complexity, superposition, and inseparability of prenatal and postnatal mechanisms that are not mutually exclusive.

Converging evidence from human and animal studies supports that exposure to stress during pregnancy negatively affects maternal behavior towards, and the care of, offspring [167-169]. On the other hand, maternal stress can affect offspring mental outcomes through prenatal programming, particularly epigenetic mechanisms causing permanent neuronal impairments and poor offspring outcomes that persist throughout life [170-172]. Yet, it is difficult to test the mechanistic involvement of prenatal stress independent of stress effects on the mother's care. The limitations in our understanding of the neurobiological and pathophysiological mechanisms of stress-induced depression, particularly the lack of measurable biochemical and molecular alterations, hamper effective pharmacological interventions to prevent or ameliorate the behavioral deficits.

Therefore, the goal of this work is to we examine the distinctive behavioral impacts and neurobiological mechanisms of in utero exposure alone (prenatal one-hit stress) versus impaired maternal care alone (postnatal one-hit stress) or combined exposure (prenatal and postnatal two-hits stress). We hypothesized that prenatal stress acts as a priming factor that synergistically interacts with subsequent early-life challenges (inadequate caregiving by traumatized mothers) to exacerbate the tendency for offspring of traumatized mothers to develop psychiatric disorders later in life.

To recapitulate intergenerational trauma experience, we modeled stress by exposing mouse dams in the last four days of their pregnancy to a predator odor. We applied cross-fostering procedures to evaluate the distinct contributions to adult behavioral deficits of prenatal trauma and subsequent postnatal inadequate caregiving. We used a comprehensive approach combining metabolomic, transcriptomic, and bioinformatic analyses to determine the molecular processes that are associated with stress-induced behavioral deficits. Based on our findings of the mechanisms involved, which revealed a role for mitochondria metabolism dysfunctions, we examined whether the behavioral deficits can be reversed by early and/or late supplementation with acetyl-L-carnitine (ALCAR).

6.2 MATERIALS AND METHODS

Animals and breeding procedures

Eight-week-old Swiss Webster mice were obtained from Charles River Laboratories (Wilmington, MA). Mice were maintained on a 12-h light/dark cycle (light on at 7:00 am). One male and two female mice were group-housed, and pregnant mice were individually housed from the fourteenth day of pregnancy (gestational day 14) until delivery. After weaning (postnatal day 21), male mice were group-housed separately (Figure 6.1a). All experimental procedures were approved by the Institutional Animal Care and Use Committee of University of California, Irvine and were performed in compliance with national and institutional guidelines for the care and use of laboratory animals.

Predator scent (PS) exposure and cross-fostering

On gestational day 17, the pregnant mice were exposed to a predator scent (2,5-dihydro-2,4,5-trimethylthiazoline, or TMT, a constituent of fox urine) for 1 h on each of four consecutive days in a separate cage under the fume hood and were then returned to their home cage. Bedding mixed with a few drops of distilled water (Control, C) or 0.02% TMT (Stress, S) was placed in a 60 × 15 mm polystyrene plate placed in each cage to achieve scent exposure [233-236].

Maternal behavior: pups' retrieval assay with postpartum mice

Maternal behavior was examined in predator-odor-exposed dams and control dams using pups' retrieval assay [237]. The assay was conducted on PPD2, in which, a maximum of 5 min of video recording time to calculate the mother's latency and duration. The mother was temporarily removed from the cage, and pups were removed except for three pups, which were placed on each of the three corners of the cage (not the nest corner). The mother was then returned to her nest and the latency and duration of pups' retrieval were recorded.

Cross-fostering mouse model and animal care

Pups (control, c or stress, s) of control (C) and stress (S) mothers were raised by their biological mother (c → C and s → S) or were cross-fostered to the opposite mother treatment (s → C and c → S, for control mothers with stress pups or stress mothers with control pups, respectively) within 24-h of birth. The pups remained with either their biological or foster mother until the weaning day (postnatal day 21). Subsequently, the male mice were then selected for the study and group-housed in groups ranging from 3 to 5.

Behavioral analyses

Male mice were tested from postnatal week 8 to week 13 with a battery of behavioral paradigms in the following order: locomotion and stereotypy/open field, social interaction, spontaneous T-maze alternation, novel object recognition, elevated plus maze, forced swim, contextual fear conditioning (Figure 6.1a). The sequence of specific assays spaced by 3-6 days inter-assay interval was adapted from previous reports [238,239]. In subsequent cross-fostering behavioral studies, mice were tested only in social interaction and forced swim assays. In ALCAR behavioral studies, mice were tested only in one behavioral assay (forced swim).

Locomotor activity

Mice were placed into a locomotion test chamber (Med Associates, Inc.) for 90 min as we previously described [240]. The first 30 min was allotted for the animal to habituate to the chamber before the test. The horizontal, vertical, and stereotypic activities were then recorded for the remaining 60 min and were then analyzed by the Activity Monitor 5 software (Med Associates, Inc.).

Open field assay

Prior to testing, the open field test chamber (40 × 40 cm, Med Associates, Inc.) was sectioned into a central zone, a 24 × 24 cm square in the middle of the test chamber, and a peripheral zone, the remaining outer area [241]. Mice were placed in the chamber and the time the animal spent within 10 min in the central or peripheral zones was recorded. Using the predetermined zone areas, the center-to-periphery exploration time ratio was assessed by the Activity Monitor 5 software (Med Associates, Inc.).

Elevated plus maze

A standard elevated plus-maze, made of gray Plexiglas, was placed in a sound-proof observation room with controlled light (200 Lux) on the central platform of the maze [242]. Animals were given a 30-min period to habituate to the room before being tested. During the test, the mice were placed in the center of the plus facing an open arm and were given 5 min to explore. The behavior was recorded and scored by two independent observers blind to the animal treatments. The animals were scored based on time spent in the closed and open arms and the number of entries to the closed and open arms.

Social interaction

The social interaction test was performed using the three-chambered apparatus [241]. Two wire mesh cups were placed in the middle of both the right and left chamber (one on each side). In one of the cups on either side, a control mouse (an unfamiliar mouse of the same strain, gender, and age with no prior contact with the subject mouse) was placed. The subject mouse was placed in the middle chamber and was given 5 min to explore with the dividing doors closed. The dividing doors were then removed to allow the mouse to freely travel between the three chambers for 10 min. The duration of direct contact between the subject mouse and both the empty cup and the cup with the mouse was measured. The relative exploration time was recorded and expressed by a discrimination index: [D.I. = $(T_{mouse} - T_{empty})/(T_{mouse} + T_{empty}) \times 100\%$]. The test was video recorded and analyzed by the ANY-MAZE software (Stoelting Co.).

Spontaneous T-maze alternation assay

The T-maze has three designated parts: the main stem, the side arms, and the starting area (AccuScan Instruments, Inc.) [241]. The mice were placed in the starting area behind a sliding door, blocking the main stem and side arms and were given a 30 s acclimation period before the start of each trial. After the acclimation period, the sliding door was removed, and the mice can choose either the left or right-side arm. After a choice (all four paws in the chosen arm), the sliding door was closed behind the animal, allowing the mouse to explore the chosen arm for 30 s, before being manually returned to the start area for the next trial. A total of eight trials were completed, allowing for a total of seven total possible alternations. The alternation percentage was calculated as 100 x (number of alternations/7). The time for the animal to decide on a side arm (decision latency) was also recorded.

Novel object recognition assay

The novel object recognition (NOR) assay consists of training and testing phases [240]. Prior to training, the mice were handled for 1–2 min a day for 3 days and were given 10 min a day for 3 days inside the empty experimental apparatus to habituate to the environment. During the training phase, mice were placed in the experimental apparatus, and were given 10 min to explore and examine two identical objects. Twenty-four hours later, one of the familiar objects was replaced with a novel object and the animals were given 5 min to explore the chamber. During both the training and testing phases, the duration and number of times the mice interact with the familiar and novel objects were recorded individually. The relative exploration time was recorded and expressed by a D.I.: Equation (1) [D.I. = $(T_{novel} - T_{familiar})/(T_{novel} + T_{familiar}) \times 100\%$]. Tests were video recorded and analyzed by the ANY-MAZE software (Stoelting Co.).

Forced swim

The forced swim assay was performed as previously described [243]. During the 6-min assay, the first 2 min of activity was discarded. For the last 4 min, mice were videotaped and the immobility time was recorded. The ANY-MAZE software was used to record and analyze immobility (Stoelting Co.).

Contextual fear conditioning assay

The Contextual Fear Conditioning Assay was performed as previously described [240]. The assay was split into a training and retention session. Prior to the training session, mice were handled for 1–2 min per day for 3 days. During the training session, mice were placed in the conditioning chamber (TSE Systems, Inc.), with a striped pattern, for 2.5 min, before receiving a 0.7 mA foot shock for 2 s. After an additional 30 s, the mice were returned to their home cages. The freezing behavior (lack of movement for at least 3 s in a 5 s interval) pre-shock and post-shock were measured. Twenty-four hours after training, the mice were placed in the chamber again, with the same striped pattern, for 5 min and the freezing behavior, without shock, and was assessed. Freezing behavior was scored as freezing (1) or not (0) for every 5 s interval and the percentage of freezing behavior was calculated as 100 x (number of freezing intervals/total intervals).

Acetyl-L-carnitine (ALCAR) treatment

The ALCAR treatment protocol was adapted from a previously reported protocol [229]. The s → S mice received ALCAR (0.3%, Sigma Aldrich) in the drinking water either on postnatal day 21 (PPD 21 weaning day) and continued to week 8, or on week 7 and continued to week 8. Control groups received normal tap water. Forced swim tests were carried out on the last day of the treatment and 7 days after discontinuing ALCAR.

Immunohistochemistry

Immunohistochemistry methods to examine the Arc positive (Arc^+) neurons were conducted as we previously described [243]. Mice were perfused under isoflurane anesthesia with 4% paraformaldehyde (PFA), and brains were removed, post-fixed in 4% PFA for overnight at 4 °C, and stored in 30% sucrose. Coronal sections were cut at 20 μm thickness, and three sections were used from each region of interest. Brain regions were defined according to their anatomy using the mouse brain atlas [244]. Sections were blocked with 4% normal goat serum in PBS with 0.3% Triton X-100 for 1 h, and were then incubated in the blocking buffer that contains the primary antibodies (Arc 1:500, Sigma). The sections were then washed with PBS, incubated with the secondary antibody (1:500) for 1 h, then with 4′,6-diamidino-2-phenylindole (DAPI) for 5 min, and were then mounted on slides. Imaging was carried out using Leica Sp8 TCS confocal microscope (UCI optical biology core facility). Arc positive (Arc^+) neurons were counted in the bilateral areas of each section, and the mean counts of three non-consecutive sections per brain of 3–5 brains were calculated. Cell counts were performed using ImageJ [245], and confirmed manually by two persons blind to the experiment conditions.

Brain metabolite analyses

Tissues of one brain hemisphere (cortical-subcortical/mouse) were collected from neonatal and adult mice, and extracted following the protocols first published in [246]. Metabolic profiling was carried out by the West Coast Metabolomics Center (University of California Davis). Three metabolic platforms were profiled: (1) primary metabolites including hydroxyl acids, purines, pyrimidines, carbohydrates and sugar phosphates, amino acids, and aromatics, (2) lipids, and (3) biogenic amines and methylated and acetylated amines [247].

mRNA microarray analysis

Microarray experiments and analysis were performed as we previously described [240,248]. Total RNA was extracted (Qiagen RNA extraction kit) from one brain hemisphere of the 24-h and 13 weeks' old pups according to the manufacturer's protocol. RNA samples with A260/A280 absorbance ratios between 2.00 and 2.20 were reverse-transcribed into cDNA and analyzed by "whole-transcript transcriptomics" using the GeneAtlas microarray system (Affymetrix) and manufacturer's protocols. MoGene 2.1 ST array strips (Affymetrix) were used to hybridize to newly synthesized ss-cDNA. Each array comprised 770,317 distinct 25-mer probes to probe an estimated 28,853 transcripts, with a median 27 probes per gene. Only annotated genes were included in the differential analysis.

Real time quantitative polymerase chain reaction (RT-qPCR)

RNA was reverse-transcribed into cDNA using the Transcriptor First Strand cDNA synthesis kit (Roche Molecular Systems, Inc) following manufacturer's instructions. RT-qPCR was performed using the LightCycler480 SYBR Green I Master kit (Roche Molecular Systems, Inc), and analyzed using the amplification reactions carried out on a LightCycler® 480 instrument with gene specific primers. Samples from 5 animals were run in duplicates and averaged. The comparative CT method was used to obtain the Ct values from each RNA sample and normalized to a housekeeping gene (GAPDH) [249]. The difference between the Ct values (ΔCt) of the gene of interest and the housekeeping gene was calculated for each sample and the difference in the ΔCt values between the experimental and control samples ΔΔCt was calculated. Fold change was obtained as 2^(−ΔΔCt) [240]. The following primers were used (5′–3′):

MCM6

Forward CGACAGCTTGAGAGCATGATCC,

Reverse TGACATCAGGCGTCTCTACACG;

AVP

Forward GCTACTTCCAGAACTGCCCAAG,

Reverse CAGCAGATGCTTGGTCCGAAGC;

VGF

Forward CGGACTGGAACGAAGTACTC,

Reverse GTTTGGGAAGGGGTGATAGG;

C1QL1

Forward AG TATGTGGGCAGACCTCTGCA,

Reverse CCAGCTTGATGAAGACCTCGTC;

FOS

Forward GATGTTCT CGGGTTTCAACG,

Reverse GGAGAAGGAGTCGGCTGG;

EGR1

Forward GTCACCTCCGCC TCCCCCAACC,

Reverse GGCGGCGATAAGAATGCTGAAGGA;

GAPDH

Forward CATCCCA GAGCTGAAC,

Reverse TCAGATGCCTGCTTCAC.

Bioinformatic analysis of metabolomics and transcriptomics, and metabolites-transcriptomic Integration

The bioinformatic analysis of the differential metabolites differential genes was conducted as we described previously [247]. A differential analysis was performed between the s → S and c → C groups for both 24-h old pups and 13-week old adult mice groups using the Cyber-T program [247,251] to identify the top up- or downregulated metabolites, using p-value cutoff at 0.05. The metabolic pathway enrichment analysis was performed on the differentially expressed metabolites using Fisher exact test, which is based on a hypergeometric distribution, to identify enriched pathways from the Small Molecule Pathway Database [252,253]. The inputs of the 2×2 contingency table used for the Fisher exact test were: number of metabolite hits, number of metabolite non-hits, number of non-hits in metabolites associated with the pathway, and number of background metabolites. Pathways with *p*-value less than 0.05 were considered enriched in the given list of metabolites. Differentially expressed genes in s → S and c → C groups for both neonatal and adult mice were identified using Transcriptome Analysis Console (TAC) with *p*-value cutoff at 0.05, and the transcriptomic data underwent further analyses. These analyses were: (1) pathway enrichment analysis using fisher exact test on pathways from the Pathway Common Database [252] and the ConsensusPathDB [253], and STRING analysis (https://string-db.org/); (2) upstream transcription factor binding site (TFBS) enrichment analysis of promoters using the promoters and their target genes identified by the MotifMap database [254,255] and the CHiPSeq database from ENCODE; [256] (3) identification of transcription factors (TFs) and RNA-binding proteins (RBP) and analyses of their differentially expressed downstream targets using MotifMap and CHiPSeq databases.

For Integrated metabolite-transcriptomic analysis, metabolites were identified by InChI Key or name in Human Metabolome Database (HMDB) [257]. Enzymes and enzyme-coding genes involved in metabolic reactions of the metabolites were queried from the biological properties section of the database. The transcriptomic expression of those enzyme-coding genes in s → S and c → C groups was extracted from the microarray data. In this way, the activity of the metabolites and their enzyme-coding genes in the s → S and c → C groups were linked together for holistic analysis. Network graphs were constructed with nodes being a metabolite or a gene, and edges being a known reaction between the metabolite and enzyme coded by the gene.

Integrated mouse-human transcriptomic analysis

The DEGs in both adult and newborn mouse groups from the transcriptomic analysis were compared with DEGs in human depression [258]. The overlaps between DEGs common to stress mice and human depression were computed for adult and newborn mouse groups using Fisher exact test.

Statistics and reproducibility

Statistical analyses of behavioral data were carried out using GraphPad Prism (GraphPad Software, Inc.). Data were presented as means ± S.E.M. Results were analyzed by unpaired student *t*-test, one-way, and two-way ANOVA followed by the appropriate post hoc comparisons, and $P < 0.05$ was considered statistically significant.

6.3 RESULTS

s → S pups display depressive-like behavior, social impairment, but normal cognitive functions

Compared to the offspring of control dams (c → C), the offspring of dams exposed to the predator scent (s → S) exhibited normal locomotor activities (Figure 6.1a–c). The c → C and s → S mice travelled similar distances in the center and peripheral area in the open field assay ($P > 0.05$, unpaired *t*-test, Figure 6.1d), and displayed similar times and number of entries to the open arm of the elevated maze ($P > 0.05$, unpaired *t*-test, Figure 6.1e–h), indicating normal anxiety behavior in the s → S mice. In the social interaction assay, s → S mice displayed less interaction with the unfamiliar mice than did the c → C group ($P < 0.001$, two-way ANOVA, followed by Bonferroni posttest, Figure 6.1i), and their D.I. was significantly lower ($P < 0.001$, unpaired *t*-test, Figure 6.1j), indicating impaired sociability in the s → S mice. The s → S mice displayed depressive-like behavior, reflected by their higher immobility time in the forced swim test compared to the c → C mice ($P < 0.05$ unpaired *t*-test, Figure 6.1k).

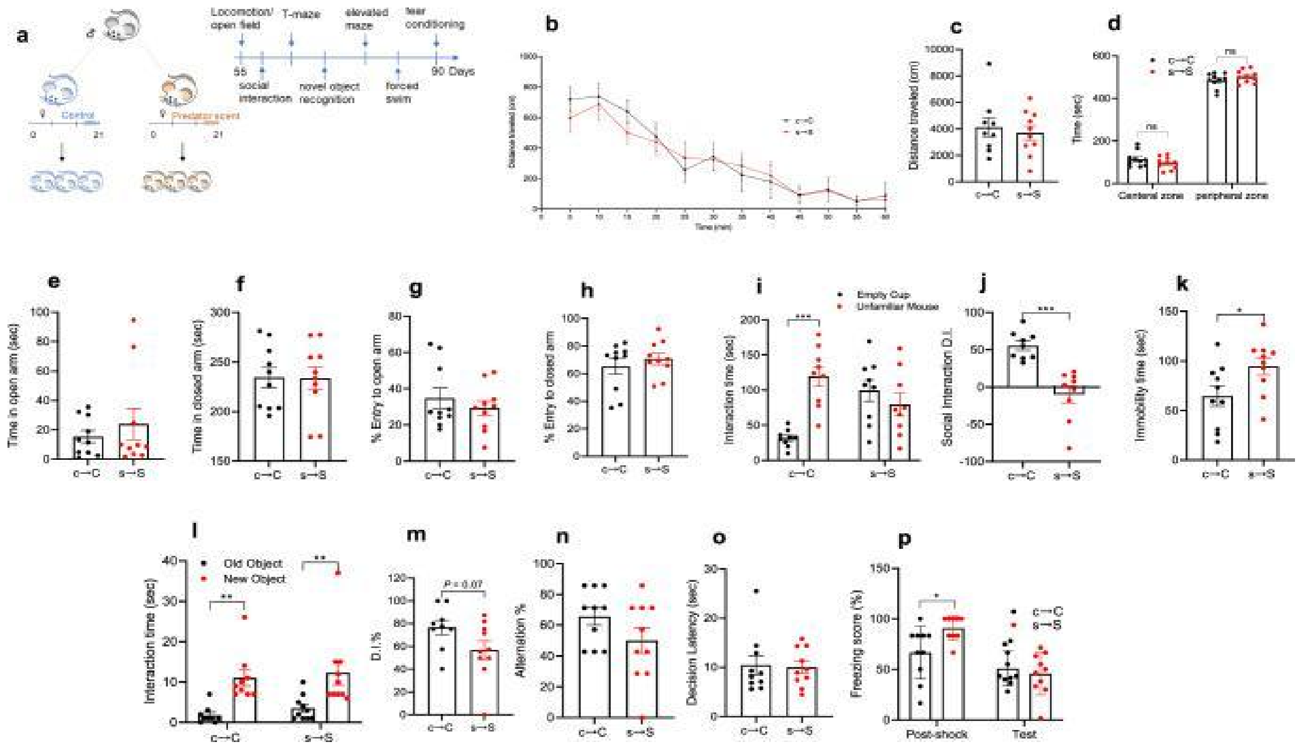

Figure 6.1. The s → S pups display depressive-like behavior, social impairment, but normal cognitive functions

(a) Schematic of the experiment design. (b,c) s → S pups display normal locomotor activity. (b) Time-course of the locomotor activity, (c) Distance mice traveled in 60 min of the locomotion assay ($n = 10$ c → C, 10 s → S). Unpaired student test ($t = 0.2723$, $P = 0.7885$): c → C vs s → S, ns not significant ($P > 0.05$). Data are presented as means ± S.E.M. (d) Time mice spent in the central and peripheral zones in 10 min in the locomotion assay ($n = 10$ c → C, 10 s → S). Two-way ANOVA revealed a significant zone effect ($F_{1,36} = 1453$, $P < 0.0001$) followed by Bonferroni post hoc test: c → C vs s → S, ns not significant ($P > 0.05$). (e, f) Elevated plus maze measure of time spent in (f) Closed (unpaired t-test; $t = 0.788$, $P = 0.44$), and (e) open arms (unpaired t-test; $t = 0.788$, $P = 0.44$). (g, h) Elevated plus maze measure of percent entry to (h) Closed (unpaired t-test; $t = 0.05$, $P = 0.95$), and (g) open arms (unpaired t-test; $t = 0.74$, $P = 0.46$). (i) Time mice spent interacting with empty cup and unfamiliar mouse in the social interaction assay ($n = 9$ c → C, 9 s → S). Two-way ANOVA: stress effect ($F_{1,32} = 6.783, P = 0.0138$), stress x object interaction ($F_{1,32} = 16.88, P = 0.0002$) followed by Bonferroni post hoc test: empty cup vs unfamiliar mouse, ****$P < 0.0001$, ns not significant ($P > 0.05$). (j) Discrimination index in the social interaction assay ($n = 9$ c → C, 9 s → S). Unpaired student test ($t = 5.053, P = 0.0001$): c → C vs s → S, ***$P < 0.001$. (k) Time mice spent immobile in the forced swim assay ($n = 10$ c → C, 10 s → S). Unpaired student test ($t = 2.27, P = 0.0358$): c → C vs s → S, *$P < 0.05$. (l) Time mice spent exploring both the new and old objects during the test session in the novel object recognition assay ($n = 9$ c → C, 10 s → S). Two-way ANOVA revealed a significant stress effect ($F_{1,34} = 21.79, P < 0.0001$) followed by Bonferroni post hoc test: old object vs new object, **$P < 0.01$. (m) Discrimination index in the novel object recognition assay ($n = 9$ c → C, 10 s → S). Unpaired student test ($t = 1.904, P = 0.074$): c → C vs s → S, ns not significant ($P > 0.05$). (n) Percentage of the alternation choice mice made in the T-maze spontaneous assay ($n = 10$ c → C, 10 s → S). Unpaired student test ($t = 1.558, P = 0.1366$): c → C vs s → S, ns not significant. (o) Time mice spent to make a decision in T-maze spontaneous assay ($n = 10$ c → C, 10 s → S). Unpaired student test ($t = 0.2029, P = 0.8415$). (p) Percentage of freezing behavior in contextual fear conditioning assay ($n = 10$ c → C, 10 s → S). Two-way ANOVA revealed a significant stage effect ($F_{1,35} = 22.82, P < 0.001$) and stress x stage interaction ($F_{1,35} = 5.260, P = 0.0279$) followed by Bonferroni post hoc test: c → C vs s → S, *$P < 0.05$, ns not significant ($P > 0.05$).

We investigated whether the prenatal stress caused cognitive dysfunction, by testing object memory, working memory, and contextual fear memory. In the novel object recognition assay, both groups spent more time exploring the new object than the old object ($P < 0.01$, two-way ANOVA, followed by Bonferroni posttest, Figure 6.1l), the D.I. in the s → S mice was not different compared to the c → C mice ($P = 0.07$, unpaired *t*-test, Figure 6.1m). In the spontaneous T-maze alternation assay, s → S and c → C mice showed a similar percentage of arm choice alternation and decision latency ($P > 0.05$, unpaired *t*-test, Figure 6.11n, o). In the contextual fear-conditioning assay, the s → S group exhibited higher freezing behavior during the stimulus session ($P < 0.05$), but not in the retention session ($P > 0.05$, two-way ANOVA, followed by Bonferroni posttest, Figure 6.11p). Together, these results suggest that s → S mice display normal cognitive function.

Mothers exposed to predator scent exhibited deficits in maternal behavior, and depressive-like behavior, but not locomotor activity or anxiety behavior

The exposure to the predator scent triggered fear-like responses in the mother mice, displayed by escape behavior (avoidance) and heart palpitations. Pup retrieval is a key indicator of maternal care. At postpartum day 2 (PPD2), stressed mothers (S) retrieved pups with significantly higher latencies (time to retrieve the first pup) and longer retrieval duration (retrieval of three pups) compared to the control mothers (C) ($P < 0.05$ and $P < 0.001$, for latency and duration respectively). In the forced swim test on PPD5, the S mothers exhibited higher immobility time than C mothers ($P < 0.001$, Figure 6.1c), indicating increased depressive-like behavior in these mice. Other behaviors of mothers including locomotor activity and anxiety behavior were normal.

Prenatal stress results in alterations in brain metabolomics

Global brain metabolomics analysis of neonatal pups revealed that prenatal exposure to stress-induced alterations in 50 brain molecules (Figure 6.2a), of which the mitochondrial metabolite 2-hydroxyglutaric acid (2-HG) displayed the highest increase in the brains of neonatal s → S pups (Figure 6.2b). 2-HG is a hypoxia and mitochondrial dysfunction marker, and an epigenetic modifier [173-176]. Therefore, its striking increase in the brains of the s → S pups within the first 24 h after birth indicates disruptions in mitochondrial respiratory functions and epigenetic processes. Alongside 2-HG elevated levels, the levels of tricarboxylic acid (TCA) cycle metabolites succinic acid and γ-aminobutyric acid (GABA) significantly increased in the brains of the neonatal s → S pups (Figure 6.2b, c). Beside its role as a neurotransmitter, GABA regulates the TCA cycle through the GABA shunt [177], in which 2-HG is formed as a by-product during conversion of GABA to succinic acid (Figure 6.2c) [178-182]. The increases in 2-HG, GABA, and succinate levels further support a mitochondrial metabolism dysfunction, particularly in the TCA cycle and GABA shunt, in the neonatal s → S pups.

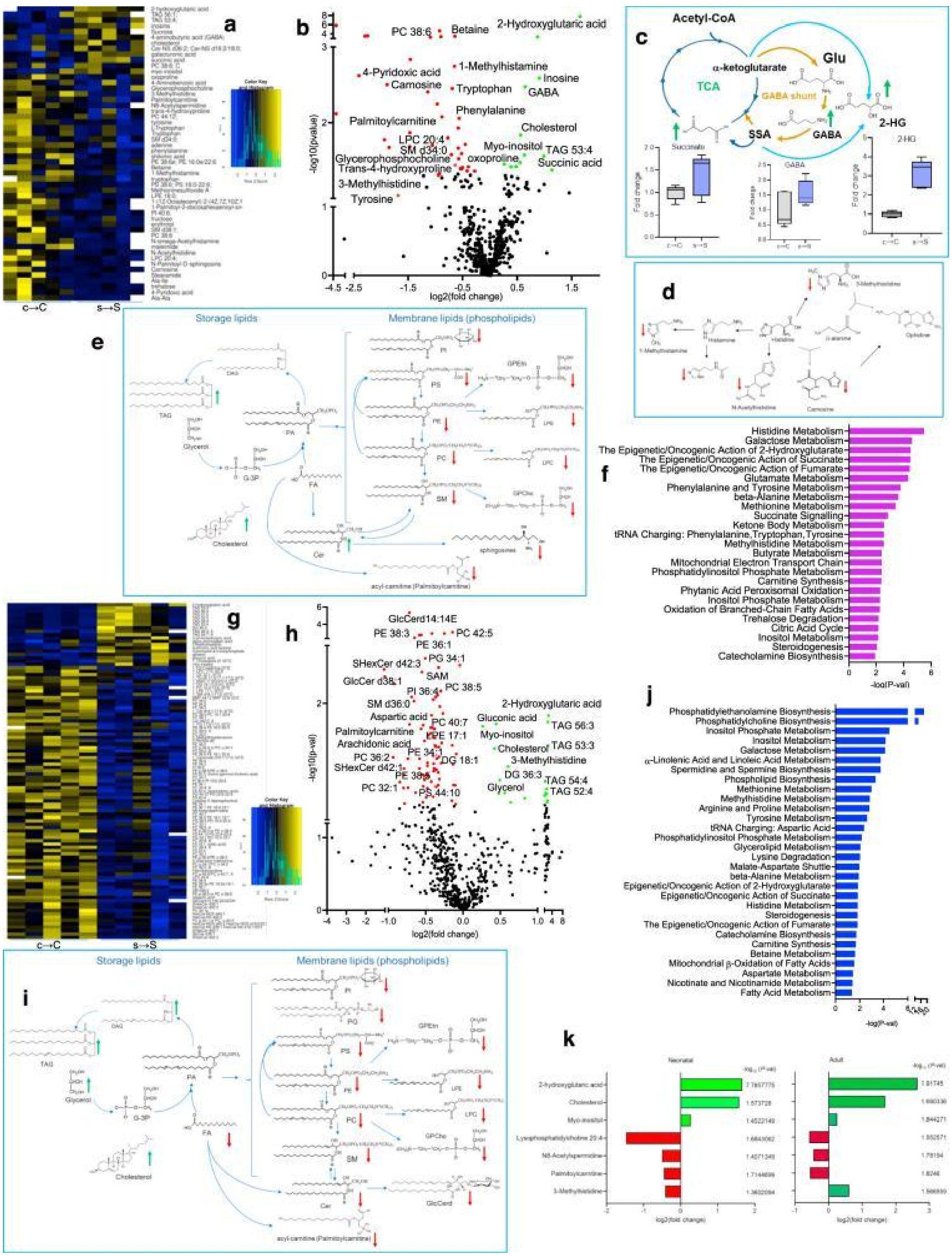

Figure 6.2. Prenatal exposure to stress causes changes in brain metabolites

(a) Heatmap of metabolites significantly changed in the brains of neonatal s → S mice ($P < 0.05$). (b) Volcano plot of metabolites significantly changed in the brains of neonatal s → S mice ($P < 0.05$). (c) Effect of prenatal exposure to stress on the tricarboxylic acid (TCA) and GABA shunt metabolism. Increased metabolites in green. (d) Changes of metabolites related to histidine metabolism, decreased metabolites in red. (e) Changes of metabolites related to lipid synthesis/metabolism in the neonatal s → S pups. Increased metabolites in green, and decreased metabolites in red. Phosphatidylcholines (PC), lysophosphatidylcholines (LPCs), phatidylethanolamines (PE), lysophosphatidylethanolamines (LPE), phosphatidylserine (PS), fatty acids (FA), arachidonic acid, glucoceramides (GlcCer), phosphtatidylglycerols (PG), and the decrease in sphingomyelins (SMs), diacylglycerols (DAG), and triglycerides (TAGs). (f) Pathway analysis of metabolites significantly changed in the neonatal MET pups. (g) Heatmap of metabolites significantly changed in the brains of adult s → S mice ($P < 0.05$). (h) Volcano plot showing differentially expressed metabolites in the brains from adult s → S mice. (i) Changes of metabolites related to lipid synthesis/metabolism in adult s → S pups. Increased metabolites in green, and decreased metabolites in red.(j) Pathway of metabolites significantly changed in the adult s → S pups. (k). Metabolites differentially expressed in neonatal and adult s → S mice with $\log_2$(fold change) and $-\log 10$ (P value).

Other metabolites that were altered in the brains of the neonatal s → S pups include molecules involved in glycolysis and energy metabolism such as myo-inositol (increased) and palmitoyl-carnitine (decreased) (Figure 6.2b). The decrease in palmitoyl-carnitine reflects reduced oxidative capacity and mitochondrial ATP production [183-186]. The mitochondrial dysfunction in neonatal s → S pups is further indicated by the marked decrease of carnosine

(>3-fold) [187,188], which was associated with decreases of other histidine metabolism components (Figure 6.2b ,d). Carnosine (β-alanyl-L-histidine) is a dipeptide that has mitochondrial pH-buffering capacity and enhancing activity on the respiratory chain complexes, and mitochondrial energy production [187-190]. The depletion of these energy-related molecules, thus, suggests that the oxygen–glucose deprivation in the neonatal s → S pups' brains creates a condition of excessive need for carnosine and its derivatives, to restore glycolysis and ATP production, and that the need exceeds the resources available of these molecules [191]. On the other hand, carnosine depletion might result in a reduction in the buffering of mitochondrial pH, thus contributing to the cellular and particularly mitochondrial acidity, associated with the production of 2-HG [174].

Metabolites of monoamine neurotransmitters' pathways displayed decreases in the brains of neonatal s → S pups including noradrenaline and dopamine precursor (tyrosine), serotonin precursor (tryptophan), and histamine-metabolism components (Figure 6.2b).

The major lipidomic changes included increases in triacylglycerols (TAGs), cholesterol, ceramides (Cer), and decreases in acyl-carnitine (palmitoyl-carnitine), and membrane phospholipids (Figure 6.2a, e). Bioinformatic analysis of metabolites altered in the brains of neonatal s → S pups substantiated enrichment of pathways associated with epigenetic processes, energy metabolism, mitochondrial functions, fatty acid oxidation, and complex lipid metabolism ($FDR < 0.05$, Figure 6.2f).

In the adult brains, 2-HG again exhibited the highest change (>6-fold increase) in the brains of the s → S pups, indicating mitochondrial dysfunction (Figure 6.2g, h). Other metabolites whose levels increased are molecules involved in energy and lipid metabolism/storage (myo-inositol, glycerol, TAGs, and cholesterol). There were profound abnormalities in the membrane, mitochondria, and signaling lipidomics. Except for cholesterol, glycerol, TAGs and diacylglycerol (DGs), which were increased in the S adult brains, all other lipids were decreased (Figure 6.2h–i). Among the notable metabolites whose levels decreased in the s → S mice were aspartic acid, palmitoyl-carnitine, and S-Adenosyl-methionine (SAM).

Bioinformatic analysis revealed similar biochemical pathways enrichments in the brain' metabolites of adult s → S mice to those significantly enriched in the neonatal s → S pups, indicating early but long-lasting metabolomic signatures produced by prenatal stress ($\mathrm{FDR} < 0.05$, Figure 6.2j). This is further supported by the finding that seven metabolites exhibited changes in the same directions in both neonatal and adult s → S mice: 2-HG, myo-inositol, N8-Acetylspermidine, palmitoyl-carnitine, cholesterol, LPC 20:4, and methylhistidine (Figure 6.2k). Hence, metabolic pathways enriched in the brains' metabolites of both neonatal and adult s → S mice included epigenetic/oncogenic action of 2-HG and succinate, mitochondrial GABA metabolism, carnitine synthesis, mitochondrial beta-oxidation of long-chain fatty acids, catecholamine biosynthesis, glutathione metabolism, inositol metabolism, histidine metabolism, methionine metabolism, and phosphatidylinositol-phosphate metabolism (Figure 6.2f, j).

Prenatal stress results in distinct alterations in brain transcriptomics

Global brain transcriptomic analysis of differentially expressed genes (DEGs) revealed a subset of genes that exhibited *a* ≥ 1.5-fold change in the neonatal s → S mice ($P < 0.05$); *Avp, Egr1, C1ql1, Fos, Crhbp* (downregulated) and *Baiap2l1, mt-Tqm, Irak1bp1*, and 11 microRNAs (Mirs) (upregulated) (Figure 6.3a). To verify the microarray results, we conducted RT-qPCR on six genes (*Egr1, Fos, Avp, Vgf, Mcm6, and C1ql1*) that were shown by microarray to display significant changes in the neonatal s → S mice ($P < 0.05$); the RT-qPCR results confirmed the microarray findings (Figure 6.3b).

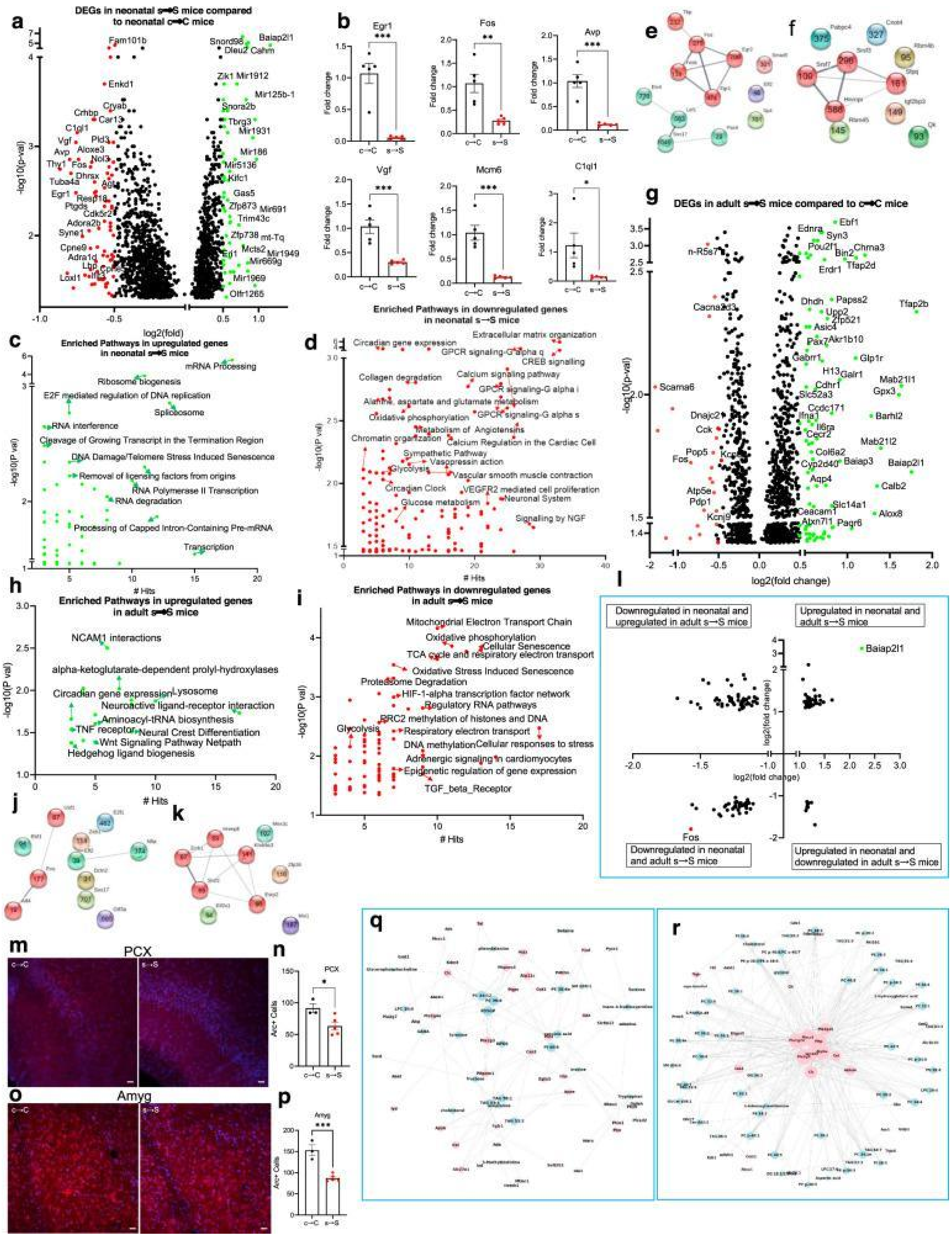

Figure 6.3. Prenatal exposure to stress causes alteration in brain transcriptomic signature

(a) Volcano plot showing differentially expressed genes in brains from neonatal s → S versus c → C mice. Baiap2l1 exhibited the largest expression change among the upregulated genes (green symbols, log(fold) > 0.5); Thy1 exhibited the largest expression change among the downregulated genes (red symbols log(fold) < −0.5). (b) Real-time qPCR validation of microarray analysis in the brains of neonatal mice. Relative global mRNA levels of Egr1, Fos, Avp, Vgf, Mcm6, and C1ql1 genes in the mice brain assessed by quantitative real-time PCR ($n = 5$). Results were normalized to Gapdh. Unpaired student test (Egr1: $t = 6.346$, $P = 0.0002$; Fos: $t = 4.027$, $P = 0.0038$; Avp: $t = 6.807$, $P = 0.0001$; Vgf: $t = 5.172$, $P = 0.0009$, Mcm6: $t = 5.950$, $P = 0.0003$; C1q11: $t = 2.563$, $P = 0.0335$): neonatal c → C vs neonatal s → S, $^{*}P < 0.05$, $^{**}P < 0.01$, $^{***}P < 0.01$. Data are presented as means ± S.E.M. (c, d) Significantly enriched biological pathways in the (c) upregulated and (d) downregulated genes in the neonatal mice with number of genes' hits. Hypergeometric test, $P < 0.05$. (e, f) Differential (e) TFs and (f) RBPs, whose target genes are DEGs in the neonatal mice. STRING network visualization, using Markov clustering algorithm (MCL), with the number of their differential target genes. (g) Volcano plot showing differentially expressed genes (DEGs) in brains from adult s → S versus c → C mice. (h, i) Significantly enriched biological pathways in the (h) upregulated and (i) downregulated genes in the adult mice with number of genes' hits. Hypergeometric test, $P < 0.05$. (j, k) Differential (j) TFs and (k) RBPs whose target gens are DEGs in adult s → S mice. STRING network visualization, using Markov clustering algorithm (MCL), with the number of their differential target genes. (l) Volcano plot of genes showing similar and opposite directions of change in neonatal and adult s → S pups. (m–p) Immunohistochemistry analysis of Arc in the brains of adult s → S and c → C mice; m, o Representative images of Arc-immunoreactivity in the (m) PCX, (o) Amyg, n, p quantification of Arc immuno-positive cells in the (n) PCX, (p) Amyg. Unpaired *t*-test, PCX: $t = 2.83$, $P = 0.029$, $n = 3$ C 5 s; Amyg: $t = 6.165$, $P = 0.0008$, $n = 3$ C 5 s; Scale bar = 50 μM. Values represent mean ± SEM. piriform cortex (PCX), and amygdala (Amyg). (q, r) Network graphs visualizing the metabolite-transcriptome interaction in (q) neonatal s → S pups and (r) adult s → S pups, using "spring" layout from the NetworkX package with Python. Each blue node presents a metabolite, and each red node presents the enzyme-coding gene. If a gene was involved in the metabolic reaction of a metabolite, an edge was drawn to connect these two nodes. The size of the node is proportional to its connectedness in the graph: the more connected the node is, the bigger its size.

Pathway analysis using hypergeometric test and Pathway Common Database and the ConsensusPathDB in neonatal s → S mice revealed the enrichment of mRNA processing, extracellular matrix organization, mitochondrial transport, GPCR signaling, glutamate transmission, glycolytic processes, ATP production, sympathetic system activation, and circadian regulation of gene expression (Figure 6.3c, d). After correction for multiple testing (FDR $q < 0.05$), mRNA processing remained enriched.

Aligned with the gene regulation enriched pathways, 57 transcription factors (TFs) and 13 RNA-binding proteins (RBPs) were differentially expressed in the s → S mice. Bioinformatic analyses using MotifMap and ChiPseq databases reveal that many of the DEGs in the neonatal s → S mice are indeed targets (differential target genes (DTGs)) for more than one of the differential TFs and RBPs (Figure 6.3e, f, Figure 6.2a–h).

In the adult s → S mice, the top downregulated genes were *Fos, Cacna2d3, Zfp874b, mt-Ts1*, and several small nucleolar RNAs and ribosomal proteins (Figure 6.3g). Among the top upregulated genes were mitochondrial genes and genes known to regulate energy metabolism: *Glp1r, Tfap2b/d, Gpx3, Calb2, Alox8, Chrna3, Galr1, Ebf1, Paqr6, Gdpd2, Akr1b10, Syn3, Aqp4, Il6ra, and Tacr3* (Figure 6.3g).

The hypergeometric test identified enrichment of pathways that are associated with cellular responses to stress, oxidative phosphorylation, electron transport chain, glycolysis, TCA cycle and respiratory electron transport, acyl-carnitine pathways, HIF-1-alpha transcription factor network, oxidative stress-induced senescence, circadian gene expression, DNA and histone methylation, sympathetic signaling in cardiovascular system, and epigenetic regulation of gene expression ($P < 0.05$, Figure 6.3h, i). After correction for multiple testing (FDR $q < 0.05$), mitochondrial Electron Transport Chain remained significantly enriched.

Aligned with the gene regulation enriched pathways, 52 TFs (40 upregulated and 12 downregulated), and nine RBPs were differentially expressed in the brains of the adult s → S mice (Figure 6.3j, k). Several differential genes were identified as targets for these differential TFs and RBPs (Figure 6.3j, k).

Eighty-three genes followed the same change direction in neonatal and adult s → S mice, whereas 62 genes exhibited opposite alterations (Figure 6.3l). The genes exhibiting the greatest degree of differential expression that changed in the same direction in neonatal and adult s → S mice were Baiap2l1 and Fos (Figure 6.3l).

Given the alteration in many genes involved in synaptic plasticity and glutamate transmission in both neonatal and adult s → S mice, we analyzed relative expression of activity-regulated cytoskeleton-associated protein (Arc/Arg3.1), a critical gene for proper glutamatergic synaptic function and plasticity [192,193]. We found that in the s → S adult pups, there were lower numbers of Arc positive cells in the amygdala, hippocampus, striatum, and piriform cortex, with no change in the frontal cortex and nucleus accumbens, compared to c → C adult pups (Figure 6.3m–p, Figure 6.4a–h), though the total numbers of cells in these regions were not altered in s → S group, evidenced by the similar number of DAPI-stained nuclei.

Bioinformatic integration of transcriptomic and metabolomic data substantiates mitochondrial and epigenetic mechanisms

Our metabolic profiling was in good agreement with gene expression data. The activities of the metabolites and their corresponding genes involved in the metabolic reactions were linked together through known enzymatic reactions from HMDB. The linkage analysis of the changes in gene expression levels with the changes in metabolite levels in the neonatal pups confirm the master biological pathways including mRNA modification, response to stress and hypoxia, oxidative-reduction process, phospholipid metabolic process, and DNA demethylation. The molecular functions enrichment analysis identified enzymatic activities of 2-ketoglutarate-dependent dioxygenase, phospholipase, and cytidine deaminase (Figure 6.3q, r). The linkage analysis of the DEGs with the changes in metabolite levels in the adult pups revealed master pathways including chromatin modification, lipid metabolism, and glutamate pathways. Enriched chromatin modification (histone methylation (H4-R3 and H3-K27)) was associated with enrichment in histone methyltransferase activity. Enriched lipid metabolism was linked with phospholipase activity, and phospholipid transporter activity (transferring acyl group) (Figure 6.3q, r).

Distinct behavioral impacts of in utero exposure vs. impaired maternal care

Since mothers exposed to stress during pregnancy exhibited impaired maternal care and increased depressive-like behavior, we applied cross-fostering procedures to examine the distinctive effects of the in utero exposure vs. impaired maternal care upon the behavioral phenotype in adulthood (Figure 6.4a). In the cross-fostering behavioral studies, mice were tested only in social interaction and forced swim assays, since these were the only two behaviors that were impaired in s → S. We found that pups born to control mothers and reared by stressed mothers (c → S mice) displayed similar behavioral phenotypes to those born to and raised by their stressed biological mothers: the c → S mice displayed social deficits ($P < 0.001$, two-way ANOVA followed by Bonferroni posttest, Figure 6.4b), and increased immobility time in the forced swim test ($P < 0.01$, one-way ANOVA, followed by Tukey posttest, Figure 6.4c). These results support a crucial role for the early life environment in the observed phenotypes. However, the caregiving by control females of mice born to stressed females (s → C) did not reverse the behavioral deficits. Thus, although s → C mice spent more time with the unfamiliar mice than the empty cup, the difference in time spent was not statistically significant (Figure 6.4b). Similarly, caregiving by control mothers slightly reduced immobility time of s → C mice in the forced swim test; however, the levels were not significantly different from those of s → S mice ($P > 0.05$, when compared to c → C or s → S mice, Figure 6.4c).

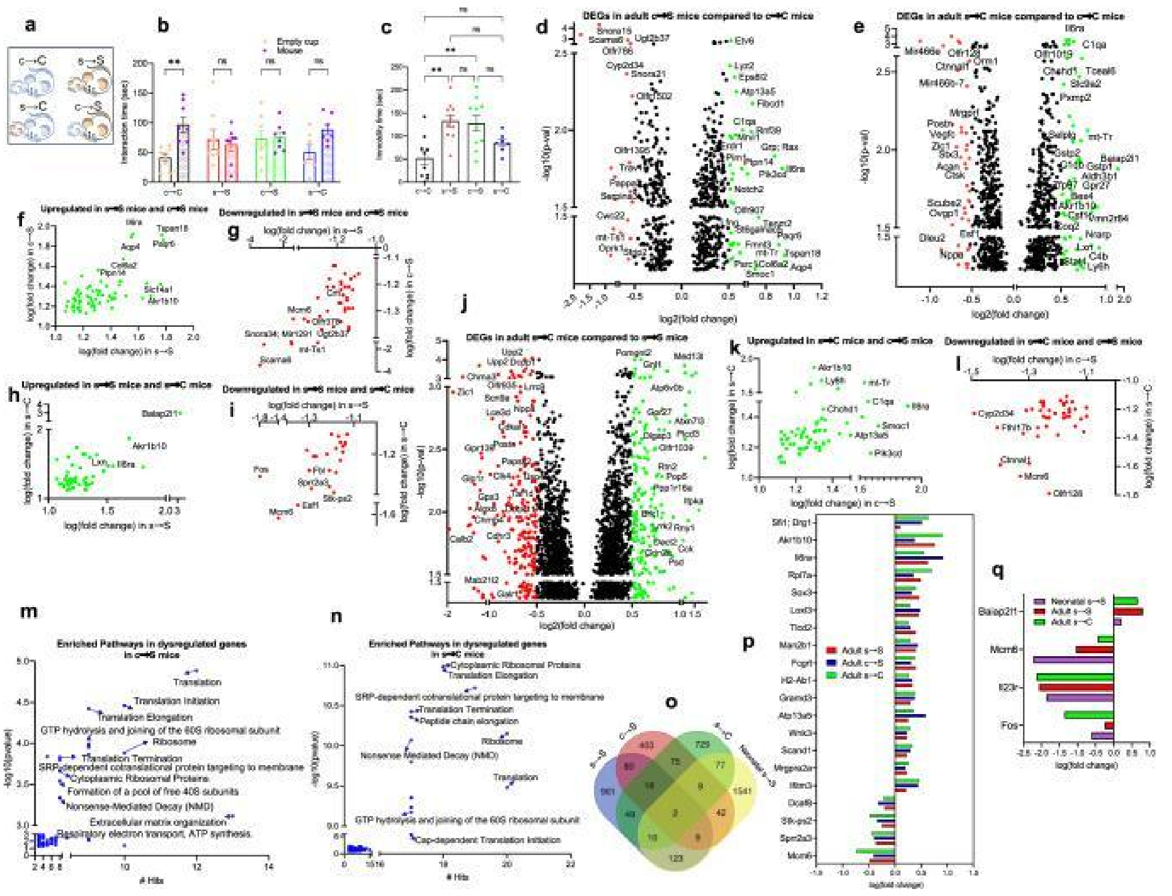

Figure 6.4. Cross-fostering effects on behavioral phenotype and transcriptomic profile

(a) Schematic of the Cross-fostering experiment design. (b) Time mice spent interacting with empty cup and unfamiliar mouse in the social interaction assay ($n = 8$ c → C, 8 s → S, 8 c → S, 7 s → C). Two-way ANOVA: object effect ($F_{1,54} = 7.255$, $P = 0.0094$), exposure to stress effect ($F_{3,54} = 0.1260$, $P = 0.9443$), stress x object interaction ($F_{3,54} = 3.422$, $P = 0.0235$) followed by Bonferroni post hoc test: empty cup vs unfamiliar mouse, $^{**}P < 0.01$, ns not significant ($P > 0.05$). Data are presented as means ± S.E.M. (c) Time mice spent immobile in the forced swim assay ($n = 10$ c → C, 10 s → S, 10 c → S, 7 s → C). One way ANOVA revealed a significant stress effect ($F_{3,33} = 7.531$, $P = 0.0006$) followed by Tukey post hoc test: c → C vs s → S vs c → S, $^{**}P < 0.01$, ns not significant ($P > 0.05$). (d) Volcano plot showing DEGs in brains from adult c → S versus c → C mice. (e) Volcano plot showing DEGs in brains from adult s → C versus c → C mice. (f, g) Volcano plot of genes showing similar direction of change in c → S and s → S: (f) upregulated and (g) downregulated genes. (h, i) Volcano plot of genes showing similar direction of change in s → C and s → S: (h) upregulated and (i) downregulated genes. (j) Volcano plot showing DEGs in brains from adult s → C versus s → S mice. (k, l) Volcano plot of genes showing similar direction of change in c → S and s → C mice: (k) downregulated and (l) upregulated genes. (m, n) Enriched biological pathways in the DEGs of (g) c → S and (h) s → C mice with number of genes' hits. Hypergeometric test, $P < 0.05$. (o) Venn diagram showing the overlap of DEGs in all mouse groups. p Overlap of DEGs in adult mouse groups that received one hit of stress, prenatally only (s → C), postnatally only (c → S) or two hits of stress (s → S). (q) Overlap of DEGs in neonatal and adult mice that received one hit of stress prenatally with or without postnatal hit of stress.

Distinct Transcriptomic impacts of in utero exposure vs. impaired maternal care

Transcriptomic analysis in adult c → S and s → C mice revealed 640 and 973 DEGs, respectively, compared to c → C mice, of which 108 and 69 genes in adult c → S and s → C mice, respectively, were altered in the same direction of the s → S DEGs (Figure 6.4d, e).

Among the top DEGs that displayed the same direction of change in both s → S and c → S mice were *Il6ra, Aqp4, Atp13a5, Akr1b10, Tspan18, and Paqr6*(upregulated) (Figure 6.4f), and *Scarna6, Snora34, Mcm6, Akr1c20, Mir1291, and Crh*, (downregulated) (Figure 6.4g). On the other hand, among the top DEGs that displayed similar changes in s → S and s → C mice were *Il6ra, Baiap2l1, Akr1b10, Gstp1, and Lxn* (upregulated) and *Fos, Mcm6, Fbl, Stk-ps2, and Esf1* (Figure 6.4h, i). Most interestingly, caregiving by control mothers reversed the alterations in 559 genes (Figure 6.4j). Among the top DEGs in s → C group compared to s → S group are *Gpx3, Galr1, Chrna3, Alox8, Calb2, Glp1r, Tfap2d, and Mab21l2*, which were downregulated, and *Atp5e, Crhbp, Cck, and Pop5*, which were upregulated (Figure 6.4j).

Mice exposed to one hit of stress either prenatally (s → C mice) or postnatally (c → S mice) shared 103 DEGs, which exhibited changes in the same directions in both s → C and c → S mice (Figure 6.4k, l).

Hypergeometric distribution and Fisher's exact test revealed common significant enriched pathways between s → C and c → S mice, including mRNA translation (initiation, elongation, and termination) and mRNA decay (FDR $q < 0.05$, Figure 6.4m, n).

Further, 20 DEGs overlapped across the three adult groups that were exposed to one hit (s → C and c → S mice) or two hits (s → S) of stress (Figure 6.4o, p). When considering the neonatal transcriptomic changes, we found only four genes that exhibited early- and long-lasting expression changes in the animals that were exposed at least prenatally to stress (neonatal s → S, s → S, and s → C) (Figure 6.4q). Only one gene (Mcm6) displayed the same change in all animals that were exposed to stress prenatally and/or postnatally and was changed as early as 24-hr after birth.

Transcriptomic-overlapping between human MDD and the four stress mouse groups

The transcriptomics linkage analysis of the DEGs in the four groups of S mice with gene expression changes in human major depressive disorder (MDD) revealed 203, 137, 105, and 74 DEGs in the neonatal s → S, adult s → S, s → C, and c → S mice respectively that overlap with human MDD (Figure 6.5). Fisher exact test revealed significant overlaps between human MDD and all the stress mouse groups, with *P* values of 1.33E–31, 3.34E–21, 1.09E–19, and 4.58E–11 for intersections between MDD and neonatal s → S, adult s → S, s → C, and c → S respectively.

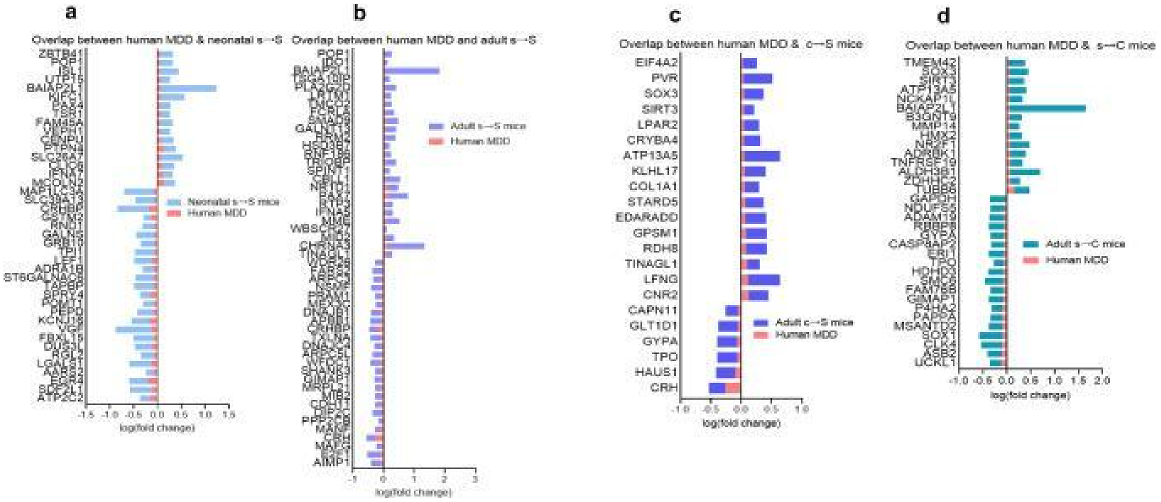

Figure 6.5. Integrated mouse-human transcriptomic analysis reveals overlap between genes whose expressions changed in mice exposed to stress and MDD patients

(a) Top common DEGs and their log(fold change) in MDD patients and 24-h s → S mice with same direction changes. (b) Top common DEGs and their log(fold change) in MDD patients and adult s → S mice with same direction changes. (c) Top common DEGs and their log(fold change) in MDD patients and c → S mice with same direction changes. (d) Top common DEGs and their log(fold change) in MDD patients and s → C mice with same direction changes.

Acetyl-L-carnitine (ALCAR) protected against and reversed depressive-like behavior induced by prenatal trauma

Given that the behavioral deficits in the s → S mice were associated with a decrease in palmitoyl-carnitine, increase in 2-HG, and impairments in the mitochondrial functions, lipid β-oxidation and phospholipid metabolism, we tested whether the behavioral deficits could be rescued by an agent, acetyl-L-carnitine (ALCAR), that is known to restore these functions. ALCAR is known to elicit its antidepressant effects through a number of mechanisms including rescuing mitochondrial functions and lipid β-oxidation metabolism, improving glutamate transmission, and enhancing chromatin acetylation by providing an acetyl group to chromatin [194,195]. ALCAR was supplemented in the drinking water of s → S mice either from weaning to adulthood (3–8 weeks), or for one week in adulthood (7–8 weeks) (Figure 6.6a). ALCAR supplementation for 1 week during adulthood rescued the depressive-like behavior ($P < 0.001$, Figure 6.6b) in s → S mice. One week after ALCAR cessation, however, the anti-depressant effect of ALCAR was diminished (Figure 6.6c). ALCAR supplementation from weaning rendered s → S mice resistant to developing depressive-like behavior ($P < 0.01$, Figure 6.6b). Strikingly, ALCAR antidepressant effects lasted 1 week after its cessation ($P < 0.001$, Figure 6.6c).

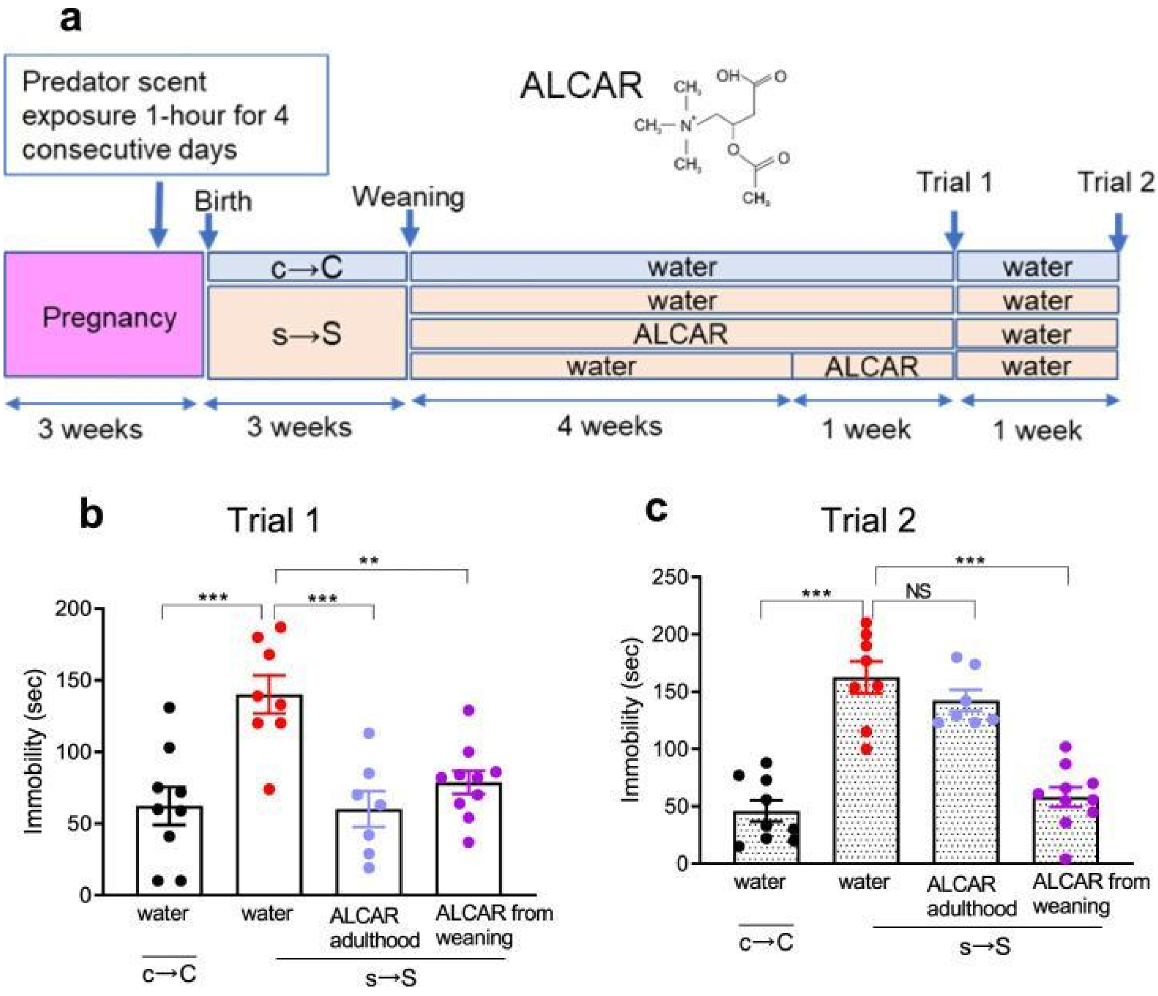

Figure 6.6. Acetyl-L-carnitine (ALCAR) reverses depressive-like behavior after its cessation

(a) Schematic of the two ALCAR administration regimes, and the chemical structure of ALCAR. (b) Time mice spent immobile in the forced swim assay following the treatment of ALCAR for 5 weeks from weaning, and 1 week during the adult stage, ($n = 9$ c → C, 8 s → S, 7 s → S + ALCAR from Weaning, 10 s → S + ALCAR in Adulthood). One-way ANOVA: treatment effect ($F_{3,30} = 9.72, P = 0.0001$) followed by Tukey post hoc test, $^{**}P < 0.01$, $^{***}P < 0.001$, ns not significant ($P > 0.05$). (c) Time mice spent immobile in the forced swim assay 1 week after the cessation of ALCAR treatment, One-way ANOVA revealed a significant treatment effect ($F_{3,30} = 32, P = 0.0001$) followed by Tukey post hoc test, $^{***}P < 0.001$, ns not significant ($P > 0.05$). Data are presented as means ± S.E.M.

6.4 DISCUSSION

The long-term devastating impacts of prenatal traumatic stress are well established in humans and animals [160,162,163,196]. Yet, the mechanistic involvement of prenatal stress independent of stress effects on maternal care is largely unknown.

Here, we present results demonstrating that exposure to trauma during pregnancy induces in the offspring long-lasting depressive-like behavior and social deficits, without affecting cognitive functions. Using cross-fostering experiments, we demonstrate that these behavioral deficits are associated with divergent and convergent mechanisms of both in-utero and early-life parenting environments. Thus, the exposure to postnatal early-life hit of stress, through raising of normal pups by traumatized mothers, produces a behavioral phenotype that is similar to that induced by a double-hit of stress (in pups born and raised by their biological traumatized mothers). Good caregiving by normal mothers of pups that were exposed to prenatal hits of stress, however, did not completely prevent the manifestation of trauma- induced behavioral deficits. Thus, our data demonstrate distinctive behavioral impacts of one-hit exposure to stress (either prenatally through or postnatally) or two-hits stress (prenatal and postnatal exposures).

Associated with the distinct behavioral deficits we found, through metabolomic, transcriptomic and bioinformatic analyses, mechanisms that involve stress- and hypoxia-response energy metabolic pathways, especially mitochondrial ATP production. These acute responses seem to have resulted in long-lasting adaptations in glycolysis, homeostasis of energy lipids, and epigenetic processes pertaining to DNA and chromatin modifications, as evidenced by the disruptions of these pathways in the brains of adult mice. We therefore propose a model through which stress exposure during pregnancy induces, in progeny, early and long-lasting mitochondrial metabolism dysfunctions and epigenetic changes, associated with social behavioral deficits (Figure 6.7a). According to our model, the striking increase in the mitochondrial metabolite and epigenetic modifier 2-hydroxyglutarate (2-HG) in the brains of neonatal mice, whose mothers were exposed to extreme stress during pregnancy, likely forms the first step of the consequent stress-response events.

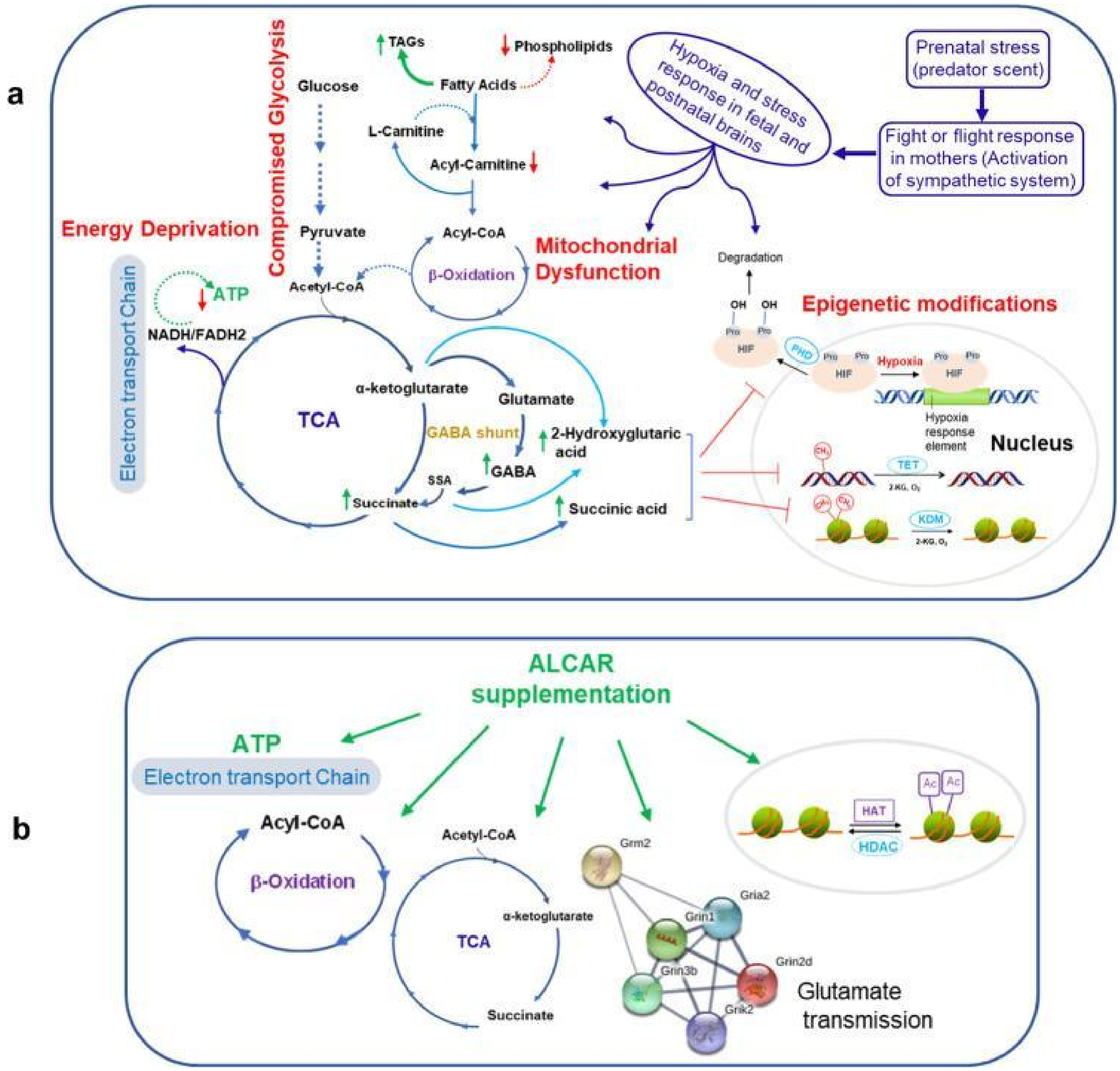

Figure 6.7. Model for proposed mechanism

(a) Prenatal exposure to stress elicits depression through a number of mechanisms that may begin with hypoxia, which results in compromised glycolysis, energy deprivation, mitochondrial dysfunction (oxidative phosphorylation and ATP production), and altered epigenetic processes. (b) Possible mechanisms through which ALCAR may produce its antidepressant effects.

Exposure to extreme stress during pregnancy is known to activate the maternal fight-or-flight sympathetic system, and produce fetal reduction of oxygen (hypoxia), which might be detected in the infants several months postnatally [197-201]. The mitochondrial metabolite 2-HG is an established marker for hypoxia, defective mitochondria, decreased electron transport chain activity, and acidic cellular conditions [173,174,202,203]. Accumulation of 2-HG in hypoxia occurs as a result of the TCA cycle dysfunction and, in turn, 2-HG inhibits electron transport and glycolysis to counterbalance the deleterious consequences of hypoxia [202]. Therefore, 2-HG accumulation in the neonatal s → S pups, accompanied by succinate accumulation and activated GABA shunt, indicates a hypoxic state and a disruption of the mitochondrial metabolism. The hypoxic state in newborn s → S mice seems to trigger adaptation mechanisms, particularly in metabolic and energy demand [204-206]. Accordingly, acute stress-hypoxia responses in the neonatal s → S mice affect glycolysis and shift mitochondrial-energy metabolism (disruption in ATP production, accumulation of TAGs and depletion of membrane phospholipids). In addition to its role in hypoxia, 2-HG is an epigenetic modifier, which regulates epigenetic programming through its competitive inhibition of 2-ketoglutarate (2-KG)-dependent enzymes [207]. 2-KG-dependent enzymes known to be inhibited by 2-HG include TET(1-3) DNA demethylase enzymes, Jumonji family of histone lysine demethylases (JmjC-KDMs), and prolyl hydroxylases (PHDs 1–3), which hydroxylate proline in hypoxia-inducible factors (HIFs), as a post-translational modification [208-212].

Through these mechanisms, 2-HG alters DNA and histone methylation [208,209,213,214] and increases HIFs accumulation, resulting in selective upregulation of HIF-target genes [215,216]. In support of HIFs accumulation, we found lower levels in the neonatal s → S pups of 4-hydroxyproline, a marker for the degradation of the proline-containing HIFs [217]. The reduced levels of 4-hydroxyproline in the neonatal s → S pups indicate decreased hydroxylation and, hence, lower degradation of HIFs, causing HIFs accumulation.

HIFs target genes include practically all genes of the glycolytic pathway [218-220]. While these metabolic and epigenetic changes aim to protect the brain from hypoxia during development, their effects may persist and confer the susceptibility for psychiatric disorders including depression later in life. First, the perturbation of the glycolysis pathways during stress triggers the activation of GABA shunt as an alternative pathway to enhance energy production [182,221-223]. Ultimately, the stress-associated depletion of the brain's energy resources leads to alteration in GABA and glutamate transmission and results in impaired neuronal plasticity underlying depression [224-225], reflected by the decreased Arc expression in brain regions involved in emotion and stress. Second, the disruption of glycerolipids homeostasis exacerbates neural dysfunction and has acute and long-lasting impacts through directing the lipid flux toward energy storage rather than membrane extension or signaling. Lastly, while the early life 2-HG-triggered epigenetic modifications serve to offset mitochondrial dysfunction in response to stress [225], they may produce long-lasting adaptations by altering methylation states and the expression of key genes involved in neurodevelopment, neuron maturation and differentiation, axon-genesis, and synaptic plasticity [226,227].

Our findings indicate a two-hits mechanism of convergence as well as divergence of some key metabolic, epigenetic and neuronal pathways induced by prenatal and early life trauma, which are involved in the pathophysiology of depression. This is supported by the overlap in specific sets of genes and pathway networks among s → S, s → C and c → S mice. Our finding of common genes in human depression and the four experimental animal groups (neonatal s → S, adult s → S, s → C and c → S) provides a translational aspect of our model and support for our convergent pathways hypothesis of the emergence of stress-induced depression. Strikingly, among the different stress mouse groups, the neonatal s → S mice exhibited the highest overlap in DEGs with human MDD. This finding strongly indicates the importance of our model in identifying biomarkers that serve as predictive markers in early life for the risk of the development of depression in adulthood, and in providing a potential target for early preventive approaches and therapeutic strategies.

Thus, a pharmacological intervention that restores the perturbed pathways at the appropriate time of life would be predicted to protect against depression. ALCAR possesses unique features that make it an ideal candidate, providing a rare opportunity for preventive rather than therapeutic intervention for depression. First, ALCAR has long been known to enhance mitochondrial function and facilitate ATP production [194,195]. Second, ALCAR promotes transportation of fatty acids into the mitochondria for subsequent oxidation and ATP generation and, thus, corrects the lipid profile, and directs the flow of lipids toward membrane production and energy production and TAGs reduction [228,229]. Third, ALCAR produces epigenetic modifications that involve histone acetylation (through providing acetyl group from ALCAR to chromatin) [194,195]. Through its epigenetic actions, ALCAR regulates the expression of key genes crucial for synaptic plasticity [194,195]. Fourth, ALCAR has been shown to correct glutamate transmission in animal models of stress [194,195]. Lastly, and most importantly, several randomized clinical studies demonstrated the effectiveness of ALCAR supplementation to decrease depressive symptoms [230,231]. Indeed, the antidepressant effects of ALCAR have been speculated to occur through more than one of these mechanisms including enhancing mitochondrial function and facilitating ATP production [194,195].

We found that ALCAR antidepressant effects outlasted its treatment end when it was administered early in life (at weaning time), but not when it was administered in adulthood. The timing and duration of ALCAR administration might be deterministic factors in the long-lasting anti-depressant effect of ALCAR, given that animals administered ALCAR from weaning time received the drug for 5 weeks, whereas those administered ALCAR in postnatal week 7 received it for 1 week. However, considering that 1 week cessation of ALCAR is sufficient as a washout period, the long-lasting effect of ALCAR seems to be more likely due to the administration timing (weaning time vs adulthood) rather than duration (1 week vs 5 weeks).

This long-lasting anti-depressant effect of ALCART after its cessation suggests epigenetic mechanisms, through which ALCART likely increases histone acetylation causing chromatin structure remodeling. Since prenatal stress induced in $s \rightarrow S$ mice changes in all pathways that can be improved by ALCAR (mitochondrial functions and lipid β-oxidation metabolism, glutamate transmission, and epigenetic modifications), and given the distinctive effects of 1 week vs 5 weeks of ALCAR administration, it is likely that ALCAR elicited its antidepressant effects on $s \rightarrow S$ mice via more than one mechanism (Figure 6.7b). These findings provide a unique opportunity for utilizing ALCAR as a prophylactic supplementation to young children and adolescents to protect against depression in high-risk populations. Remarkably, ALCAR levels are low in depression patients, and the declines are greater in patients with a history of childhood trauma and emotional neglect [232].

Given the unique features of ALCAR, this natural supplement can represent an innovative and unique prophylactic and therapeutic strategy, should it be administered at the appropriate time of life. This has the potential to change the lives of millions of people who suffer from major depression or have the risk of developing this disabling disorder, particularly those in which the depression arose from prenatal traumatic stress.

In conclusion, we demonstrate that intergenerational trauma induces social deficits and depressive-like behavior through divergent and convergent mechanisms of both in utero and early-life parenting environments. We establish 2-HG as an early predictive biomarker for trauma-induced behavioral deficits and demonstrate that early pharmacological correction of mitochondria metabolism dysfunction by ALCAR can permanently reverse the behavioral deficits.

CHAPTER 7:

CONCLUSIONS

PD continues to impact millions of people worldwide and tens of thousands get diagnosed each year. Searching for alternative ways to combat the motor symptoms of the disease seems to not be something that people are interested in, despite it being very important to search for alternative treatments to L-DOPA. Although it is the gold standard, L-DOPA falls short when treating long term and could result in debilitating symptoms worse than the disease itself. Studying alternative systems that we can target aside from the dopamine system allows us to develop new drugs to target those systems and avoid the complications that arise when working with a delicate system, such as the dopamine system. There are still so many unknown therapeutic targets that we may not know about that require so much more research.

In this thesis, we explore the locomotor induced by L-DOPA and NSD1015 in mouse models of PD. We identified that this treatment is able to induce locomotor activity in these mouse models and identified OA as the possible metabolite responsible for the hyperactivity (see Chapter 2). We also identified an interaction between L-DOPA, Scn, and iron, providing an explanation for why L-DOPA becomes less effective over time, despite larger doses being administered to patients (see Chapter 3). We observed the hyperactivity of L-DOPA and NSD1015 in the MPTP mouse model for PD and we were able to induce locomotor activity in this model by treating the animals with OA through an ICV injection. The ICV injection was necessary as we also showed that OA was unable to cross the blood-brain barrier (see Chapter 4). Finally, we were able to investigate the mechanism by which OA induced locomotor activity. Through radioligand binding and cAMP assays, we were able to confirm that OA does indeed bind to the CaSR and is able to activate the receptor as well. We also found that L-DOPA also has some affinity to the CaSR and in combination with calcium and OA, it is able to promote and enhance binding to the receptor. Lastly, we were able to confirm this is the correct mechanism by blocking the locomotor activity induced by both the L-DOPA and NSD1015 treatment and by injecting OA directly through the use of a CaSR antagonist, NPS2143 (Chapter 5).

Overall, this work has helped contribute to the search for an alternative treatment for PD. Given that the CaSR, when activated, is able to induce locomotor activity in PD modeled mice, it can now serve as a target for future drugs. Assuming that there are no adverse or harmful side effects, targeting the CaSR could be an alternative method to treating PD patients without targeting the dopamine system or using L-DOPA as a whole. Even if there were to be some shortcomings to the CaSR as a target, this work shows that there could be alternatives to the dopamine system when we look at treating motor dysfunction and hopefully encourages scientists to search for others that may exist.

In chapter 6, we were able to investigate the intricacies of intergenerational trauma, as the long-term devastating impacts of this have been well established [160,162,163,196]. What we found was that mice birthed from traumatized mothers seem to suffer distinct behavioral defects, namely in their social behavior and they expressed more depressive-like behaviors. We also recognized a number of biomarkers, such as 2-hydroxyglutaric acid, that was dramatically increased in the brains of the neonates, as well as, in the adults exposed prenatally to trauma. We were able to identify defects in many metabolic pathways, specifically ones that produced alterations in mitochondrial energy metabolism and epigenetic processes. Lastly, we were able to reverse the depression induced by intergenerational trauma through early intervention using ALCAR, which provided long-lasting protection even after stopping the supplement during adulthood.

Overall, this work aimed to provide a better understanding of intergenerational trauma and its harmful impact. Simply bringing attention to the idea that what we do has long lasting impacts on our future generation can be extremely beneficial as it may raise awareness against certain behaviors that we may not deem harmful at the time, but may cause issues in the future. We also showed that ALCAR can permanently reverse the behavioral deficits, showing that early pharmacological intervention is massively important and if we are able to identify biomarkers that could mean a person is high-risk for developing certain deficits we may be able to treat them before it becomes too late.

REFERENCES

1. Goedert, M., & Jakes, R. (2005). Mutations causing neurodegenerative tauopathies. Biochimica et Biophysica Acta (BBA)-Molecular Basis of Disease, 1739(2-3), 240-250. doi: 10.1016/j.bbadis.2004.08.015
2. Schapira, A. H., & Jenner, P. (2011). Etiology and pathogenesis of Parkinson's disease. Movement Disorders, 26(6), 1049-1055. doi: 10.1002/mds.23732
3. McGeer, P. L., & McGeer, E. G. (2004). Inflammation and neurodegeneration in Parkinson's disease. Parkinsonism & Related Disorders, 10(Suppl 1), S3-S7. doi: 10.1016/j.parkreldis.2004.01.005
4. Xilouri, M., & Stefanis, L. (2011). Autophagic pathways in Parkinson disease and related disorders. Expert Review of Molecular Medicine, 13(e8), 1-22. doi: 10.1017/S1462399410001755
5. Wichmann, T., & DeLong, M. R. (2016). Basal ganglia circuits in movement and movement disorders. In Handbook of Clinical Neurology (Vol. 139, pp. 137-157). Elsevier.
6. Graybiel, A. M. (2000). The basal ganglia. Current biology, 10(14), R509-R511.
7. Haber, S. N. (2016). Corticostriatal circuitry. In Handbook of Clinical Neurology (Vol. 139, pp. 235-252). Elsevier.
8. Mink, J. W. (1996). The basal ganglia: focused selection and inhibition of competing motor programs. Progress in neurobiology, 50(4), 381-425.
9. Albin, R. L., Young, A. B., & Penney, J. B. (1989). The functional anatomy of basal ganglia disorders. Trends in neurosciences, 12(10), 366-375.

10. Doyon, J., & Benali, H. (2005). Reorganization and plasticity in the adult brain during learning of motor skills. Current opinion in neurobiology, 15(2), 161-167.
11. Hikosaka, O., Nakamura, K., Sakai, K., & Nakahara, H. (2002). Central mechanisms of motor skill learning. Current opinion in neurobiology, 12(2), 217-222.
12. Frank, M. J. (2005). Dynamic dopamine modulation in the basal ganglia: a neurocomputational account of cognitive deficits in medicated and nonmedicated Parkinsonism. Journal of cognitive neuroscience, 17(1)
13. Lees, A. J., & Hardy, J. (2011). Revesz T. Parkinson's disease. Lancet, 373(9680), 2055-2066.
14. Walker, F. O. (2007). Huntington's disease. The Lancet, 369(9557), 218-228.
15. Hallett, M. (2011). Neurophysiology of dystonia: The role of inhibition. Neurobiology of disease, 42(2), 177-184.
16. Gross, C. G. (2014). The striatum: a historical perspective. Frontiers in neuroanatomy, 8, 74. doi: 10.3389/fnana.2014.00074
17. Gerfen, C. R., Engber, T. M., Mahan, L. C., Susel, Z., Chase, T. N., Monsma Jr, F. J., & Sibley, D. R. (1990). D1 and D2 dopamine receptor-regulated gene expression of striatonigral and striatopallidal neurons. Science, 250(4986), 1429-1432. doi: 10.1126/science.2147780
18. Wichmann, T., & DeLong, M. R. (1996). Functional and pathophysiological models of the basal ganglia. Current opinion in neurobiology, 6(6), 751-758.
19. Jenner P. The contribution of the MPTP-treated primate model to the development of new treatment strategies for Parkinson's disease. Parkinsonism Relat Disord. 2003;9(3):131-7.

20. Nambu A, Tachibana Y, Okada A, et al. A mesopontine relay for tonic inhibition of substantia nigra pars reticulata and mesencephalic locomotor region by the pedunculopontine nucleus. J Neurosci. 2005;25(29):7082-91.
21. Lobb CJ, Wilson CJ, Paladini CA. High-resolution imaging of the autofluorescence in the rat substantia nigra identifies the location of dopaminergic neurons in vivo. J Neurophysiol. 2011;106(2):652-64.
22. Schultz W. Dopamine neurons and their role in reward mechanisms. Curr Opin Neurobiol. 1997;7(2):191-7.
23. Hong S, Jhou TC, Smith M, et al. Pallidal versus subthalamic nucleus deep brain stimulation for Parkinson's disease: reconciling the differences? Neurobiol Dis. 2015;85:187-97.
24. Kita H, Kitai ST. The striatopallidal system, with special reference to rat: A Golgi and electron microscopic study. J Comp Neurol. 1987 Apr 22; 260(2):159-72. doi: 10.1002/cne.902600203. PMID: 2438703.
25. Schrag A, Quinn N. Dyskinesias and motor fluctuations in Parkinson's disease. A community-based study. Brain. 2000 Dec; 123(Pt 12):2297-305. doi: 10.1093/brain/123.12.2297. PMID: 11099449.
26. Singer HS. Tourette's syndrome: from behaviour to biology. Lancet Neurol. 2005 Aug; 4(8): 149-159. doi: 10.1016/S1474-4422(05)01012-4. PMID: 16033683.
27. Jenner, P. (2003). Oxidative stress in Parkinson's disease. Annals of neurology, 53(S3), S26-S36.
28. Hirsch, E. C., & Hunot, S. (2009). Neuroinflammation in Parkinson's disease: a target for neuroprotection?. The Lancet Neurology, 8(4), 382-397.

29. Lesage, S., & Brice, A. (2009). Parkinson's disease: from monogenic forms to genetic susceptibility factors. Human molecular genetics, 18(R1), R48-R59.
30. Nalls, M. A., Pankratz, N., Lill, C. M., Do, C. B., Hernandez, D. G., Saad, M., ... & Singleton, A. B. (2014). Large-scale meta-analysis of genome-wide association data identifies six new risk loci for Parkinson's disease. Nature genetics, 46(9), 989-993.
31. Tanner, C. M., & Goldman, S. M. (1996). Epidemiology of Parkinson's disease. Neurologic clinics, 14(2), 317-335.
32. Schapira, A. H. V., & Jenner, P. (2011). Etiology and pathogenesis of Parkinson's disease. Movement Disorders, 26(6), 1049-1055. doi: 10.1002/mds.23732
33. Jankovic, J., & Poewe, W. (2012). Therapies in Parkinson's disease. Current Opinion in Neurology, 25(4), 433-447. doi: 10.1097/WCO.0b013e328355d0a8
34. Jankovic J. Parkinson's disease: clinical features and diagnosis. J Neurol Neurosurg Psychiatry. 2008 May;79(5):368-76. doi: 10.1136/jnnp.2007.131045. PMID: 18344392.
35. Postuma RB, Berg D. Advances in markers of prodromal Parkinson disease. Nat Rev Neurol. 2016 Jul;12(7):385-96. doi: 10.1038/nrneurol.2016.80. Epub 2016 Jun 3. PMID: 27255461.
36. Bloem BR, Okun MS, Klein C. Parkinson's disease. Lancet. 2021 Feb 27;397(10272):2284-2303. doi: 10.1016/S0140-6736(21)00670-8. PMID: 33891881.
37. Aarsland D, Pahlhagen S, Ballard CG, Ehrt U, Svenningsson P. Depression in Parkinson disease--epidemiology, mechanisms and management. Nat Rev Neurol. 2012 Mar 13;8(1):35-47. doi: 10.1038/nrneurol.2011.189. PMID: 22453131.

38. Chaudhuri KR, Healy DG, Schapira AH; National Institute for Clinical Excellence. Non-motor symptoms of Parkinson's disease: diagnosis and management. Lancet Neurol. 2006 Mar;5(3):235-45. doi: 10.1016/S1474-4422(06)70373-8. PMID: 16488383.
39. Muslimovic D, Post B, Speelman JD, Schmand B. Cognitive profile of patients with newly diagnosed Parkinson disease. Neurology. 2005 Jul 26;65(2):123-8. doi: 10.1212/01.wnl.0000167924.38237.1e. PMID: 16043800.
40. Chaudhuri KR, Prieto-Jurcynska C, Naidu Y, et al. The Nondeclaration of Nonmotor Symptoms of Parkinson's Disease to Health Care Professionals: An International Study Using the Nonmotor Symptoms Questionnaire. Mov Disord. 2010;25(6):704-709. doi: 10.1002/mds.22768. PMID: 20310027.
41. LeWitt PA. Levodopa therapy for Parkinson's disease: pharmacokinetics and pharmacodynamics. Mov Disord. 2015;30(1):64-72. doi:10.1002/mds.26166
42. Stocchi F, Rascol O, Kieburtz K, et al. Initiating levodopa/carbidopa therapy with and without entacapone in early Parkinson disease: the STRIDE-PD study. Ann Neurol. 2010;68(1):18-27. doi:10.1002/ana.22078
43. Olanow CW, Kieburtz K, Odin P, et al. Continuous intrajejunal infusion of levodopa-carbidopa intestinal gel for patients with advanced Parkinson's disease: a randomised, controlled, double-blind, double-dummy study. Lancet Neurol. 2014;13(2):141-149. doi:10.1016/S1474-4422(13)70293-X
44. Antonini A, Poewe W, Chaudhuri KR, et al. Levodopa-carbidopa intestinal gel in advanced Parkinson's: final results of the GLORIA registry. Parkinsonism Relat Disord. 2017;45:13-20. doi:10.1016/j.parkreldis.2017.09.018

45. Espay AJ, Hausdorff JM, Sánchez-Ferro Á, et al. A roadmap for implementation of patient-centered digital outcome measures in Parkinson's disease obtained using mobile health technologies. Mov Disord. 2019;34(5):657-663. doi:10.1002/mds.27671
46. DeMaagd G, Philip A. Parkinson's disease and its management: part 3: treatment of motor symptoms. P&T. 2015;40(12):832-837.
47. Tomlinson CL, Stowe R, Patel S, Rick C, Gray R, Clarke CE. Systematic review of levodopa dose equivalency reporting in Parkinson's disease. Mov Disord. 2010;25(15):2649-2653. doi:10.1002/mds.23429
48. Borregaard, N.; Cowland, J. B. Neutrophil gelatinase-associated lipocalin, a siderophore-binding eukaryotic protein. Biometals 2006, 19, 211– 215, DOI: 10.1007/s10534-005-3251-7
49. Correnti, C.; Strong, R. K. Mammalian siderophores, siderophore-binding lipocalins, and the labile iron pool. J. Biol. Chem. 2012, 287, 13524– 13531, DOI: 10.1074/jbc.R111.311829
50. Flo, T. H.; Smith, K. D.; Sato, S.; Rodriguez, D. J.; Holmes, M. A.; Strong, R. K.; Akira, S.; Aderem, A. Lipocalin 2 mediates an innate immune response to bacterial infection by sequestrating iron. Nature 2004, 432, 917– 921, DOI: 10.1038/nature03104
51. Devireddy, L. R.; Gazin, C.; Zhu, X.; Green, M. R. A cell-surface receptor for lipocalin 24p3 selectively mediates apoptosis and iron uptake. Cell 2005, 123, 1293– 1305, DOI: 10.1016/j.cell.2005.10.027
52. Lee, S.; Lee, W. H.; Lee, M. S.; Mori, K.; Suk, K. Regulation by lipocalin-2 of neuronal cell death, migration, and morphology. J. Neurosci. Res. 2012, 90, 540– 550, DOI: 10.1002/jnr.22779

53. Jha, M. K.; Lee, S.; Park, D. H.; Kook, H.; Park, K. G.; Lee, I. K.; Suk, K. Diverse functional roles of lipocalin-2 in the central nervous system. Neurosci. Biobehav. Rev. 2015, 49, 135– 156, DOI: 10.1016/j.neubiorev.2014.12.006
54. Bi, Yanqin, et al. “Lipocalin 2 Promotes Breast Cancer Progression.” Cancer Biology & Medicine, vol. 17, no. 2, 2020, pp. 496–508., doi:10.20892/j.issn.2095-3941.2019.0325.
55. Lee, Sang Hoon, et al. “Lipocalin-2 Is Elevated in the Cerebrospinal Fluid of Alzheimer’s Disease Patients.” Scientific Reports, vol. 9, no. 1, 2019, doi:10.1038/s41598-019-47788-1.
56. Mishra, Alok, et al. “Neutrophil Gelatinase-Associated Lipocalin (NGAL) as a Biomarker for Acute Heart Failure: A Systematic Review.” Heart Failure Reviews, vol. 24, no. 6, 2019, pp. 867–874., doi:10.1007/s10741-019-09825-x.
57. Ferreira, A. C.; Sousa, N.; Bessa, J. M.; Sousa, J. C.; Marques, F. Metabolism and adult neurogenesis: Towards an understanding of the role of lipocalin-2 and iron-related oxidative stress. Neurosci. Biobehav. Rev. 2018, 95, 73– 84, DOI: 10.1016/j.neubiorev.2018.09.014
58. Ferreira, A. C.; Da Mesquita, S.; Sousa, J. C.; Correia-Neves, M.; Sousa, N.; Palha, J. A.; Marques, F. From the periphery to the brain: Lipocalin-2, a friend or foe?. Prog. Neurobiol. 2015, 131, 120– 136, DOI: 10.1016/j.pneurobio.2015.06.005
59. Kim, H.; Lee, S.; Park, H. C.; Lee, W. H.; Lee, M. S.; Suk, K. Modulation of glial and neuronal migration by lipocalin-2 in zebrafish. Immune Network2011, 11, 342– 347, DOI: 10.4110/in.2011.11.6.342
60. Xing, C.; Wang, X.; Cheng, C.; Montaner, J.; Mandeville, E.; Leung, W.; van Leyen, K.; Lok, J.; Wang, X.; Lo, E. H. Neuronal production of lipocalin-2 as a help-me signal for

glial activation. Stroke 2014, 45, 2085– 2092, DOI: 10.1161/STROKEAHA.114.005733

61. Kim, B. W.; Jeong, K. H.; Kim, J. H.; Jin, M.; Kim, J. H.; Lee, M. G.; Choi, D. K.; Won, S. Y.; McLean, C.; Jeon, M. T.Pathogenic Upregulation of Glial Lipocalin-2 in the Parkinsonian Dopaminergic System. J. Neurosci. 2016, 36, 5608– 5622, DOI: 10.1523/JNEUROSCI.4261-15.2016
62. Kalia, L. V., & Lang, A. E. (2015). Parkinson's disease. The Lancet, 386(9996), 896-912. doi:10.1016/s0140-6736(14)61393-3
63. Fernagut, P. O., Diguet, E., Bioulac, B., & Tison, F. (2002). MPTP and MPP+ models of Parkinson's disease in rodents. Brain Research Reviews, 40(1-3), 77-96. doi:10.1016/s0165-0173(02)00198-0
64. Rangasamy, S. B., Soderstrom, K., Bakay, R. A., Kordower, J. H., & Burke, R. E. (2010). Neurotrophic factor therapy for Parkinson's disease. Progress in Brain Research, 184, 237-264. doi:10.1016/s0079-6123(10)84013-1
65. Schneider JS, Roeltgen DP. Delayed onset and long duration of reserpine-induced motor deficits in monkeys. Pharmacol Biochem Behav. 1993 Mar;44(3):535-40. doi: 10.1016/0091-3057(93)90360-v. PMID: 8453408.
66. Fornai F, Schlüter OM, Lenzi P, et al. Parkinson-like syndrome induced by continuous MPTP infusion: convergent roles of the ubiquitin-proteasome system and alpha-synuclein. Proc Natl Acad Sci U S A. 2005 Apr 5;102(14):5013-8. doi: 10.1073/pnas.0409643102. Epub 2005 Mar 23. PMID: 15788537; PMCID: PMC556143.
67. Zheng Z, Wang Y, Guo L, et al. Reserpine exposure disturbs metabolism and immune responses via gut microbiota alteration in zebrafish. Sci Total Environ. 2021 Jan

20;752:141915. doi: 10.1016/j.scitotenv.2020.141915. Epub 2020 Aug 20. PMID: 32898869.

68. Fernandez, H. H., Lapane, K. L., & Ott, B. R. (2014). The relevance of animal models in Parkinson's disease research. Parkinson's disease, 2014, 1-9. doi: 10.1155/2014/718527
69. Langston, J. W. (2017). The MPTP story. Journal of Parkinson's Disease, 7(s1), S11-S19. doi: 10.3233/JPD-179005
70. Cai, H., Liu, G., Sun, L., Ding, J., & Alper, J. (2010). MPTP-induced parkinsonian-like symptoms and oxidative stress in mice are reduced by ethyl pyruvate. Journal of neuroscience research, 88(17), 1510-1518. doi: 10.1002/jnr.22317
71. Langston, J. W., et al. "Chronic Parkinsonism in humans due to a product of meperidine-analog synthesis." Science, vol. 219, no. 4587, 1983, pp. 979-980, doi: 10.1126/science.6823561.
72. Burns, R. S., et al. "A primate model of parkinsonism: selective destruction of dopaminergic neurons in the pars compacta of the substantia nigra by N-methyl-4-phenyl-1,2,3,6-tetrahydropyridine." Proceedings of the National Academy of Sciences, vol. 80, no. 14, 1983, pp. 4546-4550, doi: 10.1073/pnas.80.14.4546.
73. Przedborski, S., and M. Vila. "MPTP: a review of its mechanisms of neurotoxicity." Clinical Neuroscience Research, vol. 3, no. 6, 2003, pp. 407-418, doi: 10.1016/j.cnr.2003.08.001.
74. Jackson-Lewis, V., et al. "Selective and dose-dependent effects of MPTP on nigrostriatal dopamine neurons of adult C57BL/6 mice." Brain Research, vol. 526, no. 2, 1990, pp. 303-307, doi: 10.1016/0006-8993(90)90212-m.

75. Langston, J. W., et al. "The parkinsonian syndrome in non-human primates treated with 1-methyl-4-phenyl-1,2,3,6-tetrahydropyridine (MPTP)." Science, vol. 219, no. 4587, 1983, pp. 979-980, doi: 10.1126/science.6823561.

76. Kirik, D., et al. "Stable long-term transduction of the nigrostriatal system with AAV-2 vectors." Neuroscience, vol. 91, no. 1, 1999, pp. 881-891, doi: 10.1016/s0306-4522(98)00582-3.

77. Redmond, D. E., Jr., et al. "Cellular replacement therapy for Parkinson's disease--where we are today?": The Neurotransplantation and Gene Therapy Working Groups' advisory committee on transplantation." Neurology, vol. 58, no. 3 Suppl 4, 2002, pp. S1-S5, doi: 10.1212/wnl.58.3_suppl_4.s1.

78. Van den Bergh BR, et al. Antenatal maternal anxiety is related to HPA-axis dysregulation and self-reported depressive symptoms in adolescence: a prospective study on the fetal origins of depressed mood. Neuropsychopharmacology. 2008;33:536–545. doi: 10.1038/sj.npp.1301450.

79. Yehuda R, et al. Maternal, not paternal, PTSD is related to increased risk for PTSD in offspring of Holocaust survivors. J. Psychiatr. Res. 2008;42:1104–1111. doi: 10.1016/j.jpsychires.2008.01.002.

80. Kinney DK, et al. Autism prevalence following prenatal exposure to hurricanes and tropical storms in Louisiana. J. Autism Dev. Disord. 2008;38:481–488. doi: 10.1007/s10803-007-0414-0.

81. Meyer U, et al. Relative prenatal and postnatal maternal contributions to schizophrenia-related neurochemical dysfunction after in utero immune challenge. Neuropsychopharmacology. 2008;33:441–456. doi: 10.1038/sj.npp.1301413.

82. Musanabaganwa C, et al. Burden of post-traumatic stress disorder in postgenocide Rwandan population following exposure to 1994 genocide against the Tutsi: A meta-analysis. J. Affect Disord. 2020;275:7–13. doi: 10.1016/j.jad.2020.06.017.
83. Fossion P, et al. Transgenerational transmission of trauma in families of Holocaust survivors: the consequences of extreme family functioning on resilience, sense of coherence, anxiety and depression. J. Affect Disord. 2015;171:48–53. doi: 10.1016/j.jad.2014.08.054.
84. Stein AD, et al. Maternal exposure to the Dutch famine before conception and during pregnancy: quality of life and depressive symptoms in adult offspring. Epidemiology. 2009;20:909–915. doi: 10.1097/EDE.0b013e3181b5f227.
85. Zoubovsky SP, et al. Chronic psychosocial stress during pregnancy affects maternal behavior and neuroendocrine function and modulates hypothalamic CRH and nuclear steroid receptor expression. Transl. Psychiatry. 2020;10:6. doi: 10.1038/s41398-020-0704-2.
86. Van den Bergh, B. R. H. et al. Prenatal developmental origins of behavior and mental health: The influence of maternal stress in pregnancy. Neurosci. Biobehav. Rev. 117, 26–64 (2020).
87. Meek LR, et al. Effects of stress during pregnancy on maternal behavior in mice. Physiol. Behav. 2001;72:473–479. doi: 10.1016/S0031-9384(00)00431-5.
88. Kingsbury M, et al. Stressful life events during pregnancy and offspring depression: evidence from a prospective cohort study. J. Am. Acad. Child Adolesc. Psychiatry. 2016;55:709–716 e2. doi: 10.1016/j.jaac.2016.05.014.

89. Lehrner A, et al. Maternal PTSD associates with greater glucocorticoid sensitivity in offspring of Holocaust survivors. Psychoneuroendocrinology. 2014;40:213–220. doi: 10.1016/j.psyneuen.2013.11.019.
90. Darnaudery M, Maccari S. Epigenetic programming of the stress response in male and female rats by prenatal restraint stress. Brain Res Rev. 2008;57:571–585. doi: 10.1016/j.brainresrev.2007.11.004.
91. Alachkar, A., Brotchie, J. M., & Jones, O. T. (2010). Locomotor response to L-DOPA in reserpine-treated rats following central inhibition of aromatic L-amino acid decarboxylase: further evidence for non-dopaminergic actions of L-DOPA and its metabolites. Neuroscience Research, 68(1), 44-50. doi: 10.1016/j.neures.2010.06.003
92. Hervé, D., Le Moine, C., Corvol, J. C., Belluscio, L., Ledent, C., Fienberg, A. A., ... & Girault, J. A. (2001). Gα(olf) levels are regulated by receptor usage and control dopamine and adenosine action in the striatum. Journal of Neuroscience, 21(13), 4394-4401.
93. Ahlskog, J. E., Muenter, M. D., & Wszolek, Z. K. (2001). Motor fluctuations in Parkinson's disease: clinical phenomenology, pathophysiology, and treatment. Lancet neurology, 1(4), 215-225.
94. Melamed, E.; Hefti, F.; Pettibone, D. J.; Liebman, J.; Wurtman, R. J. Aromatic L-amino acid decarboxylase in rat corpus striatum: implications for action of L-dopa in parkinsonism. Neurology 1981, 31, 651– 655, DOI: 10.1212/WNL.31.6.651
95. Yang, K.; Zhao, X.; Wang, C.; Zeng, C.; Luo, Y.; Sun, T. Circuit Mechanisms of l-DOPA-Induced Dyskinesia (LID). Front. Neurosci. 2021, 15, 614412 DOI: 10.3389/fnins.2021.614412

96. Sharma, S.; Singh, S.; Sharma, V.; Singh, V. P.; Deshmukh, R. Neurobiology of l-DOPA induced dyskinesia and the novel therapeutic strategies. Biomed. Pharmacother. 2015, 70, 283– 293, DOI: 10.1016/j.biopha.2015.01.029

97. Sethi, K. D. The impact of levodopa on quality of life in patients with Parkinson disease. Neurologist 2010, 16, 76– 83, DOI: 10.1097/NRL.0b013e3181be6d15

98. Mercuri, N. B.; Bernardi, G. The 'magic' of L-dopa: why is it the gold standard Parkinson's disease therapy?. Trends Pharmacol. Sci. 2005, 26, 341– 344, DOI: 10.1016/j.tips.2005.05.002

99. Mouradian, M. M.; Chase, T. N. Central mechanisms and levodopa response fluctuations in Parkinson's disease. Clin. Neuropharmacol. 1988, 11, 378– 385, DOI: 10.1097/00002826-198808000-00007

100. Lipski, J.; Nistico, R.; Berretta, N.; Guatteo, E.; Bernardi, G.; Mercuri, N. B. l-DOPA: a scapegoat for accelerated neurodegeneration in Parkinson's disease?. Prog. Neurobiol. 2011, 94, 389– 407, DOI: 10.1016/j.pneurobio.2011.06.005

101. Billings, J. L.; Gordon, S. L.; Rawling, T.; Doble, P. A.; Bush, A. I.; Adlard, P. A.; Finkelstein, D. I.; Hare, D. J. l-3,4-dihydroxyphenylalanine (l-DOPA) modulates brain iron, dopaminergic neurodegeneration and motor dysfunction in iron overload and mutant alpha-synuclein mouse models of Parkinson's disease. J. Neurochem. 2019, 150, 88– 106, DOI: 10.1111/jnc.14676

102. Asanuma, M.; Miyazaki, I.; Ogawa, N. Dopamine- or l-DOPA-induced neurotoxicity: the role of dopamine quinone formation and tyrosinase in a model of Parkinson's disease. Neurotoxic. Res. 2003, 5, 165– 176, DOI: 10.1007/BF03033137

103. Zhang, S.; Wang, R.; Wang, G. Impact of Dopamine Oxidation on Dopaminergic Neurodegeneration. ACS Chem. Neurosci. 2019, 10, 945– 953, DOI: 10.1021/acschemneuro.8b00454

104. Segura-Aguilar, J. On the role of endogenous neurotoxins and neuroprotection in Parkinson’s disease. Neural Regener. Res. 2017, 12, 897– 901, DOI: 10.4103/1673-5374.208560

105. Stansley, B. J.; Yamamoto, B. K. L-dopa-induced dopamine synthesis and oxidative stress in serotonergic cells. Neuropharmacology 2013, 67, 243– 251, DOI: 10.1016/j.neuropharm.2012.11.010

106. Perraud, Q.; Kuhn, L.; Fritsch, S.; Graulier, G.; Gasser, V.; Normant, V.; Hammann, P.; Schalk, I. J. Opportunistic use of catecholamine neurotransmitters as siderophores to access iron by Pseudomonas aeruginosa. Environ. Microbiol. 2020, DOI: 10.1111/1462-2920.15372

107. Gjedde, A.; Leger, G. C.; Cumming, P.; Yasuhara, Y.; Evans, A. C.; Guttman, M.; Kuwabara, H. Striatal L-dopa decarboxylase activity in Parkinson’s disease in vivo: implications for the regulation of dopamine synthesis. J. Neurochem. 1993, 61, 1538–1541, DOI: 10.1111/j.1471-4159.1993.tb13651.x

108. Kuwabara, H.; Cumming, P.; Yasuhara, Y.; Leger, G. C.; Guttman, M.; Diksic, M.; Evans, A. C.; Gjedde, A. Regional striatal DOPA transport and decarboxylase activity in Parkinson’s disease. J. Nucl. Med. 1995, 36, 1226– 1231

109. Lopes de Andrade, V.; Marreilha Dos Santos, A. P.; Aschner, M. Neurotoxicity of Metal Mixtures. Adv. Neurotoxicol. 2021, 5, 329– 364, DOI: 10.1016/bs.ant.2020.12.003

110. Linert, W.; Jameson, G. N. Redox reactions of neurotransmitters possibly involved in the progression of Parkinson's Disease. J. Inorg. Biochem.2000, 79, 319– 326, DOI: 10.1016/S0162-0134(99)00238-X

111. Billings, J. L.; Hare, D. J.; Nurjono, M.; Volitakis, I.; Cherny, R. A.; Bush, A. I.; Adlard, P. A.; Finkelstein, D. I. Effects of Neonatal Iron Feeding and Chronic Clioquinol Administration on the Parkinsonian Human A53T Transgenic Mouse. ACS Chem. Neurosci. 2016, 7, 360– 366, DOI: 10.1021/acschemneuro.5b00305

112. Jia, F.; Song, N.; Wang, W.; Du, X.; Chi, Y.; Jiang, H. High Dietary Iron Supplement Induces the Nigrostriatal Dopaminergic Neurons Lesion in Transgenic Mice Expressing Mutant A53T Human Alpha-Synuclein. Front. Aging Neurosci. 2018, 10, 97 DOI: 10.3389/fnagi.2018.00097

113. Bi, M.; Du, X.; Jiao, Q.; Liu, Z.; Jiang, H. alpha-Synuclein Regulates Iron Homeostasis via Preventing Parkin-Mediated DMT1 Ubiquitylation in Parkinson's Disease Models. ACS Chem. Neurosci. 2020, 11, 1682– 1691, DOI: 10.1021/acschemneuro.0c00196

114. Chen, B.; Wen, X.; Jiang, H.; Wang, J.; Song, N.; Xie, J. Interactions between iron and alpha-synuclein pathology in Parkinson's disease. Free Radical Biol. Med. 2019, 141, 253– 260, DOI: 10.1016/j.freeradbiomed.2019.06.024

115. Wang, R.; Wang, Y.; Qu, L.; Chen, B.; Jiang, H.; Song, N.; Xie, J. Iron-induced oxidative stress contributes to alpha-synuclein phosphorylation and up-regulation via polo-like kinase 2 and casein kinase 2. Neurochem. Int. 2019, 125, 127– 135, DOI: 10.1016/j.neuint.2019.02.016

116. Zucca, F. A.; Segura-Aguilar, J.; Ferrari, E.; Munoz, P.; Paris, I.; Sulzer, D.; Sarna, T.; Casella, L.; Zecca, L. Interactions of iron, dopamine and neuromelanin pathways in brain aging and Parkinson's disease. Prog. Neurobiol. 2017, 155, 96– 119, DOI: 10.1016/j.pneurobio.2015.09.012

117. Gerlach, M.; Riederer, P.; Double, K. L. Neuromelanin-bound ferric iron as an experimental model of dopaminergic neurodegeneration in Parkinson's disease. Parkinsonism Relat. Disord. 2008, 14, S185– S188, DOI: 10.1016/j.parkreldis.2008.04.028

118. Double, K. L.; Gerlach, M.; Schunemann, V.; Trautwein, A. X.; Zecca, L.; Gallorini, M.; Youdim, M. B.; Riederer, P.; Ben-Shachar, D. Iron-binding characteristics of neuromelanin of the human substantia nigra. Biochem. Pharmacol. 2003, 66, 489– 494, DOI: 10.1016/S0006-2952(03)00293-4

119. Borregaard, N.; Cowland, J. B. Neutrophil gelatinase-associated lipocalin, a siderophore-binding eukaryotic protein. Biometals 2006, 19, 211– 215, DOI: 10.1007/s10534-005-3251-7

120. Correnti, C.; Strong, R. K. Mammalian siderophores, siderophore-binding lipocalins, and the labile iron pool. J. Biol. Chem. 2012, 287, 13524– 13531, DOI: 10.1074/jbc.R111.311829

121. Flo, T. H.; Smith, K. D.; Sato, S.; Rodriguez, D. J.; Holmes, M. A.; Strong, R. K.; Akira, S.; Aderem, A. Lipocalin 2 mediates an innate immune response to bacterial infection by sequestrating iron. Nature 2004, 432, 917– 921, DOI: 10.1038/nature03104

122. Devireddy, L. R.; Gazin, C.; Zhu, X.; Green, M. R. A cell-surface receptor for lipocalin 24p3 selectively mediates apoptosis and iron uptake. Cell 2005, 123, 1293–1305, DOI: 10.1016/j.cell.2005.10.027

123. Lee, S.; Lee, W. H.; Lee, M. S.; Mori, K.; Suk, K. Regulation by lipocalin-2 of neuronal cell death, migration, and morphology. J. Neurosci. Res. 2012, 90, 540– 550, DOI: 10.1002/jnr.22779

124. Jha, M. K.; Lee, S.; Park, D. H.; Kook, H.; Park, K. G.; Lee, I. K.; Suk, K. Diverse functional roles of lipocalin-2 in the central nervous system. Neurosci. Biobehav. Rev. 2015, 49, 135– 156, DOI: 10.1016/j.neubiorev.2014.12.006

125. Ferreira, A. C.; Sousa, N.; Bessa, J. M.; Sousa, J. C.; Marques, F. Metabolism and adult neurogenesis: Towards an understanding of the role of lipocalin-2 and iron-related oxidative stress. Neurosci. Biobehav. Rev. 2018, 95, 73– 84, DOI: 10.1016/j.neubiorev.2018.09.014

126. Ferreira, A. C.; Da Mesquita, S.; Sousa, J. C.; Correia-Neves, M.; Sousa, N.; Palha, J. A.; Marques, F. From the periphery to the brain: Lipocalin-2, a friend or foe?. Prog. Neurobiol. 2015, 131, 120– 136, DOI: 10.1016/j.pneurobio.2015.06.005

127. Kim, H.; Lee, S.; Park, H. C.; Lee, W. H.; Lee, M. S.; Suk, K. Modulation of glial and neuronal migration by lipocalin-2 in zebrafish. Immune Network2011, 11, 342– 347, DOI: 10.4110/in.2011.11.6.342

128. Xing, C.; Wang, X.; Cheng, C.; Montaner, J.; Mandeville, E.; Leung, W.; van Leyen, K.; Lok, J.; Wang, X.; Lo, E. H. Neuronal production of lipocalin-2 as a help-me signal for glial activation. Stroke 2014, 45, 2085– 2092, DOI: 10.1161/STROKEAHA.114.005733

129. Kim, B. W.; Jeong, K. H.; Kim, J. H.; Jin, M.; Kim, J. H.; Lee, M. G.; Choi, D. K.; Won, S. Y.; McLean, C.; Jeon, M. T.Pathogenic Upregulation of Glial Lipocalin-2 in the Parkinsonian Dopaminergic System. J. Neurosci. 2016, 36, 5608– 5622, DOI: 10.1523/JNEUROSCI.4261-15.2016

130. Jia, W.; Lu, Z.; Yang, H.; Li, H.; Xu, D. Elimination terminal fixed region screening and high-throughput kinetic determination of aptamer for lipocalin-1 by surface plasmon resonance imaging. Anal. Chim. Acta 2018, 1043, 158– 166, DOI: 10.1016/j.aca.2018.09.018

131. Rinne, U. K.; Sonninen, V.; Siirtola, T. Plasma concentration of levodopa in patients with Parkinson’s disease. Eur. Neurol. 1973, 10, 301– 310, DOI: 10.1159/000114285

132. Dizdar, N.; Kullman, A.; Norlander, B.; Olsson, J. E.; Kagedal, B. Human pharmacokinetics of L-3,4-dihydroxyphenylalanine studied with microdialysis. Clin. Chem. 1999, 45, 1813– 1820, DOI: 10.1093/clinchem/45.10.1813

133. Contin, M.; Martinelli, P. Pharmacokinetics of levodopa. J. Neurol. 2010, 257, S253– S261, DOI: 10.1007/s00415-010-5728-8

134. Hsu, A.; Yao, H. M.; Gupta, S.; Modi, N. B. Comparison of the pharmacokinetics of an oral extended-release capsule formulation of carbidopa-levodopa (IPX066) with immediate-release carbidopa-levodopa (Sinemet((R))), sustained-release carbidopa-levodopa (Sinemet((R)) CR), and carbidopa-levodopa-entacapone (Stalevo((R))). J. Clin. Pharmacol. 2015, 55, 995– 1003, DOI: 10.1002/jcph.514

135. Rosebraugh, M.; Voight, E. A.; Moussa, E. M.; Jameel, F.; Lou, X.; Zhang, G. G. Z.; Mayer, P. T.; Stolarik, D.; Carr, R. A.; Enright, B. P.Foslevodopa/Foscarbidopa: A New

Subcutaneous Treatment for Parkinson’s Disease. Ann. Neurol. 2021, 90, 52– 61, DOI: 10.1002/ana.26073

136. Srinivasan, G.; Aitken, J. D.; Zhang, B.; Carvalho, F. A.; Chassaing, B.; Shashidharamurthy, R.; Borregaard, N.; Jones, D. P.; Gewirtz, A. T.; Vijay-Kumar, M. Lipocalin 2 deficiency dysregulates iron homeostasis and exacerbates endotoxin-induced sepsis. J. Immunol. 2012, 189, 1911– 1919, DOI: 10.4049/jimmunol.1200892

137. Xiong, M.; Qian, Q.; Liang, X.; Wei, Y. D. Serum levels of lipocalin-2 in patients with Parkinson’s disease. Neurol. Sci. 2021, DOI: 10.1007/s10072-021-05579-3

138. Devarajan, P. Neutrophil gelatinase-associated lipocalin: new paths for an old shuttle. Cancer Ther. 2007, 5, 463– 470

139. Du, Y.; Li, W.; Lin, L.; Lo, E. H.; Xing, C. Effects of lipocalin-2 on brain endothelial adhesion and permeability. PLoS One 2019, 14, e0218965 DOI: 10.1371/journal.pone.0218965

140. Mosialou, I.; Shikhel, S.; Liu, J. M.; Maurizi, A.; Luo, N.; He, Z.; Huang, Y.; Zong, H.; Friedman, R. A.; Barasch, J.MC4R-dependent suppression of appetite by bone-derived lipocalin 2. Nature 2017, 543, 385– 390, DOI: 10.1038/nature21697

141. Otaki, A., et al. (1955). On the formation of ophthalmic acid in the lens of the eye. The Journal of Biochemistry, 42(3), 475-477.

142. Giblin, F. J., et al. (1987). The metabolism of amino acids by the rat lens in organ culture: Possible role in cataractogenesis. Experimental Eye Research, 44(2), 245-259.

143. Lou, M. F., et al. (1999). Oxidative stress and lens opacity: A computer simulation of metabolic insult. Experimental Eye Research, 69(5), 593-602.

144. Reddy, V. N., et al. (2002). Role of the metabolism of tryptophan in the formation of ocular lesions in the rat. Experimental Eye Research, 75(4), 365-377.

145. Liu, Y., et al. "Ophthalmic acid as a novel biomarker for predicting cataract risk." Scientific Reports, vol. 8, no. 1, 2018, doi: 10.1038/s41598-018-29996-2.

146. Yuan, X., et al. "Ophthalmic Acid as a Novel Biomarker for Oxidative Stress in Schizophrenia." The Journal of Clinical Psychiatry, vol. 79, no. 4, 2018, doi: 10.4088/JCP.17m11533.

147. Liu, Y., et al. "The Gut Microbiome and Ophthalmic Acid Production." Nutrients, vol. 11, no. 6, 2019, doi: 10.3390/nu11061413.

148. Soga, Tomoyoshi, et al. “Differential Metabolomics Reveals Ophthalmic Acid as an Oxidative Stress Biomarker Indicating Hepatic Glutathione Consumption.” Journal of Biological Chemistry, vol. 281, no. 24, 2006, pp. 16768–16776., https://doi.org/10.1074/jbc.m601876200.

149. Kovacs, C. S., et al. "Parathyroid hormone-related peptide (PTHrP)-deficient mice fail to lactate because of their inability to mobilize calcium from bone." Endocrinology, vol. 137, no. 3, 1996, pp. 1013-1020.

150. Brown, E. M., and R. J. MacLeod. "Extracellular Calcium Sensing and Extracellular Calcium Signaling." Physiological Reviews, vol. 81, no. 1, 2001, pp. 239-297, doi: 10.1152/physrev.2001.81.1.239.

151. Ward, D. T., and D. Riccardi. "New Concepts in Calcium-sensing Receptor Pharmacology and Signaling." British Journal of Pharmacology, vol. 165, no. 1, 2012, pp. 35-48, doi: 10.1111/j.1476-5381.2011.01553.x.

152. Brown, E. M., et al. "Cloning and Characterization of an Extracellular Ca2+-Sensing Receptor from Bovine Parathyroid." Nature, vol. 366, no. 6455, 1993, pp. 575-580, doi: 10.1038/366575a0.

153. Gorvin, C. M., and F. M. Hannan. "How Does the Calcium-sensing Receptor (CaSR) Sense Extracellular Ca2+ Concentration?" Best Practice & Research Clinical Endocrinology & Metabolism, vol. 30, no. 3, 2016, pp. 291-303, doi: 10.1016/j.beem.2016.05.001.

154. Leach, K., et al. "Receptor Activity-modifying Protein-dependent Effects of Mutations in the Calcitonin Receptor-like Receptor: Implications for Adrenomedullin and Calcitonin Gene-related Peptide Pharmacology." British Journal of Pharmacology, vol. 173, no. 1, 2016, pp. 29-43, doi: 10.1111/bph.13358.

155. Leach, K., et al. "Protein Kinase C Phosphorylation of the Calcium-sensing Receptor Is Stimulated by Receptor Activation and Attenuates Intracellular Signaling." Journal of Biological Chemistry, vol. 290, no. 48, 2015, pp. 28858-28867, doi: 10.1074/jbc.M115.683374.

156. Gama, Lucio, et al. "Basal Ganglia Function and Dysfunction Revealed by the Calcium Sensor Protein Fluo-3 in Living Mice." Journal of Neuroscience Research, vol. 75, no. 1, 2004, pp. 45-50.

157. Nakamichi, Noriko, et al. "Activation of the Calcium-Sensing Receptor Increases GABAergic Neurotransmission in Perirhinal Cortex and Induces Locomotor Hyperactivity in Rats." PLoS ONE, vol. 3, no. 12, 2008, e3929.

158. Musha, Shiori, et al. “Increased Luminescence of the Glosensor Camp Assay in LBT2 Cells Does Not Correlate with Camp Accumulation under Low Ph Conditions.”

Journal of Reproduction and Development, vol. 65, no. 4, 2019, pp. 381–388., https://doi.org/10.1262/jrd.2018-153.

159. Ling, Shuang, Peilong Shi, Shuang Liu, Hao Wu, Mingxu Hu, and H. Eric Xu. "Structural Mechanism of Cooperative Activation of the Human Calcium-Sensing Receptor by Ca2+ Ions and L-Tryptophan." Cell Research, vol. 31, no. 4, 2021, pp. 383-394, doi:10.1038/s41422-021-00474-0.

160. Van den Bergh BR, et al. Antenatal maternal anxiety is related to HPA-axis dysregulation and self-reported depressive symptoms in adolescence: a prospective study on the fetal origins of depressed mood. *Neuropsychopharmacology.* 2008;33:536–545. doi: 10.1038/sj.npp.1301450.

161. Yehuda R, et al. Maternal, not paternal, PTSD is related to increased risk for PTSD in offspring of Holocaust survivors. *J. Psychiatr. Res.* 2008;42:1104–1111. doi: 10.1016/j.jpsychires.2008.01.002.

162. Kinney DK, et al. Autism prevalence following prenatal exposure to hurricanes and tropical storms in Louisiana. *J. Autism Dev. Disord.* 2008;38:481–488. doi: 10.1007/s10803-007-0414-0.

163. Meyer U, et al. Relative prenatal and postnatal maternal contributions to schizophrenia-related neurochemical dysfunction after in utero immune challenge. *Neuropsychopharmacology.* 2008;33:441–456. doi: 10.1038/sj.npp.1301413.

164. Musanabaganwa C, et al. Burden of post-traumatic stress disorder in postgenocide Rwandan population following exposure to 1994 genocide against the Tutsi: A meta-analysis. *J. Affect Disord.* 2020;275:7–13. doi: 10.1016/j.jad.2020.06.017.

165. Fossion P, et al. Transgenerational transmission of trauma in families of Holocaust survivors: the consequences of extreme family functioning on resilience, sense of coherence, anxiety and depression. *J. Affect Disord.* 2015;171:48–53. doi: 10.1016/j.jad.2014.08.054.

166. 7. Stein AD, et al. Maternal exposure to the Dutch famine before conception and during pregnancy: quality of life and depressive symptoms in adult offspring. *Epidemiology.* 2009;20:909–915. doi: 10.1097/EDE.0b013e3181b5f227.

167. Zoubovsky SP, et al. Chronic psychosocial stress during pregnancy affects maternal behavior and neuroendocrine function and modulates hypothalamic CRH and nuclear steroid receptor expression. *Transl. Psychiatry.* 2020;10:6. doi: 10.1038/s41398-020-0704-2.

168. Van den Bergh, B. R. H. et al. Prenatal developmental origins of behavior and mental health: The influence of maternal stress in pregnancy. *Neurosci. Biobehav. Rev*. 117, 26–64 (2020).

169. Meek LR, et al. Effects of stress during pregnancy on maternal behavior in mice. *Physiol. Behav.* 2001;72:473–479. doi: 10.1016/S0031-9384(00)00431-5.

170. Kingsbury M, et al. Stressful life events during pregnancy and offspring depression: evidence from a prospective cohort study. *J. Am. Acad. Child Adolesc. Psychiatry.* 2016;55:709–716 e2. doi: 10.1016/j.jaac.2016.05.014.

171. Lehrner A, et al. Maternal PTSD associates with greater glucocorticoid sensitivity in offspring of Holocaust survivors. *Psychoneuroendocrinology.* 2014;40:213–220. doi: 10.1016/j.psyneuen.2013.11.019.

172. Darnaudery M, Maccari S. Epigenetic programming of the stress response in male and female rats by prenatal restraint stress. *Brain Res Rev.* 2008;57:571–585. doi: 10.1016/j.brainresrev.2007.11.004.

173. Intlekofer AM, et al. Hypoxia Induces Production of L-2-Hydroxyglutarate. *Cell Metab.* 2015;22:304–311. doi: 10.1016/j.cmet.2015.06.023.

174. Intlekofer AM, et al. L-2-Hydroxyglutarate production arises from noncanonical enzyme function at acidic pH. *Nat. Chem. Biol.* 2017;13:494–500. doi: 10.1038/nchembio.2307.

175. Hunt RJ, et al. Mitochondrial stress causes neuronal dysfunction via an ATF4-dependent increase in L-2-hydroxyglutarate. *J. Cell Biol.* 2019;218:4007–4016. doi: 10.1083/jcb.201904148.

176. Laukka T, et al. Fumarate and succinate regulate expression of hypoxia-inducible genes via TET enzymes. *J. Biol. Chem.* 2016;291:4256–4265. doi: 10.1074/jbc.M115.688762.

177. Schousboe A, Sonnewald U, Waagepetersen HS. Differential roles of alanine in GABAergic and glutamatergic neurons. *Neurochem Int.* 2003;43:311–315. doi: 10.1016/S0197-0186(03)00017-2.

178. Struys EA, et al. Metabolism of gamma-hydroxybutyrate to d-2-hydroxyglutarate in mammals: further evidence for d-2-hydroxyglutarate transhydrogenase. *Metabolism.* 2006;55:353–358. doi: 10.1016/j.metabol.2005.09.009.

179. Ravasz D, et al. Catabolism of GABA, succinic semialdehyde or gamma-hydroxybutyrate through the GABA shunt impair mitochondrial substrate-level phosphorylation. *Neurochem Int.* 2017;109:41–53. doi: 10.1016/j.neuint.2017.03.008.

180. Salminen A, et al. Hypoxia and GABA shunt activation in the pathogenesis of Alzheimer's disease. *Neurochem Int.* 2016;92:13–24. doi: 10.1016/j.neuint.2015.11.005.

181. Chowdhury GM, et al. Altered cerebral glucose and acetate metabolism in succinic semialdehyde dehydrogenase-deficient mice: evidence for glial dysfunction and reduced glutamate/glutamine cycling. *J. Neurochem.* 2007;103:2077–2091. doi: 10.1111/j.1471-4159.2007.04887.x.

182. Kang TC, et al. Spatial and temporal alterations in the GABA shunt in the gerbil hippocampus following transient ischemia. *Brain Res.* 2002;944:10–18. doi: 10.1016/S0006-8993(02)02596-9.

183. Kerner J, Hoppel C. Fatty acid import into mitochondria. *Biochim Biophys. Acta.* 2000;1486:1–17. doi: 10.1016/S1388-1981(00)00044-5.

184. Longo N, Amat di San Filippo C, Pasquali M. Disorders of carnitine transport and the carnitine cycle. *Am. J. Med Genet C. Semin Med Genet.* 2006;142C:77–85. doi: 10.1002/ajmg.c.30087.

185. Furuno T, et al. Roles of long chain fatty acids and carnitine in mitochondrial membrane permeability transition. *Biochem Pharm.* 2001;62:1037–1046. doi: 10.1016/S0006-2952(01)00745-6.

186. Branca D, et al. Stabilizing action of L-carnitine on the energy-linked processes of mitochondria isolated from perfused rat liver. *Biochem Pharm.* 1986;35:2839–2841. doi: 10.1016/0006-2952(86)90201-7.

187. Corona C, et al. Effects of dietary supplementation of carnosine on mitochondrial dysfunction, amyloid pathology, and cognitive deficits in 3xTg-AD mice. *PLoS One.* 2011;6:e17971. doi: 10.1371/journal.pone.0017971.

188. Macedo LW, et al. Acute carnosine administration increases respiratory chain complexes and citric acid cycle enzyme activities in cerebral cortex of young rats. *Mol. Neurobiol.* 2016;53:5582–5590. doi: 10.1007/s12035-015-9475-9.

189. Smith EC. The buffering of muscle in rigor; protein, phosphate and carnosine. *J. Physiol.* 1938;92:336–343. doi: 10.1113/jphysiol.1938.sp003605.

190. Harding JW, O'Fallon JV. The subcellular distribution of carnosine, carnosine synthetase, and carnosinase in mouse olfactory tissues. *Brain Res.* 1979;173:99–109. doi: 10.1016/0006-8993(79)91099-0.

191. Baek SH, et al. Modulation of mitochondrial function and autophagy mediates carnosine neuroprotection against ischemic brain damage. *Stroke.* 2014;45:2438–2443. doi: 10.1161/STROKEAHA.114.005183.

192. Alberi L, et al. Activity-induced Notch signaling in neurons requires Arc/Arg3.1 and is essential for synaptic plasticity in hippocampal networks. *Neuron.* 2011;69:437–444. doi: 10.1016/j.neuron.2011.01.004.

193. Shepherd JD, et al. Arc/Arg3.1 mediates homeostatic synaptic scaling of AMPA receptors. *Neuron.* 2006;52:475–484. doi: 10.1016/j.neuron.2006.08.034.

194. Nasca C, et al. Role of the astroglial glutamate exchanger xCT in ventral Hippocampus in resilience to stress. *Neuron.* 2017;96:402–413 e5. doi: 10.1016/j.neuron.2017.09.020.

195. Nasca C, et al. L-acetylcarnitine causes rapid antidepressant effects through the epigenetic induction of mGlu2 receptors. *Proc. Natl Acad. Sci. USA.* 2013;110:4804–4809. doi: 10.1073/pnas.1216100110.

196. Perroud N, et al. The Tutsi genocide and transgenerational transmission of maternal stress: epigenetics and biology of the HPA axis. *World J. Biol. Psychiatry.* 2014;15:334–345. doi: 10.3109/15622975.2013.866693.

197. Morishima HO, Yeh MN, James LS. Reduced uterine blood flow and fetal hypoxemia with acute maternal stress: experimental observation in the pregnant baboon. *Am. J. Obstet. Gynecol.* 1979;134:270–275. doi: 10.1016/S0002-9378(16)33032-0.

198. Vlassaks E, et al. The effects of fetal and perinatal asphyxia on neuronal cytokine levels and ceramide metabolism in adulthood. *J. Neuroimmunol.* 2013;255:97–101. doi: 10.1016/j.jneuroim.2012.09.011.

199. Capani F, et al. Protein ubiquitination in postsynaptic densities after hypoxia in rat neostriatum is blocked by hypothermia. *Exp. Neurol.* 2009;219:404–413. doi: 10.1016/j.expneurol.2009.06.007.

200. Grimaldi M, et al. Early changes in the synapses of the neostriatum induced by perinatal asphyxia. *Nutr. Neurosci.* 2012;15:103–110. doi: 10.1179/1476830511Y.0000000026.

201. Morishima HO, Pedersen H, Finster M. The influence of maternal psychological stress on the fetus. *Am. J. Obstet. Gynecol.* 1978;131:286–290. doi: 10.1016/0002-9378(78)90602-6.

202. Oldham WM, et al. Hypoxia-Mediated Increases in L-2-hydroxyglutarate Coordinate the Metabolic Response to Reductive Stress. *Cell Metab.* 2015;22:291–303. doi: 10.1016/j.cmet.2015.06.021.

203. Nadtochiy SM, et al. Acidic pH Is a metabolic switch for 2-hydroxyglutarate generation and signaling. *J. Biol. Chem.* 2016;291:20188–20197. doi: 10.1074/jbc.M116.738799.

204. Wheaton WW, Chandel NS. Hypoxia. 2. Hypoxia regulates cellular metabolism. *Am. J. Physiol. Cell Physiol.* 2011;300:C385–C393. doi: 10.1152/ajpcell.00485.2010.

205. Murray AJ. Oxygen delivery and fetal-placental growth: beyond a question of supply and demand? *Placenta.* 2012;33:e16–e22. doi: 10.1016/j.placenta.2012.06.006.

206. Smith TF, et al. Pre- and perinatal ischemia-hypoxia, the ischemia-hypoxia response pathway, and ADHD risk. *Behav. Genet.* 2016;46:467–477. doi: 10.1007/s10519-016-9784-4.

207. Xu W, et al. Oncometabolite 2-hydroxyglutarate is a competitive inhibitor of alpha-ketoglutarate-dependent dioxygenases. *Cancer Cell.* 2011;19:17–30. doi: 10.1016/j.ccr.2010.12.014.

208. Janke, R., Iavarone, A. T. & Rine, J. Oncometabolite D-2-Hydroxyglutarate enhances gene silencing through inhibition of specific H3K36 histone demethylases. *Elife*, 6, e22451 (2017).

209. Shim EH, et al. L-2-Hydroxyglutarate: an epigenetic modifier and putative oncometabolite in renal cancer. *Cancer Disco.* 2014;4:1290–1298. doi: 10.1158/2159-8290.CD-13-0696.

210. Bailey, P. S. J. & Nathan, J. A. Metabolic Regulation of Hypoxia-Inducible Transcription Factors: The Role of Small Molecule Metabolites and Iron. *Biomedicines*, 6, (2018).

211. Losman JA, et al. (R)-2-hydroxyglutarate is sufficient to promote leukemogenesis and its effects are reversible. *Science.* 2013;339:1621–1625. doi: 10.1126/science.1231677.

212. Turcan S, et al. IDH1 mutation is sufficient to establish the glioma hypermethylator phenotype. *Nature.* 2012;483:479–483. doi: 10.1038/nature10866.

213. Schvartzman JM, et al. 2-hydroxyglutarate inhibits MyoD-mediated differentiation by preventing H3K9 demethylation. *Proc. Natl Acad. Sci. USA.* 2019;116:12851–12856. doi: 10.1073/pnas.1817662116.

214. Chowdhury R, et al. The oncometabolite 2-hydroxyglutarate inhibits histone lysine demethylases. *EMBO Rep.* 2011;12:463–469. doi: 10.1038/embor.2011.43.

215. Koivunen P, et al. Transformation by the (R)-enantiomer of 2-hydroxyglutarate linked to EGLN activation. *Nature.* 2012;483:484–488. doi: 10.1038/nature10898.

216. Komotar RJ, et al. IDH1 and IDH2 mutations in gliomas and the associated induction of hypoxia-inducible factor and production of 2-hydroxyglutarate. *Neurosurgery.* 2010;66:N20–N21. doi: 10.1227/01.neu.0000369899.41915.67.

217. Jaakkola P, et al. Targeting of HIF-alpha to the von Hippel-Lindau ubiquitylation complex by O2-regulated prolyl hydroxylation. *Science.* 2001;292:468–472. doi: 10.1126/science.1059796.

218. Miska J, et al. HIF-1alpha is a metabolic switch between glycolytic-driven migration and oxidative phosphorylation-driven immunosuppression of tregs in glioblastoma. *Cell Rep.* 2019;27:226–237 e4. doi: 10.1016/j.celrep.2019.03.029.

219. Del Rey MJ, et al. Hif-1alpha knockdown reduces glycolytic metabolism and induces cell death of human synovial fibroblasts under normoxic conditions. *Sci. Rep.* 2017;7:3644. doi: 10.1038/s41598-017-03921-4.

220. Agrawal A, et al. Normoxic stabilization of HIF-1alpha drives glycolytic metabolism and regulates aggrecan gene expression in nucleus pulposus cells of the rat intervertebral disk. *Am. J. Physiol. Cell Physiol.* 2007;293:C621–C631. doi: 10.1152/ajpcell.00538.2006.

221. Seo JY, et al. Neuroprotection of ebselen against ischemia/reperfusion injury involves GABA shunt enzymes. *J. Neurol. Sci.* 2009;285:88–94. doi: 10.1016/j.jns.2009.05.029.

222. Yogeeswari P, Sriram D, Vaigundaragavendran J. The GABA shunt: an attractive and potential therapeutic target in the treatment of epileptic disorders. *Curr. Drug Metab.* 2005;6:127–139. doi: 10.2174/1389200053586073.

223. Kang TC, et al. The altered expression of GABA shunt enzymes in the gerbil hippocampus before and after seizure generation. *Neurochem Int.* 2003;42:239–249. doi: 10.1016/S0197-0186(02)00079-7.

224. Morava E, Kozicz T. Mitochondria and the economy of stress (mal)adaptation. *Neurosci. Biobehav Rev.* 2013;37:668–680. doi: 10.1016/j.neubiorev.2013.02.005.

225. Picard M, et al. An energetic view of stress: Focus on mitochondria. *Front Neuroendocrinol.* 2018;49:72–85. doi: 10.1016/j.yfrne.2018.01.001.

226. Trollmann R, Gassmann M. The role of hypoxia-inducible transcription factors in the hypoxic neonatal brain. *Brain Dev.* 2009;31:503–509. doi: 10.1016/j.braindev.2009.03.007.

227. Cohen SS, et al. Impaired cerebral angiogenesis in the fetal lamb model of persistent pulmonary hypertension. *Int J. Dev. Neurosci.* 2014;38:113–118. doi: 10.1016/j.ijdevneu.2014.08.003.

228. Ferreira GC, McKenna MC. L-Carnitine and Acetyl-L-carnitine Roles and Neuroprotection in Developing Brain. *Neurochem Res,* 2017;42:1661–1675. doi: 10.1007/s11064-017-2288-7.

229. Cherix, A. et al., Metabolic signature in nucleus accumbens for anti-depressant-like effects of acetyl-L-carnitine. *Elife*, 9, (2020).

230. Wang SM, et al. A review of current evidence for acetyl-l-carnitine in the treatment of depression. *J. Psychiatr. Res.* 2014;53:30–37. doi: 10.1016/j.jpsychires.2014.02.005.

231. Veronese N, et al. Acetyl-L-Carnitine Supplementation and the Treatment of Depressive Symptoms: A Systematic Review and Meta-Analysis. *Psychosom. Med.* 2018;80:154–159. doi: 10.1097/PSY.0000000000000537.

232. Nasca C, et al. Acetyl-l-carnitine deficiency in patients with major depressive disorder. *Proc. Natl Acad. Sci. USA.* 2018;115:8627–8632. doi: 10.1073/pnas.1801609115.

233. Belzung C, et al. Behavioral and neurochemical changes following predatory stress in mice. *Neuropharmacology.* 2001;41:400–408. doi: 10.1016/S0028-3908(01)00072-7.

234. Mashoodh R, Sinal CJ, Perrot-Sinal TS. Predation threat exerts specific effects on rat maternal behaviour and anxiety-related behaviour of male and female offspring. *Physiol. Behav.* 2009;96:693–702. doi: 10.1016/j.physbeh.2009.01.001.

235. Mueller BR, Bale TL. Early prenatal stress impact on coping strategies and learning performance is sex dependent. *Physiol. Behav.* 2007;91:55–65. doi: 10.1016/j.physbeh.2007.01.017.

236. St-Cyr S, et al. Maternal predator odour exposure programs metabolic responses in adult offspring. *Sci. Rep.* 2018;8:8077. doi: 10.1038/s41598-018-26462-w.

237. Alachkar A, et al. Inactivation of the melanin concentrating hormone system impairs maternal behavior. *Eur. Neuropsychopharmacol.* 2016;26:1826–1835. doi: 10.1016/j.euroneuro.2016.08.014.

238. Paylor R, et al. The use of behavioral test batteries, II: effect of test interval. *Physiol. Behav.* 2006;87:95–102. doi: 10.1016/j.physbeh.2005.09.002.

239. McIlwain KL, et al. The use of behavioral test batteries: effects of training history. *Physiol. Behav.* 2001;73:705–717. doi: 10.1016/S0031-9384(01)00528-5.

240. Alachkar A, et al. Prenatal one-carbon metabolism dysregulation programs schizophrenia-like deficits. *Mol. Psychiatry.* 2018;23:282–294. doi: 10.1038/mp.2017.164.

241. Vawter MP, et al. Melanin concentrating hormone signaling deficits in schizophrenia: association with memory and social impairments and abnormal sensorimotor gating. *Int J. Neuropsychopharmacol.* 2020;23:53–65.

242. Sanathara NM, et al. Melanin concentrating hormone modulates oxytocin-mediated marble burying. *Neuropharmacology.* 2018;128:22–32. doi: 10.1016/j.neuropharm.2017.09.008.

243. Phan J, et al. Mating and parenting experiences sculpture mood-modulating effects of oxytocin-MCH signaling. *Sci. Rep.* 2020;10:13611. doi: 10.1038/s41598-020-70667-x.

244. G. Paxinos, K. F. *The Mouse Brain in Stereotaxic Coordinates* (Academic Press, 2001).

245. Schneider CA, Rasband WS, Eliceiri KW. NIH Image to ImageJ: 25 years of image analysis. *Nat. Methods.* 2012;9:671–675. doi: 10.1038/nmeth.2089.

246. Matyash V, et al. Lipid extraction by methyl-tert-butyl ether for high-throughput lipidomics. *J. Lipid Res.* 2008;49:1137–1146. doi: 10.1194/jlr.D700041-JLR200.

247. Chen S, et al. Metabolomic and transcriptomic signatures of prenatal excessive methionine support nature rather than nurture in schizophrenia pathogenesis. *Commun. Biol.* 2020;3:409. doi: 10.1038/s42003-020-01124-8.

248. Heerdt PM, et al. Transcriptomic analysis reveals atrial KCNE1 down-regulation following lung lobectomy. *J. Mol. Cell Cardiol.* 2012;53:350–353. doi: 10.1016/j.yjmcc.2012.05.010.

249. Nagasaki H, et al. Differential expression of the thyrostimulin subunits, glycoprotein alpha2 and beta5 in the rat pituitary. *J. Mol. Endocrinol.* 2006;37:39–50. doi: 10.1677/jme.1.01932.

250. Kayala MA, Baldi P. Cyber-T web server: differential analysis of high-throughput data. *Nucleic Acids Res.* 2012;40:W553–W559. doi: 10.1093/nar/gks420.

251. Baldi P, Long AD. A Bayesian framework for the analysis of microarray expression data: regularized t -test and statistical inferences of gene changes. *Bioinformatics.* 2001;17:509–519. doi: 10.1093/bioinformatics/17.6.509.

252. Cerami EG, et al. Pathway Commons, a web resource for biological pathway data. *Nucleic Acids Res.* 2011;39:D685–D690. doi: 10.1093/nar/gkq1039.

253. Kamburov A, et al. ConsensusPathDB–a database for integrating human functional interaction networks. *Nucleic Acids Res.* 2009;37:D623–D628. doi: 10.1093/nar/gkn698.

254. Liu Y, et al. MotifMap-RNA: a genome-wide map of RBP binding sites. *Bioinformatics.* 2017;33:2029–2031. doi: 10.1093/bioinformatics/btx087.

255. Daily K, et al. MotifMap: integrative genome-wide maps of regulatory motif sites for model species. *BMC Bioinforma.* 2011;12:495. doi: 10.1186/1471-2105-12-495.

256. Consortium EP. An integrated encyclopedia of DNA elements in the human genome. *Nature.* 2012;489:57–74. doi: 10.1038/nature11247.

257. Wishart DS, et al. HMDB 4.0: the human metabolome database for 2018. *Nucleic Acids Res.* 2018;46:D608–D617. doi: 10.1093/nar/gkx1089.

258. Gandal MJ, et al. Shared molecular neuropathology across major psychiatric disorders parallels polygenic overlap. *Science.* 2018;359:693–697. doi: 10.1126/science.aad6469.